

# JUICE: In-mission synergy of science and navigation ephemeris products

Application to potential benefits for statistical Delta-V expenditure.

Jonas Hener



# JUICE: In-mission synergy of science and navigation ephemeris products

Application to potential benefits for statistical Delta-V expenditure.

by

**Jonas Hener**

to obtain the degree of Master of Science  
at the Delft University of Technology,  
to be defended publicly on Friday July 1, 2022 at 9:00 AM.

Student number:	4430166	
Project duration:	September 4 <sup>th</sup> , 2021 – July 1 <sup>st</sup> , 2022	
Thesis committee:	Prof. dr. L.L.A. Vermeersen	Committee chair
	Dr. ir. D. Dirkx,	Supervisor
	Ir. M. Fayolle,	Supervisor
	Dr. A. Menicucci	External examiner

An electronic version of this thesis is available at <http://repository.tudelft.nl/>.

Cover picture: "Jupiter's Magnificent Swirling Clouds - A multitude of magnificent, swirling clouds in Jupiter's dynamic North North Temperate Belt is captured in this image from NASA's Juno spacecraft."  
Image credit: NASA



# Preface

This work marks the end of my M.Sc. studies at the Space Flight department of TU Delft. I would like to thank the academic staff for the setup and teaching of the curriculum, which has proven invaluable during this thesis and has opened many doors for my future.

Special thanks go to my supervisors Dominic and Marie, who through their reliable and considerate guidance have kept me engaged and - more so - excited during the whole project. Bringing me along to expert seminars and allowing me to get in touch with the academic authorities in the field was an exceptionally generous move and made the project all the more interesting to me. I will happily think back to these days.

Lastly I want to thank my friends and family for the unwavering support over the past 7 (seven!) years and beyond.

*Jonas Hener*  
*Delft, June 2022*



# Abstract

This thesis project investigates navigational aspects of the upcoming JUICE (JUperiter ICy moons Explorer) mission, which is expected to deliver valuable data products for the scientific study of the Jovian system, and the three Galilean moons Europa, Ganymede and Callisto in particular. One such data product comes from the 3GM radio science payload, which is expected to contribute towards more accurate ephemerides of the Galilean moons and a refined study of their gravity fields. Accurate and reliable acquisition of these data depends greatly on the successful Guidance, Navigation and Control (GNC) operations, where an efficient GNC performance can unlock excess  $\Delta V$  capabilities. It is the goal of this work to identify statistical  $\Delta V$  savings from integration of in-mission radio science ephemeris improvements into the GNC operations. The resulting excess  $\Delta V$  could be used to effectuate one of the mission enhancement and extension options (*e.g.* coverage of the Jupiter's mid-high latitudes or a lower-altitude Ganymede orbit), the enablement of which ultimately motivates this thesis project.

A navigational orbit determination (OD) framework was set up, modelled closely after the OD setup from the JUICE mission analysis team. An interface for simulating moon state knowledge updates from external ephemeris products was implemented. This setup was then extended to support a simplified statistical  $\Delta V$  analysis. The external ephemeris products were modelled using an adopted high-fidelity OD setup with a coupled filter configuration, which simulates the uncertainty of in-mission ephemeris updates from the 3GM radio science data. These results were then used to simulate external ephemeris updates to the navigation OD and to evaluate their impact on the statistical  $\Delta V$  expenditure.

It was found that external moon ephemerides in general, and the simulated science data based OD solution in particular, are not suitable for reducing the statistical  $\Delta V$  cost of post-flyby correction manoeuvres. Within one to two encounters of a given flyby body, the nominal (update-free) navigation OD has improved moon state knowledge to a point where it no longer contributes significantly to size of the correction manoeuvres. To generate statistical  $\Delta V$  savings, the moon state knowledge must be improved for the navigation of the mission's first encounters. It was thus concluded that moon ephemeris improvements should not be provided from JUICE science data, but from observations that have been collected prior to mission. It was furthermore found that due to its extensive coverage, the navigation tracking data captures system information that the radio science data is less sensitive to. It could therefore be considered in the post-mission efforts to improve the high-accuracy ephemerides of the Galilean moons.



# Contents

1	Introduction	1
1.1	Research Questions	2
1.2	Report Outline	2
2	Journal Paper	3
3	Conclusions & Recommendations	27
3.1	Conclusions	27
3.2	Recommendations for future work	29
A	Numerical implementation of the JUICE mission trajectory	31
A.1	Mission trajectory simplifications	31
A.2	Integrator & Propagator selection	34
A.2.1	Requirements on numerical solver	34
A.2.2	Integrator settings selection	34
A.2.3	Numerical accuracy quantification	35
B	Verification & Validation	37
B.1	Verification & Validation: Navigation OD	37
B.1.1	Consistency of Navigation OD Results (Verification)	37
B.1.2	Comparison to reference data (Validation)	40
B.2	Validation: Manoeuvre Design Algorithm	44
C	Supplementary material on selected OD solutions	47
C.1	System knowledge evolution with gravity estimation	47
C.2	System knowledge evolution with transfer factor ( $f=3$ )	51
C.3	System knowledge evolution from simulated 3GM data	52



# Nomenclature

## Abbreviations and Acronyms

CReMA	Consolidated Report on the Mission Analysis
DCO	Data Cut-Off (time)
DSM	Deep Space Manoeuvre
ESA	European Space Agency
ESOC	European Space Operations Centre
ESTRACK	European Space Tracking Network
GC0-500	Ganymede Circular Orbit at altitude of 500km (JUICE mission phase)
GNC	Guidance, Navigation & Control
ICRF	International Celestial Reference Frame
IMCCE	Institut de mécanique céleste et de calcul des éphémérides
JANUS	Optical imaging system onboard the JUICE spacecraft
JOI	Jupiter Orbit Insertion
JUICE	Jupiter ICy moons Explorer
MC	Monte Carlo (Analysis)
Nav OD	Navigation Orbit Determination, referring specifically to the setup implemented by this work
OD	Orbit Determination
OpNavs	Optical Navigation measurements
PRIDE	Planetary Radio Interferometry and Doppler Experiment of the JUICE mission
RFK	Runge-Kutta-Fehlberg
TCM	Trajectory Correction Manoeuvre
VLBI	Very-Long Baseline Interferometry
3GM	Radio science experiment onboard the JUICE spacecraft
p/e	pre-encounter (manoeuvre)
c/u	clean-up (manoeuvre)
c/a	(point of) closest approach

**Latin Symbols**

<b>A</b>	Sampling factor matrix
<b><math>c_i</math></b>	Arc-wise empirical acceleration terms [m/s <sup>2</sup> ]
<b>C</b>	Covariance matrix of the consider parameters
<b><math>C_q</math></b>	Matrix containing the information contribution coefficients $c_q$
<b><math>c_q</math></b>	Information contribution coefficients, [-]
<b><math>\mathcal{C}</math></b>	Transformation function for correcting corrupted a-priori matrices
<b><math>f</math></b>	Numerical value of the transfer factor, [-]
<b><math>\mathbf{f}</math></b>	Factoring vector of the transfer factor
<b>H</b>	Design matrix
<b><math>\mathbf{h}</math></b>	Set of simulated observations
<b><math>h</math></b>	Altitude w.r.t. surface of flyby body, [m]
<b>I</b>	Identity matrix
<b><math>N_{obs}</math></b>	Number of observations
<b><math>\mathbf{p}</math></b>	Set of dynamical system parameters
<b>P</b>	Covariance matrix
<b><math>\mathbf{P}^b</math></b>	Covariance matrix, containing the parameters <i>base</i> covariance
<b><math>\mathbf{P}_0</math></b>	Covariance matrix, containing the parameters a-priori covariance
<b><math>\mathbf{P}_c</math></b>	Covariance matrix, containing the parameters consider covariance
<b><math>\mathbf{q}</math></b>	Set of estimated parameters
<b><math>S</math></b>	Statistical model for the trajectory dispersion
<b><math>\bar{S}</math></b>	Trajectory dispersion sample
<b>S</b>	Sensitivity matrix
<b><math>\mathbf{s}</math></b>	Set of observational model parameters
<b>T</b>	Generic data cut-off time
<b>W</b>	Weight matrix
<b><math>\mathbf{x}</math></b>	State vector of a single body
<b>X</b>	<i>in the context of corrective manoeuvre design</i> : Spacecraft trajectory error, composed of position components ( $\mathbf{x}$ ) and velocity components ( $\mathbf{v}$ )
<b><math>\mathbf{y}</math></b>	State vector of the entire system
<b><math>\dot{\mathbf{y}}</math></b>	Time derivative of the system state vector $\mathbf{y}$
<b><math>z</math></b>	Individual observation from the observation set $\mathbf{h}$
<b><math>\mathcal{P}</math></b>	Covariance matrix, derived from external ephemeris product
<b><math>\hat{\mathbf{x}}</math></b>	State parameter estimate from external ephemeris product
<b><math>l</math></b>	External ephemeris product data cut-off lag

**Greek symbols**

<b><math>\Delta V</math></b>	Impulse per unit of spacecraft mass that is needed to perform a manoeuvre, [m/s]
<b><math>\rho</math></b>	Correlation coefficient, [-]
<b><math>\sigma</math></b>	Uncertainty (1 standard deviation)
<b><math>\Sigma</math></b>	Covariance matrix, reduced to contain only covariance for spacecraft state parameters
<b><math>\Phi</math></b>	State transition matrix

# 1

## Introduction

The JUICE (JUper ICy moons Explorer)<sup>1</sup> mission is an interplanetary space mission designed and run by ESA, which is bound to explore Jupiter and the Jovian system. Its high-level science goals are to study the Jovian system as an archetype of gas giants in and outside our solar system, and to study the Galilean moons with regards to their aptitude to sustain life. After launch in 2023, the spacecraft will perform an exploratory tour of the Jovian system, focusing on the outer three Galilean moons Europa, Ganymede and Callisto. Between 2032 and mid-2034, JUICE will have multiple close encounters of these moons - 2, 7 and 21 flybys of Europa, Ganymede and Callisto, respectively (CReMA 5.0)<sup>2</sup>. The multi-flyby tour phase of the mission is followed by the Ganymede orbital phase, which starts off as a highly eccentric orbit (eccentricities up to 0.6) and ends with a circular orbit at 500 km altitude. Scheduled at a nominal duration of 4 months, the circular orbit phase (GCO-500) constitutes the final phase of the mission. This analysis presented in this work was performed using a slightly different mission profile, which was published with the CReMA 3.2 and which will be described in more detail at a later stage of the report.

The availability of propellant (or  $\Delta V$  budget) is a decisive factor in the design of any space mission (Wertz et al., 1999) and interplanetary missions like JUICE in particular (ESA, 2014). When a shortage of  $\Delta V$  occurs in-mission, it may well force a premature end-of-mission. An excess  $\Delta V$  capacity on the other hand can enable mission extensions and beneficial modifications to the mission profile, such as the case for *e.g.* Cassini Equinox/Solstice (Buffington et al., 2008) and Mars Express (Titov et al., 2016). In the case of the JUICE mission, excess  $\Delta V$  can be used to enable a higher-inclination in the Jovian system or a lower-altitude Ganymede orbit (ESA, 2014), which can both significantly increase scientific value (Grasset et al., 2013). It is thus of great interest to the JUICE mission to investigate options for improving in-mission GNC operations to eventually reduce  $\Delta V$  expenditure throughout the course of the mission.

When discussing in-mission  $\Delta V$  savings, one needs to consider the stochastic manoeuvres, such as trajectory correction manoeuvres (TCMs), which cannot be described deterministically ahead of the mission. They are designed in-mission as part of the Guidance, Navigation & Control (GNC) operations and respond to the observed deviation from the spacecraft's nominal trajectory. In order to ensure the availability of sufficient  $\Delta V$  to conduct TCMs, they have to be considered prior to mission in what is called a statistical  $\Delta V$  analysis (*e.g.* ESOC, 2017–2019; Raofi et al., 2000). For these analyses, the uncertainties associated with the navigational orbit determination (OD) solution are estimated in a covariance analysis, which are then translated into a probability-distribution of the necessary corrective manoeuvres. The  $\Delta V$  expense associated with this distribution dictates the allocation of statistical  $\Delta V$  during the mission design, which makes up a substantial part of the total budget - 20% in the case of the JUICE mission (ESA, 2014). By upgrading the GNC operations and delivering the mission trajectory more efficiently than assumed during the allocation of the budget, in-mission  $\Delta V$  savings can be effectuated. Such GNC enhancements could be achieved by improving the moon state knowledge that is underlying the navigational operations.

Together with ground-based observation, the science return from past missions in the Jovian system has significantly improved the knowledge of the satellites dynamics and has already contributed to large improvements of satellite ephemerides since Galileo (Archinal et al., 2011; Greenberg, 2010; Lainey et al., 2004b).

---

<sup>1</sup><https://sci.esa.int/web/juice>

<sup>2</sup><https://www.cosmos.esa.int/web/spice/spice-for-juice>

Various properties of the Galilean moons and Jupiter itself have been constrained from the successful reconstruction of the system's dynamics. This includes the tidal dissipation in the system (Lainey et al., 2009), which in turn may give insight into the formation and evolution of the Jovian system (Lainey and Tobie, 2005), the moon's interior structure and geophysical processes (e.g. Schubert et al., 2004; Vance et al., 2014) and the possible habitability of the Galilean moon Ganymede (Hussmann et al., 2006). Moon ephemeris improvements have enabled the design and more efficient delivery of subsequent missions (Lynam and Longuski, 2012; Murrow and Jacobson, 1988). While the JUICE mission will profit from these ephemerides, it will also significantly contribute to improving them further. By providing an unprecedented amount of high-accuracy tracking data from Galilean moon flybys (Cappuccio et al., 2020; Grasset et al., 2013), the 3GM radio science instrument onboard of JUICE is expected to allow for an even better reconstruction of the Jovian system dynamics (e.g. Dirx et al., 2017; Fayolle et al., 2022) and Jovian satellites ephemerides.

Considering the wealth of information from a total of 30 moon flybys, significant in-mission ephemeris improvements may be achieved using the 3GM radio science data from early JUICE tour encounters. This is a promising option for improving GNC operations: the in-mission natural body ephemerides products of the sophisticated scientific OD setups can be adopted in the navigation OD. Such practices have been successfully implemented in previous missions (most notably Cassini, see e.g. Bellerose et al., 2016), but they have not yet been studied in the context of JUICE. The goal of this work is to evaluate the applicability and effectiveness of this option to the JUICE mission.

## 1.1. Research Questions

Analysing the use of scientific ephemeris products in the operations of the JUICE mission, this work aims to answer the following research question:

### Leading Research Question

To what extent can in-mission ephemeris updates from the on-board radio science instrument be used in the JUICE GNC operations to relax the constraints on the mission's statistical  $\Delta V$  budget?

which breaks down into the lower level questions:

- Q1.** How can external ephemerides be integrated into the GNC operations of the JUICE mission?
- Q2.** How strongly is the statistical  $\Delta V$  expense of corrective manoeuvres driven by moon state uncertainty?
- Q3.** How does the in-mission uncertainty evolution of the radio science ephemeris solution compare to the moon knowledge improvement from the navigation operations?
- Q4.** To what extent can external ephemeris updates effectuate  $\Delta V$  savings by improving moon knowledge? At what point in time are ephemeris updates most effective?

and the extended research question:

### Extended Research Question

How do JUICE navigation tracking data and 3GM radio science experiment products complement each other and how could such data synergies be exploited?

## 1.2. Report Outline

The core part of the work is documented in the form of a journal paper, which can be found in the following Chapter 2. Elaborate answers to the leading research questions, as well as recommendations for future work are given in Chapter 3. The Appendices provide additional information on the numerical implementation of the JUICE mission trajectory (Appendix A), the verification and validation of the analysis' core components (Appendix B) and complementary figures on some of the solutions that this report will touch upon (Appendix C).

# 2

## Journal Paper

The core methods and results of this work have been documented in a journal paper. The manuscript of the paper is given in this chapter. It adheres to the formatting requirements of the journal.

# JUICE: In-mission synergy of science and navigation ephemeris products - Application to potential benefits for statistical Delta-V expenditure.

Jonas Hener<sup>a</sup>

<sup>a</sup>Department of Aerospace Engineering, Delft University of Technology, Delft, 2629HS, The Netherlands

## Abstract

In the upcoming decade, the JUICE spacecraft will go on a multi-flyby tour of the Jovian system, including over 20 close encounters of the three outer Galilean moons Europa, Ganymede and Callisto. The efficient navigation of the tour depends on the uncertainty of the available moon ephemerides and how well moon state knowledge can be improved during the mission. Excess  $\Delta V$  from improved tour navigation could enable mission enhancements or extensions. This work investigates an enhanced strategy for in-mission moon state knowledge improvement, which integrates high-fidelity moon ephemerides from the 3GM radio science instrument into the navigational operations and examines their impact on the statistical  $\Delta V$  expense of corrective manoeuvres.

A navigation orbit determination (OD) was simulated for the multi-flyby tour of JUICE. It was extended by an interface for high-fidelity moon ephemeris updates. Using an adopted high-fidelity OD setup with a coupled filter configuration, the uncertainty of in-mission ephemeris updates from the radio science data was quantified. Through the interface, these updates were introduced into the navigation OD simulation. By implementing a corrective manoeuvre design scheme, the setup was extended into a simplified statistical  $\Delta V$  analysis and the impact of the in-mission ephemeris updates was mapped onto the  $\Delta V$  cost of corrective manoeuvres.

The comparative analysis of the statistical  $\Delta V$  budgets showed that the adoption of radio science ephemeris products is mostly disadvantageous for the moon knowledge evolution and can not generate significant  $\Delta V$  savings. Even in the limit case, in which the external ephemerides were assumed to constrain moon state knowledge perfectly,  $\Delta V$  savings could only be recorded for corrective manoeuvres on the first flyby of Ganymede and the first and second flyby of Europa. For all subsequent flybys, the nominal navigational OD already constrains the state knowledge of encountered moons so well, that corrective manoeuvre expenditure is mostly driven by trajectory uncertainties of the spacecraft. It was found that the navigational tracking data coverage of the long, early tour arcs is the driving factor for the rapid moon state knowledge improvement in the covariance analysis. Due to concerns about the accurate modelling of the spacecraft along the long tracking arcs, it is unclear to what extent the full-arc coverage of the navigation data can be exploited in practice. Nonetheless, the analysis highlights potential synergies between the navigation and science tracking data, specifically with respect to the comparatively strong signature of Io's dynamics in the navigation data.

## 1. Introduction

The upcoming JUICE mission (JUper ICy moons Explorer)<sup>1</sup> will perform an exploratory tour of the Jovian system, focusing on the outer three Galilean moons Europa, Ganymede and Callisto (Grasset et al. (2013)). The tour phase of the mission will include multiple flybys of these moons. The mission profile adopted for this work was published<sup>2</sup> with version 3.2 of the CReMA (Consolidated Report on the Mission Analysis) and includes flybys of Europa (2), Ganymede (15) and Callisto (12) (see fig. 1). The multi-flyby tour of the Galilean moons is followed by the Ganymede orbital phase. Figure 1 shows the Ganymede orbit phases through 2032 and 2033, starting at a semi-major axis of 8000 km and eccentricities up to 0.6 and ending with a circular orbit at 500 km altitude. Scheduled at a nominal duration of 4 months, the circular orbit phase (GCO-500) constitutes the final phase of the mission.

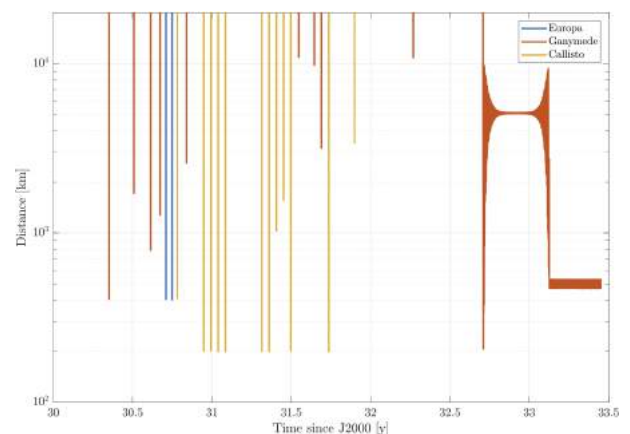


Figure 1: Distance between the JUICE spacecraft and the Galilean moons during the flyby and orbital phases, based on version 3.2 of CReMA. The vertical lines mark satellite flybys and show the associated closest-approach distances. The first flyby of the tour-phase is taken as flyby "2G2". The earlier 1G1 flyby (Ganymede,  $h=400$ km), which marks the insertion into the Jovian system (JOI), is omitted. Figure credit: Dirkx and Lainey (2019).

Email address: jonas.hener@student.tudelft.nl (Jonas Hener)

<sup>1</sup><https://sci.esa.int/web/juice>

<sup>2</sup><https://www.cosmos.esa.int/web/spice/spice-for-juice>

Via the 3GM radio-science payload, JUICE collects high-accuracy radiometric tracking data for reconstructing the spacecraft trajectory, which through the multitude of flybys is tightly coupled to the Galilean moons (Cappuccio et al. (2020)). Through these observables, but also additional data from *e.g.* the PRIDE experiment (angular position, Gurvits et al. (2013)) and the JANUS payload (optical imaging, Della Corte et al. (2014)) or even past and future missions, JUICE is expected to contribute towards more accurate ephemerides of the Galilean moons (Dirkx et al. (2017); Lari and Milani (2019); Fayolle et al. (2022)).

Long-term, high-accuracy ephemerides have significant scientific implications: they can help determine dissipation coefficients (Lainey and Tobie (2005); Lainey et al. (2009)) and enable other insights into the origin (Peale (1999)), long-term thermal-orbital evolution (Husmann and Spohn (2004); Hay et al. (2020)) and the interior processes of natural satellites (Greenberg (2010); Schubert et al. (2004)). High-accuracy ephemerides from (amongst other data types) Cassini tracking data re-opened discussions about the migrations of the Saturnian moons and the evolution of the system as a whole (Lainey et al. (2020)), which has motivated a reconsideration of the mechanisms that drive natural satellite evolution in general (Fuller et al. (2016)).

Moon ephemerides also play a significant role in the practical aspects of the JUICE mission, specifically in the Guidance, Navigation and Control (GNC) operations. In the scope of a navigational orbit determination (OD), moon state knowledge is constantly re-evaluated, such that with each flyby the a-priori moon ephemerides are constrained as closely as possible (Ionasescu et al. (2014)). These navigation OD ephemeris solutions and the high-fidelity ephemeris products generated for scientific purposes differ qualitatively: navigation OD solutions prioritise the determination of the instantaneous spacecraft state around its central body and not necessarily the accurate reconstruction of the long-term satellite dynamics (Bellerose et al. (2016); Boone et al. (2017)). Furthermore, navigation OD is based on different radiometric data, that is typically of lower quality (see table 1, or compare ESOC (2017–2019) and Cappuccio et al. (2020)), and includes fewer observable types. This motivates the notion that there is also a quantitative difference in the two types of moon ephemerides.

In an early study on the Galileo mission (Murrow and Jacobson (1988)), navigation reports of the Cassini mission (Bellerose et al. (2016), Boone et al. (2017)) and more recently in the context of Europa Clipper (Ionasescu et al. (2014)), the uncertainties of moon ephemerides were identified as dominant error sources in the navigation OD solutions. Degraded moon ephemerides increase the uncertainty of the spacecraft state relative to potential flyby bodies, leading to larger target misses during flyby and increased trajectory dispersions downstream of the flyby. This has direct negative consequences on the mission operations, which manifest themselves in less accurate delivery of the designed spacecraft trajectory and larger  $\Delta V$  expense for corrective manoeuvres (*e.g.* Martin-Mur et al. (2014)).

To mitigate the impact of moon ephemeris uncertainty on flyby targeting performance, Bellerose et al. (2016) report the bi-annual implementation of moon ephemeris updates using external ephemeris products during the Cassini "Solstice" mission report. These external ephemerides were generated in more sophisticated setups, estimating on longer tracking arcs and integrating various other data types, such as astrometry from Earth-based observations and the Hubble Space Telescope, radiometric tracking from past missions and even ring occultation data.

This practice could prove an interesting option for the JUICE mission, specifically for  $\Delta V$  savings during the navigation of the multi-flyby tour. Such savings could become important during the consideration of possible mission extensions and enhancements, such as *e.g.* the a lower-altitude option of the GCO-500 phase (ESA (2014)). This work investigates the effectiveness of incorporating high-fidelity ephemeris products from radio science data into the operations of the JUICE mission, specifically with regards to the  $\Delta V$  expense of post-flyby correction manoeuvres. In the process, the characteristics of the navigation tracking data and the efficacy of constraining moon state knowledge from it are analysed.

For this investigation, a statistical  $\Delta V$  analysis was conducted. The methodological setup of the analysis is summarised in fig. 2. It consists of two blocks: a navigation OD framework, which models the knowledge of the JUICE-Jovian system via a covariance analysis (section 2), and a framework for the computation of the  $\Delta V$  expense of corrective manoeuvres (section 3). An interface for simulating the use of external ephemeris products was added to the navigation OD framework and the coupled ephemeris covariance analysis from Fayolle et al. (2022) was adopted as a reference for high-fidelity moon ephemerides from JUICE (section 4).

The impact of external ephemeris updates is examined following a comparative approach. Using the nominal (*i.e.* update-free) Navigation OD, baseline values are established for quantities of interest, such as the formal error evolution and the statistical manoeuvre cost. By introducing external ephemeris updates (and other parameters), the Navigation OD is then modified, the quantities of interest are re-computed and the impact of the modifications on these quantities is examined. The comparative approach allows for several simplifying assumptions in the setup of the statistical  $\Delta V$  analysis, so as long as the simplifications affect the baseline and modified cases to the same extent.

Simulations in this work rely on the numerical modelling and estimation capabilities of the *Tudat* software<sup>3</sup>, developed at the Astrodynamics & Space Missions department of the Delft University of Technology.

## 2. Methodology (I) - Orbit Determination for Navigation

The analysis setup (fig. 2) includes the simulation of a navigational orbit determination (hereafter "Nav OD setup"). Its main purpose is to provide and update the covariance of the

<sup>3</sup>Documentation: <https://tudat-space.readthedocs.io>

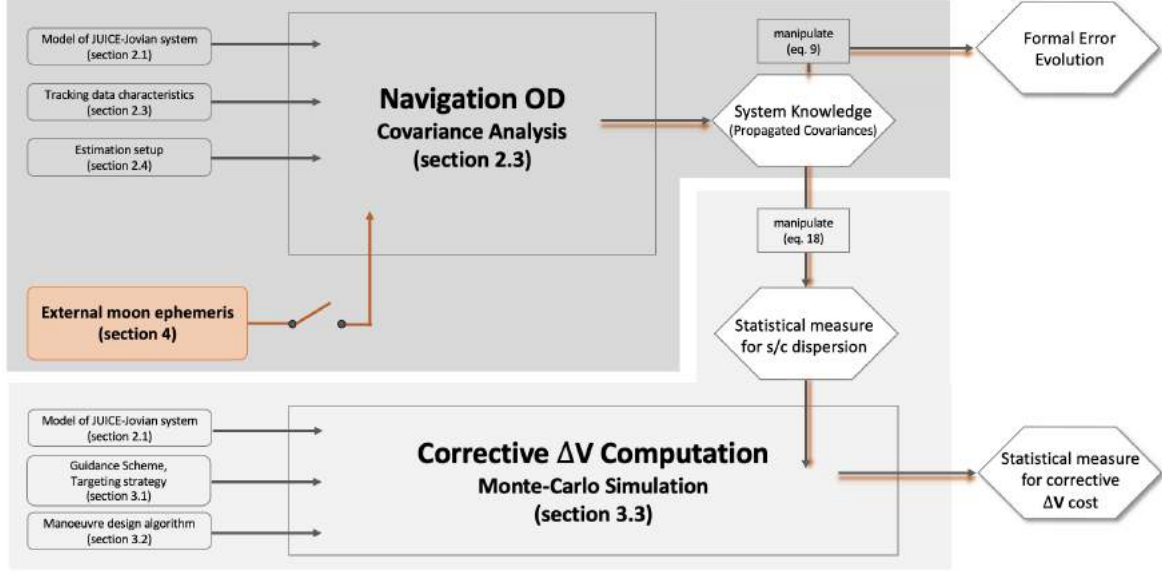


Figure 2: Schematic overview of the methodological setup of the comparative statistical  $\Delta V$  analysis. Elements with round edges denote settings and design decisions. Box-like elements represent (an assembly of) implemented functions, that facilitate the computation of relevant results. Results are framed by the hexagonal shapes. The interface for external ephemeris updates is highlighted in orange. The orange trace symbolises the flow of external moon ephemeris knowledge, if introduced via the update interface. When applicable, reference is given to the methodology section, in which the given aspect is presented in more detail.

orbit determination, which constitutes the expected statistical knowledge of the dynamical system for navigation and lays the foundation for the design of corrective manoeuvres (section 3). In order to make the analysis as realistic - and therefore mission-relevant - as possible, the tool was modelled after the Navigation OD setup from ESOC (2017–2019). Simplifications and significant deviations from this reference will be emphasised throughout this section. Furthermore, the results produced by our navigation OD implementation, and specifically the moon state covariance evolution, to which the comparative analysis of this work is most sensitive, were validated using the covariance data from the reference OD.

In the context of the statistical  $\Delta V$  analysis presented in this paper, the Nav OD setup serves as a tool for predicting the quality of the system knowledge during the JUICE multi-flyby phase. The implementation of such a tool requires the dynamical modelling of the JUICE spacecraft in the Jovian system, which are discussed in section 2.1. Section 2.2 introduces the concept of covariance analysis, which is used to compute the system knowledge quality the is expected from the Nav OD setup. Covariance analyses rely on simulated observation data, the characteristics of which are given in section 2.3. The Nav OD filter setup and the choice of estimated parameters is presented in section 2.4. Section 2.5 shows how the Nav OD setup was extended by two "optional" features, which aim to enhance the analysis.

### 2.1. Modelling the JUICE-Jovian System

For the description of the system dynamics, the system state vector is denoted by  $\mathbf{y}$ . It is propagated numerically from the initial time  $t_0$  along arc  $i$ , using

$$\dot{\mathbf{y}} = \mathbf{f}_i(\mathbf{y}, \mathbf{p}, t) \quad (1)$$

where  $\mathbf{p}$  denotes parameters of the system dynamics and  $\mathbf{f}_i$  is the dynamical model of the JUICE-Jovian system, which will be introduced hereafter. State transition matrices  $\Phi(t, t_0)$  and sensitivity matrix  $\mathbf{S}(t)$ , which are defined as

$$\Phi(t, t_0) = \frac{\partial \mathbf{y}(t)}{\partial \mathbf{y}(t_0)} \quad (2)$$

$$\mathbf{S}(t) = \frac{\partial \mathbf{y}(t)}{\partial \mathbf{p}} \quad (3)$$

are numerically solved for alongside the state on each arc.

The dynamical model employed in this work primarily serves the covariance analysis of the Navigation OD (section 2.2) and is later on also used for the manoeuvre design (section 3.2). Both applications do not require the dynamical model to be of great accuracy. The focus is on capturing the gravitational interaction between Jupiter and the Galilean moons, as well as an accurate modelling of the forces acting on the JUICE probe. Smaller Jovian satellites as well as planets outside the Jovian system are excluded from the dynamical model.

The translational states of the JUICE probe (sc) and all Galilean moons ( $j = 1, 2, 3, 4$ ) are propagated w.r.t. the centre of mass of Jupiter, with the orientation fixed w.r.t. the ICRF (J2000). The system state vector  $\mathbf{y}$  thus becomes

$$\mathbf{y} = \begin{pmatrix} \mathbf{x}_{sc} \\ \mathbf{x}_1 \\ \dots \\ \mathbf{x}_4 \end{pmatrix} \quad (4)$$

Initial states and system parameters for the natural bodies were obtained from the latest IMCCE ephemerides NOE-5-2021<sup>4</sup>, solar system ephemeris DE432 (Folkner et al. (2014)) was used for the position of Sun. Rotational states of the moons are not propagated, but modelled to be tidally locked with the planet (as is done by e.g. Lainey et al. (2004a)), which results in a synchronous rotation of the satellites w.r.t. their orbit around Jupiter. When propagating the dynamics of the Galilean moons, the following accelerations were taken into account:

- the mutual spherical harmonic acceleration between Jupiter and each Galilean moon  $j$  - in this context Jupiter's gravity field was expanded up to degree 8 and order 0, gravity fields of the Galilean moons were considered to degree and order 2.
- the mutual spherical harmonic accelerations between all Galilean moons, with their gravity fields expanded up to degree and order 2.

Matching the mission profile disseminated in the spice kernels (Acton Jr (1996)) for the JUICE CReMA 3.2, the trajectory of the JUICE probe was simulated for selected arcs of the multi-flyby tour. The selection was limited to arcs including a close flyby ( $h < 20000$  km) of a Galilean moon (fig. 1). Deep space manoeuvres (DSMs) were omitted from the simulated arcs. In order to preserve the relevance of the numerically modelled spacecraft trajectories, the arcs were constrained such that the simulated flybys meet the flyby conditions specified in the mission profile. An exemplary illustration of a simulated JUICE arc and the milestones along the arc is given by fig. 3.

When propagating the dynamics of the spacecraft during arc  $i$ , that contains a flyby with moon  $k$ , the following accelerations were taken into account:

- the gravitational acceleration of Jupiter's gravity field, up to degree 2 and order 0.
- the gravitational acceleration of the encountered moon  $k$ , considering a gravity field up to degree and order 2.
- the point-mass acceleration of all other Galilean moons.
- acceleration by non-conservative solar radiation pressure, implemented via cannonball model.
- empirical acceleration, representing execution errors of unmodelled manoeuvres - constant (in TNW frame) on 10 h sub-arcs

Simulations were done by numerical integration of the described dynamical model. The numerical integration was performed using a Runge-Kutta-Fehlberg method (RKF78), which allows for variable step-size control. At an absolute (step-wise) tolerance of  $10^{-10}$  m and a maximum step size of 1000 s, it was tuned to ensure consistency between nominal and simulated flyby geometry and timing on each arc.

## 2.2. Covariance Analysis

Given an orbit determination setup, a covariance analysis can quantify the extent to which a-priori system knowledge and the available observations enable the estimation of the system parameters. It is therefore an important component of any OD solution: knowledge of the estimate's covariance allows for the evaluation of the uncertainties of the estimated parameter values, which is crucial for informed operational decision making, and furthermore enables the regularisation of subsequent estimates (a-priori strategy, section 2.4).

Covariance analyses can also be conducted without producing a real parameter estimate and can thus be applied to OD problems for which actual system observations are not yet available. This can be exploited for simulating the performance of future OD setups in the context of the JUICE mission, such as the Navigational OD setup (section 2.4) and the high-fidelity OD setup (section 4.1, or see Fayolle et al. (2022)).

This practice requires several limiting assumptions. Firstly, the dynamical model is taken as a perfect description of the system dynamics. Secondly, it is assumed that any sort of systemic measurement errors are accounted for in the observational model. The quality of the resulting system observations can then be characterised as uncorrelated Gaussian noise. Note that noise levels and other parameter values that are used to characterise the performance of the observational model have to be assumed and cannot be validated until the mission is operational.

Given these assumptions, a set of artificial observations can be modelled, where  $\mathbf{h}(T)$  denotes the set of all modelled observations up to time  $T$ . A design matrix  $\mathbf{H}(T)$  can be computed, which contains the sensitivity of these observations to the estimatable parameters  $\mathbf{q}$ :

$$\mathbf{H}(T) = \frac{\partial \mathbf{h}(T)}{\partial \mathbf{q}} \quad (5)$$

$$\mathbf{q} = [\mathbf{y}_0; \mathbf{p}; \mathbf{s}] \quad (6)$$

where  $\mathbf{y}_0$  denotes the initial system state (eq. (4)),  $\mathbf{p}$  and  $\mathbf{s}$  are vectors containing parameters of the dynamical and observational models, respectively. The covariance matrix of the estimate of  $\mathbf{q}$ , considering simulated observations up to time  $T$ , is denoted  $\mathbf{P}_{\mathbf{q}\mathbf{q}}(T)$  and is computed as<sup>5</sup>

$$\mathbf{P}_{\mathbf{q}\mathbf{q}}(T) = \left( \mathbf{P}_{\mathbf{q}\mathbf{q},0}^{-1} + (\mathbf{H}^T(T)\mathbf{W}(T)\mathbf{H}(T)) \right)^{-1} \quad (7)$$

where  $\mathbf{P}_{\mathbf{q}\mathbf{q},0}$  denotes the a-priori covariance matrix of the parameter set  $\mathbf{q}$  and the weight matrix  $\mathbf{W}(T)$ , with  $W_{ii} = \sigma_{h,i}^{-2}$ , accounts for the expected quality of the each individual measurement.

Using eq. (8) a figure of merit can be computed, which indicates how much the estimate of a given parameter  $q$  relies on the a-priori knowledge (Floberghagen (2001)):

<sup>4</sup><https://ftp.imcce.fr/pub/ephem/satel/NOE/JUPITER/>

<sup>5</sup>For the inversion of the right hand side, we scale the estimated parameters such that the partial derivatives in  $\mathbf{H}$  are in the range [-1, 1].

$$\mathbf{C}_q = \mathbf{I} - \mathbf{P}_{qq} \mathbf{P}_{qq,0}^{-1} \quad (8)$$

where  $\mathbf{I}$  is the identity matrix. Coefficients  $c_q$  are taken from the diagonal of  $\mathbf{C}_q$ . A coefficient value equal to 1 indicates that the parameter's estimate relies entirely on the observations, while a value of 0 shows that it is fully based on a-priori knowledge.

Taking the square-root of the variances on the diagonal of a post-fit covariance matrix  $\mathbf{P}_{qq}$ , one obtains the so-called formal error, that is the expected standard deviation on the estimate of each parameter  $q$ :

$$\sigma_q = \sqrt{\mathbf{P}_{q,q}} \quad (9)$$

The formal error must be considered a statistical quantity, which is based on a set of idealising assumptions. In the absence of systemic biases in dynamical or observational models, formal errors  $\sigma_q$  scale with  $1/\sqrt{N_{obs}}$ , reflecting the notion that the associated parameter estimate can always be improved, if only a large enough amount of observations is provided. An assessment of the **true** error can only be obtained by analysis of the final distribution of the measurement residuals and by solving for systemic errors (Montenbruck and Gill (2000)). Jones et al. (2014) indicate that true error is typically 2-3 times larger than the formal errors obtained from a classic covariance analysis.

In order to capture the effect of some systemic biases in the observational model the covariance analysis can be extended by introducing so-called consider parameters. The uncertainties associated with the consider parameters are mapped onto the post-fit covariance matrix  $\mathbf{P}_{qq}$  as follows (Montenbruck and Gill (2000))

$$\mathbf{P}_{c,qq} = \mathbf{P}_{qq} + (\mathbf{P}_{qq} \mathbf{H}^T \mathbf{W}) (\mathbf{H}_c \mathbf{C} \mathbf{H}_c^T) (\mathbf{P}_{qq} \mathbf{H}^T \mathbf{W})^T \quad (10)$$

where  $\mathbf{C}$  is the matrix containing the covariances associated with the consider parameters and  $\mathbf{H}_c$  is the design matrix relating consider parameters to the observations (analogous to eq. (7)). The values obtained from the diagonal of  $\mathbf{P}_{c,qq}$  (analogous to eq. (9)) give the consider errors. By accounting for systemic errors, the contribution of the consider terms establishes a limit to the attainable solution accuracy, giving a more realistic estimate of the true error (Montenbruck and Gill (2000)).

Using the state transition and sensitivity matrices from eqs. (2) and (3), time-variant components of covariance matrices can be propagated from a reference epoch  $t_0$  to any other epoch  $t$ :

$$\mathbf{P}_{yy}^{(t_0 \rightarrow t)} = [\Phi(t, t_0); \mathbf{S}(t, t_0)] \mathbf{P}_{qq}^{t_0} [\Phi(t, t_0); \mathbf{S}(t, t_0)]^T \quad (11)$$

where  $\mathbf{P}_{yy}$  denotes covariance of the time-variant system state vector  $\mathbf{y}$ . This is equally applicable to covariance which include consider contributions ( $\mathbf{P}_{c,qq}$ ).

### 2.3. Tracking Data

The Navigation OD of the JUICE spacecraft relies largely on radiometric two-way range and range-rate (Doppler) measurements from Earth-based tracking stations. These data types are highly effective for directly constraining the knowledge of the spacecraft state. Adopting the radiometric data characteristics from ESOC (2017–2019), Doppler data was modelled with 80  $\mu\text{m/s}$  white noise at an integration time of 1 hour, while range observables were taken at a noise level of 10 m at the same cadence (summarized in table 1). Additionally, a systemic range observation bias of 2 m was implemented as consider parameter. Occultation and elevation constraints at  $\epsilon < 10$  deg were implemented w.r.t. to the ground station in Malargüe (Argentina), which - as of now - is the only station of the European Space Tracking network (ESTRACK) to support both the X- and Ka-band tracking capabilities of JUICE. For this station, a systemic position bias of 30 cm/axis was modelled via the set of consider parameter (see section 2.4).

The JUICE Navigation OD combines the radiometric data types with optical navigation images (OpNavs) obtained from an onboard navigation camera (NavCam). This data type provides additional information of the relative state of spacecraft w.r.t. observed body. It is used primarily to measure and constrain flyby moon position priori to close encounters, but also to balance the data set by direct observations of Io and Europa. The detailed planning of OpNavs requires a complicated trade-off of observation priorities, geometry and operational constraints and results in a dedicated OpNavs schedule. Implementing this schedule, alongside the more difficult modelling of the NavCam properties, was considered outside the scope of this work and consequently OpNavs were not included in the analysis. From this simplification, the estimation of larger moon uncertainty levels can be expected, affecting especially Io and Europa which cannot be well constrained from the spacecraft tracking data alone coupled to the spacecraft dynamics (see also section 5.1).

### 2.4. Estimation Setup

The characteristics of the Navigation OD estimation setup, comprised of the choice of estimated parameters, a-priori strategy and filter type, are modelled closely after the reference OD setup (ESOC (2017–2019)). One significant difference between reference and implementation is the filter type. The sequential filter setup, that the reference setup applies arc-by-arc, has obvious advantages in operational applications. These advantages do not apply if the estimation tool is only to simulate OD solutions for the sake of a subsequent covariance analysis. The sequential filter is thus replaced by an arc-wise batch least-squares algorithm. The post-fit uncertainties from the batch inversion and the instantaneous knowledge from the sequential filter will evolve differently along the arc (section 5.1, e.g. fig. 5a). During computation of the system state uncertainties for corrective manoeuvre design (section 3), the batch inversions are implemented to follow the same operational data cut-off times (see fig. 3) as the sequential filter, such that the filter type has no implication on the outcome of the analysis.

In an arc-wise batch algorithm, the orbit determination is solved on an arc-by-arc basis. A new parameter estimate  $\hat{\mathbf{q}}$  is generated w.r.t. the initial epoch  $t_0$  of every arc  $i$ . For this estimate, the filter fuses a batch of measurement data from the given arc  $i$  with a-priori parameter information.

The implemented setup estimates the following parameters:

- arc-wise spacecraft initial states  $\mathbf{x}_{sc}(t_0^i)$ , with *base* a-priori uncertainty of 15 km on each Cartesian position component and 10 cm/s on each Cartesian velocity component.
- arc-wise initial states of Galilean moons  $\mathbf{x}_j(t_0^i)$  ( $j = 1, 2, 3, 4$ ). The *base* a-priori position uncertainty was taken at 15 km along the three TNW directions. Velocity uncertainty components of the *base* a-priori were set to the differences between the latest IMCCE and JPL ephemerides ephemerides NOE-5-2021<sup>6</sup> and JUP365<sup>7</sup>, respectively.
- empirical acceleration terms  $\mathbf{c}_i$  (one per TNW component) on the spacecraft, estimated at a constant value per 10 hour sub-arc, with *base* a-priori set to  $10^{-8} \text{ m} \cdot \text{s}^{-2}$ .

and the following parameters were introduced as consider parameters

- bias for range observables, with uncertainty fixed at 2 m.
- biases for ground station position, with uncertainty fixed at 0.3 m per axis.

The covariance  $\mathbf{P}_{\mathbf{q}\mathbf{q}}^i$ , that is associated with the parameter estimate  $\hat{\mathbf{q}}$  from arc  $i$ , is used to derive an improved a-priori knowledge for the following arc  $i + 1$ :

- a-priori covariance of the spacecraft state is reset to the *base* covariance values ( $\mathbf{P}_{sc}^b$ ) and is fully de-correlated from all other parameters. This practice mitigates the build-up of unrealistically strong correlations over the course of the flyby-tour, which in reality is prevented by dynamical and observational system noise (ESOC (2017–2019)).
- a-priori covariance of the moon states is obtained from taking the fully correlated covariance matrix of the moons' state estimate ( $\mathbf{P}_m^i$ ) from  $\mathbf{P}_{\mathbf{q}\mathbf{q}}^i$  and mapping it forward to the reference epoch of the current arc ( $t_0^{i+1}$ ), while constraining it by its *base* covariance  $\mathbf{P}_m^b$ .
- a-priori covariance of the empirical acceleration terms  $\mathbf{c}_i$  on each sub-arc is taken at its *base* a-priori covariance.

The a-priori strategy outlined for the moon state knowledge requires a more detailed description. First, the post-fit moon state covariance from arc  $i$  is mapped to the initial epoch of the subsequent arc  $i+1$ . Using the propagation method given by eq. (11), the mapped covariance matrix  $\mathbf{P}_m^{(i \rightarrow i+1)}$  is obtained. Because

$\mathbf{P}_m^{(i \rightarrow i+1)}$  relies purely on the propagated covariance of a previously obtained local parameter estimate, it may contain unrealistically large uncertainties in some moon state components which exceed the envelope of the long-term ephemeris solution from Lainey et al. (2004b). In order to prevent this, the mapped covariance is regularised, by combining it with the *base* moon covariance  $\mathbf{P}_m^{b,i}$  as follows:

$$(\mathbf{P}_{m,0}^{i+1})^{-1} = (\mathbf{P}_m^{b,i})^{-1} + (\mathbf{P}_m^{(i \rightarrow i+1)})^{-1} \quad (12)$$

On the first arc  $i=0$ , the a-priori strategy is initialised with the *base* a-priori moon covariance  $\mathbf{P}_{m,0}^0 = \mathbf{P}_m^{b,0}$ .

Besides the filter type, there are two other significant differences between reference and implemented OD setup. Firstly, OpNavs-related parameters do not appear in the implemented setup, which is the logical consequence of omitting the optical navigation data type from the analysis (section 2.3). Secondly, errors in the manoeuvre execution (mechanisation errors) are not estimated, because a valid estimation of the TCM mechanisation errors requires a much more complicated setup, in which the statistical TCM analysis is coupled with the Navigation OD setup. The effects of the latter will be addressed in section 3.1 under the aspect of Control.

### 2.5. Extensions to the Orbit Determination Setup

The locally implemented Nav OD setup was extended by optional features, which are not part of the reference setup (ESOC (2017–2019)). These features include a mode in which gravity-related parameters are estimated. For this setting,  $\mathbf{q}$  was extended by the following parameters - the a-priori covariances for these parameters were adopted from Schubert et al. (2004):

- gravitational parameter  $\mu$  of each Galilean moon.
- coefficients  $C_{2,0}$  and  $C_{2,2}$  of the SH gravity field expansion for each Galilean moon.

The second feature addresses the limiting assumption of perfect dynamical and observational models, on which the covariance analysis is based. Due to *e.g.* mismodelling of manoeuvres and other non-conservative forces, it will in practice not be possible to formulate an perfectly accurate and consistent description of the spacecraft dynamics over the full length of the tracking arcs. System state knowledge improvements are thus likely to be overestimated (*e.g.* Jones et al. (2014)), especially those concerning the state of the encountered moon. In order to contain this overestimation and to mitigate its effect on the moon state evolution along the multi-flyby tour, an empirical penalty on the transfer of moon state knowledge between arcs is introduced.<sup>8</sup> It acts as an optional extension of the a-priori strategy: the propagated post-fit covariance  $\mathbf{P}_m^{(i \rightarrow i+1)}$  is penalised, and the penalised moon covariance  $\mathbf{P}_m^*$  is then combined with the *base* covariance (eq. (12)) to form the a-priori

<sup>8</sup>The adoption of the empirical penalty as well as the value of  $f = 3$  is the result of personal correspondence with Marco Zannoni, who referred to his experience with navigational practices employed during Cassini's multi-flyby tour (Bellerose et al. (2018)).

<sup>6</sup><https://ftp.imcce.fr/pub/ephem/satel/NOE/JUPITER/>

<sup>7</sup><https://ssd.jpl.nasa.gov/sats/ephem/>

covariance for the next arc. By only penalising the propagated covariance of the previously encountered moon  $k$ , this implementation of the transfer factor focuses at containing the local uncertainty improvements that are achieved through the previous flyby. The exact implementation of the penalty is shown in eq. (13):

$$\mathbf{P}_m^* = \mathbf{f} \mathbf{P}_m^{(i \rightarrow i+1)} \mathbf{f}^T \quad (13)$$

with  $\mathbf{f} = \begin{bmatrix} \mathbf{0}_{1 \times (k-1)6}, & \sqrt{f}_{1 \times 6}, & \mathbf{0}_{1 \times (4-k)6} \end{bmatrix}$

### 3. Methodology (II) - GNC Operations and Statistical $\Delta V$

This section addresses the second block of the analysis setup (fig. 2), that is the computation of the  $\Delta V$  expense for corrective manoeuvres. The navigation OD accuracy and the statistical  $\Delta V$  cost of corrective manoeuvres are linked through the way they interact during GNC operations. Section 3.1 discusses selected GNC aspects, focusing on the interplay of Navigation OD and guidance schemes. The design and computation of trajectory correction manoeuvres is addressed in section 3.2. Section 3.3 gives a more detailed introduction to the concept of statistical  $\Delta V$  budgets and describes how they are computed in this analysis.

#### 3.1. GNC Operations

GNC is the interplay of Guidance, Navigation and Control operations, which together are responsible for keeping the spacecraft on course throughout the mission. Guidance operations determine the trajectory correction manoeuvres (TCMs) required to deliver the pre-defined trajectory. Figure 3 shows the a typical guidance strategy for a satellite flyby arc, using a "targeting" and "pre-encounter" (p/e) TCM to reduce flyby target misses and a "clean-up" (c/u) TCM for correcting trajectory errors downstream of the flyby. The JUICE mission adopts this common guidance strategy, placing the p/e and c/u manoeuvres 3 days before (upstream) and after (downstream) closest approach (c/a), respectively (ESOC (2017–2019)).

Typically, the p/e and c/u manoeuvres are purely stochastic manoeuvres, meaning that they do not include any pre-defined trajectory shaping components, in which case their expected vectorial magnitude is  $\mathbf{0}$ . Their design is only driven by the stochastic deviation of the spacecraft state w.r.t. its nominal trajectory, an estimate of which is provided by the navigation operations.

Navigation operations use a dedicated OD setup (section 2) to generate estimates of the system state (OD solutions), which consist of an estimate of all relevant system parameters and the associated covariances ( $\hat{\mathbf{q}}$  and  $\mathbf{P}_{qq}$  in section 2.2). From these, a best estimate of the trajectory error can be derived, which is then used for TCM design. In the case of the JUICE mission, the generation of OD solutions for p/e and c/u manoeuvre design requires at data cut-off (DCO) 2 days prior to the given manoeuvre. This buffer accommodates data download, orbit determination, manoeuvre design and command upload.

Figure 4 schematically illustrates the interplay of navigation and guidance operations around a flyby event. Point B

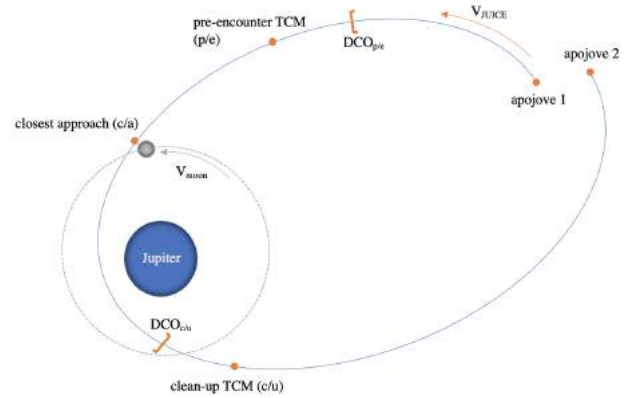


Figure 3: Typical three-maneuvre guidance scheme for flyby arcs. DCO denotes the Data Cut-off for the design of the subsequent manoeuvre. The "targeting" TCM, typically at apojoive, is not relevant for this analysis and therefore omitted from the figure.)

marks the reference state of the spacecraft w.r.t. the flyby body. Coloured elements represent the OD solutions that the navigation OD provides for the design of the scheduled TCM manoeuvres - the "X" marks the current best estimate of the spacecraft state, while the surrounding ellipse symbolises the covariance associated with the estimate. In the simple, exact targeting strategy that is adopted in this analysis, each TCM is designed such that the estimated trajectory error (difference between point B and the current best estimate of the spacecraft state) is eliminated. However, the uncertainty of the spacecraft state estimate on which the TCM design is based, is not eliminated - it is merely "re-centred" on the nominal B-plane condition "B". The uncertainty will evolve alongside the system evolution and will manifest itself in subsequent spacecraft state estimates as the "new" error, which is to be corrected by the following manoeuvre.

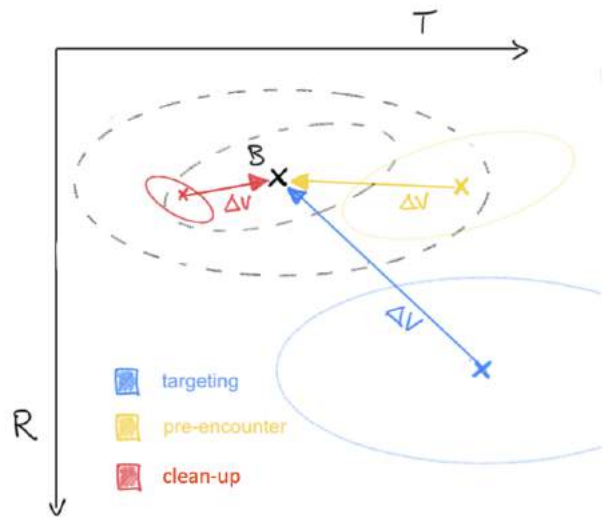


Figure 4: Schematic depiction of the TCM sequence in the B-plane, showing navigation OD solutions and manoeuvre  $\Delta V$  designs. The B point indicates the nominal target condition in the B-plane.

By introducing *trajectory dispersion* as a statistical abstraction for describing the behaviour of individual stochastic errors as a whole, it is possible to make universal observations about their occurrence and to model them. Figure 4 indicates that the trajectory dispersion is related to the covariance of the system state estimate  $\mathbf{P}_{yy}$ , on which the previous TCM was designed. It can be noted that - while trajectory dispersion upstream of the flyby is driven by the spacecraft trajectory uncertainty - moon ephemeris uncertainties make a more substantial contribution to downstream dispersion. Consequently, moon ephemeris improvements will predominantly affect the corrective manoeuvre after flyby. To show to a first degree the effect of external moon ephemeris updates on GNC operations and the statistical  $\Delta V$  budget, it is thus sufficient for this analysis to examine their impact on the clean-up manoeuvre - targeting pre-encounter TCMs are omitted.

The GNC aspect of Control is concerned with the effective execution of guidance commands and entails amongst others the issue of manoeuvre execution errors, which have been omitted from this analysis (section 2.4). These errors are typically modelled to grow proportionally with the manoeuvre magnitude (e.g. Wagner (2014)) and degrade the OD solution, which in turn leads to larger correction manoeuvres downstream of the manoeuvre (Roth et al. (2003)). Reducing the magnitude of a given manoeuvre - by for example an improved moon ephemeris - therefore has a small secondary effect on the downstream system state knowledge and subsequent corrective manoeuvres. As a consequence of the omission of the manoeuvre errors and the aspect of control as a whole, this effect will not be reproduced by the analysis in this work.

### 3.2. Corrective Manoeuvre Design

Out of the myriad of TCM targeting strategies (D’Amario et al. (1981); Wolf and Smith (1995); Buffington et al. (2005)), the next-body B-plane targeting is a common option (e.g. Cho et al. (2012)). It prescribes that every TCM targets the reference conditions of the upcoming flyby, mapped onto the B-plane of the flyby body. In some cases, this can give rise to large c/u manoeuvres, in which case targeting the reference position at upcoming apocentre is a suitable alternative (ESOC (2017–2019)). Advanced targeting strategies, such as the ones used by ESOC (2017–2019) use optimisation algorithms over multiple arcs and (biased) flyby targets.

It should be noted that for the comparative analysis of statistical  $\Delta V$  budgets (see section 3.3), the targeting strategy is not required to reproduce the exact mission-relevant manoeuvres. Instead, its function is to map spacecraft trajectory errors to c/u manoeuvre designs of a given  $\Delta V$  cost. Therefore, a simple targeting strategy is chosen, in which c/u manoeuvres target the reference position at upcoming apocentre. This option is easily implemented and compatible with the arc-wise simulation setup of the Navigation OD (sections 2.1 and 2.4).

The actual computation of the TCM manoeuvres is based on the numerical implementation of the JUICE-Jovian system dynamics, which was introduced in section 2.1. Additionally, manoeuvres are modelled as perfectly instantaneous changes of the

spacecraft velocity. Given this system model, an two-stage algorithm was defined for the computation of the c/u manoeuvre:

Letting  $\Delta \mathbf{X}(t_{c/u})$  denote the estimated trajectory error (deviation of estimated spacecraft trajectory from the reference trajectory), which the c/u manoeuvre is supposed to correct, then

**stage 1:** the velocity component  $\Delta \mathbf{v}(t_{c/u})$  of the trajectory error can be corrected by an impulsive shot of  $-\Delta \mathbf{v}(t_{c/u})$ , which constitutes the first component of the c/u manoeuvre:

$$\Delta \mathbf{V}_1 = -\Delta \mathbf{v}(t_{c/u}) \quad (14)$$

**stage 2 (a):** after the original trajectory deviation has been partially correction by  $\Delta \mathbf{V}_1$ , the propagation of the residual deviation  $\Delta \mathbf{X}'(t_{c/u})$  still gives a trajectory error  $\Delta \mathbf{X}'(t_{apo})$  at the target epoch. The propagation can be expressed by use of the state transition matrix  $\Phi$  (eq. (2)):

$$\Delta \mathbf{X}'(t_{apo}) = \Phi(t_{apo}, t_{c/u}) \Delta \mathbf{X}'(t_{c/u}) \quad (15)$$

**stage 2 (b):** a second manoeuvre component  $\Delta \mathbf{V}_2$  is needed, which mitigates the remaining target position error  $\Delta \mathbf{X}'(t_{apo})$ . A single instantaneous  $\Delta V$  change cannot be used to target a full (six-component) spacecraft state; the chosen scheme targets the reference *position* at apocentre. The manoeuvre design therefore only considers the position components  $\Delta \mathbf{x}'(t_{c/u})$  of the residual spacecraft trajectory error at target epoch. Using the partial derivatives of  $\Phi(t_{apo}, t_{c/u})$ , which relate velocity changes at manoeuvre time to position changes at target time ( $\partial \mathbf{v} / \partial \mathbf{x}$ ),  $\Delta \mathbf{x}'(t_{apo})$  can be corrected by

$$\Delta \mathbf{V}_2 = \Phi_{\partial \mathbf{v} / \partial \mathbf{x}}(t_{apo}, t_{c/u})^{-1} \Delta \mathbf{x}'(t_{apo}) \quad (16)$$

The full corrective manoeuvre is obtained by superimposing the two manoeuvre components and executing it at c/u manoeuvre time:

$$\Delta \mathbf{V}_{c/u} = \Delta \mathbf{V}_1 + \Delta \mathbf{V}_2 \quad (17)$$

Note that the computation of the second manoeuvre component in eq. (16) is based on a linear mapping between times  $t_{c/u}$  and  $t_{apo}$  and does not result in a perfectly accurate target hit. For cases in which the linearisation error becomes significant, the computation of  $\Delta \mathbf{V}_2$  can be extended to an iterative scheme, terminated by a certain target miss threshold. This was however not necessary, since linearisation errors remained negligible in all manoeuvre computations throughout the analysis. It is noted that the implemented manoeuvre computation algorithm as described above does not provide any means to constrain the velocity error components  $\Delta \mathbf{x}'(t_{apo})$  at the target. Post-correction velocity residuals were monitored and comparison with the pre-correction velocity errors shows, that the position-targeting scheme has the natural tendency to mitigate deviations in the velocity components, too. It is thus concluded that this limitation does not affect the analysis outcome - it does not impose any unintended stress on the downstream spacecraft guidance and the unmodelled contributions to the statistical  $\Delta V$  budget (i.e. targeting, pre-encounter TCMs).

### 3.3. Statistical $\Delta V$ Budgets

Statistical  $\Delta V$  analyses are performed in order to allocate sufficient resources to the performance of statistical TCMs. Its main outputs are the expected value and 99<sup>th</sup> percentile of the mission's statistical  $\Delta V$  expense. The most common method used for computing statistical  $\Delta V$  budgets, which has been found in numerous published studies (*e.g.* Martin-Mur et al. (2014); Raofi et al. (2000); Weeks (2008)) and which is adopted for this work, is the Monte-Carlo (MC) analysis.

For the MC analysis, trajectory errors are simulated by drawing statistically representative samples of the spacecraft dispersion, and a corrective manoeuvre is designed for each. The manoeuvre cost ( $\Delta V$ ) is stored for the correction of all dispersion samples. For a large enough amount of MC samples, the resulting population of  $\Delta V$  values is representative of the TCMs' statistical  $\Delta V$  expense, which can thus be characterised using the statistical properties of the  $\Delta V$  population.

Depending on the choice of targeting scheme and manoeuvre execution error model, the MC analysis would require an iterative procedure over the entire length of the considered mission phase. The setup of this analysis, which uses a simple targeting algorithm (section 3.2) and assumes perfect execution of the manoeuvres, can perform the MC analysis for each considered manoeuvre independently, arc by arc.

Recalling (from section 3.1, fig. 4) the connection between spacecraft state uncertainty during TCM design and dispersion downstream of that manoeuvre, an algorithm for the creation of dispersion samples can be defined. This algorithm, applied to generating dispersion samples for the computation of the clean-up TCM, is presented below. Note that the aforementioned setup choices allow the algorithm to be applied to the c/u manoeuvre of each flyby-arc separately.

1. The uncertainty of the system state estimate at p/e design, which is based on data cut-off time  $\text{DCO}_{p/e}$ , is propagated to c/u manoeuvre time. Using the propagation method given by eq. (11), the covariance matrix

$$\mathbf{P}_{yy}^{(t_0 \rightarrow t_{c/u})}(\text{DCO}_{p/e}) \quad (18)$$

is obtained.

2. The spacecraft state variance/covariance entries of the matrix in eq. (18) constitute the trajectory dispersion, capturing the effects of uncertainties in spacecraft and flyby body state. This measure, which is a 6x6 covariance matrix, is denoted  $\Sigma$ .
3. Using  $\Sigma$ , the trajectory dispersion at c/u manoeuvre time can be modelled using a multi-variate normal distribution

$$S \sim N_6(\mathbf{0}, \Sigma) \quad (19)$$

from which 100000 samples  $\bar{S}$  are drawn, using a factor matrix  $A A^T = \Sigma$ . This sampling effectively simulates the estimated trajectory error by the Navigation OD solution from c/u manoeuvre data cut-off ( $t_{c/u} - 2$  days).

4. Each dispersion sample  $\bar{S}$  is fed into the TCM design algorithm, where it represents the trajectory error at manoeuvre time  $\Delta \mathbf{X}(t_{c/u})$ . A corrective manoeuvre is computed and its  $\Delta V$  cost is stored.
5. The resulting  $\Delta V$  population is considered representative of the statistical  $\Delta V$  budget for the c/u manoeuvre on the given flyby-arc. It is characterised by the statistical parameters (mean, 99<sup>th</sup> percentile) of the population.

## 4. Methodology (III) - External Ephemeris Products

For scientific applications, ephemerides must - with great accuracy - capture the moon evolution over time-spans in the order of years, decades or even centuries. This requires the underlying OD setups to be build differently than the navigation OD that was presented in section 2. They typically use dynamical models of great fidelity, high-quality, complementary observations of the system and advanced filter setups. The resulting high-fidelity ephemerides are thus considered suitable as potential external ephemeris products to the GNC operations of the JUICE mission.

In section 4.1, selected characteristics of high-fidelity OD setups are discussed and differences w.r.t. the navigational OD are highlighted. The settings used by Fayolle et al. (2022), whose setup is adopted as a reference for high-fidelity ephemerides from JUICE, are given in more detail. Section 4.2 discusses methods with which high-fidelity moon ephemerides can be integrated into the Navigation OD in the form of external ephemeris updates, while section 4.3 shows how such updates are simulated in the navigation OD framework (see fig. 2).

### 4.1. High-fidelity Ephemeris Generation from JUICE

Recent publications on scientific ephemeris generation from JUICE have adopted advanced coupled filter configurations (*e.g.* Fayolle et al. (2022); Dirkx et al. (2018); Lari and Milani (2019)), which differ drastically from the strictly arc-wise setup of the navigational OD (see section 2.4). Through introduction of a coupling term, which accounts for the influence of single-arc dynamics on the multi-arc dynamics, the filter estimates single-arc initial states of the moons and multi-arc initial states of the spacecraft, in a single inversion. This approach preserves the complete dynamical couplings in the JUICE-Jovian system and unveils the full sensitivity to physical parameters of spacecraft and moon dynamics. As a consequence the risk of misinterpreting signals from spacecraft dynamics as satellite dynamics can be reduced significantly, which - given the strong dynamical couplings in the system - is anticipated to be especially relevant in the context of the JUICE mission. The authors describe this setup as the most advanced and formally correct approach and suggest it to be the method of choice for JUICE-related high-accuracy ephemeris generation applications. However, there are reservations about how applicable the coupled filter is for producing a global ephemeris solution from real observations. In practice, the concurrent estimation of the spacecraft and moon states imposes challenging requirements on the accuracy and consistency of the dynamical models, over both

	Navigation OD		High-fidelity OD	
Instrument	Nav subsystem		3GM	
Coverage	full-arc		c/a $\pm$ 4 h	
	range	Doppler	range	Doppler
Cadence	1 h	1 h	1 h	60 s
Noise	10 m	80 $\mu$ m/s	0.2 m	15 $\mu$ m/s

Table 1: Comparison of the radiometric measurements used in navigation and high-fidelity OD.

short and long timescales. The current model fidelity has for example not yet allowed a single-inversion solution to be achieved from Cassini and Juno data (e.g. Durante et al. (2019, 2020)).

The studies on ephemeris generation from JUICE consider radiometric data from the on-board 3GM instrument, which is expected to provide measurements on an 8 h arc around the time of closest approach (Cappuccio et al. (2020)), complemented by angular VLBI measurements from PRIDE (Dirkx et al. (2017)). For their ephemeris solution, Fayolle et al. (2022) simulate the radiometric range observables with a noise level of 0.2 m at a cadence of 1 h; Doppler measurements with a noise level of 15  $\mu$ m/s at an integration time of 60 s. The comparison in table 1 shows that the characteristics of the 3GM data differ substantially from the tracking data for navigational purposes.

The high-fidelity setup also employs a more sophisticated dynamical model than the navigation OD setup (section 2.1). Most notably, it models the gravity fields of the Galilean moons at greater detail and accounts for dissipative effects. Furthermore, it includes more advanced parameters, such as higher-degree gravity field coefficients, into the estimation.

#### 4.2. External Ephemeris Products in GNC Operations

Boone et al. (2017) discuss multiple ways on how an external satellite ephemeris can be incorporated into an Navigation OD setup: the ephemerides can be held fixed while their uncertainties are considered in the covariance matrices (see section 2.2, eq. (10)), or the ephemerides are used to derive an a-priori covariance for the moon initial states and the filter is given the freedom to estimate corrections to the external ephemerides. The fixed moon ephemerides can give rise to inconsistencies and eventually instabilities in the Navigation OD solution (Boone et al. (2017)). The latter option, allowing for an externally regularised re-estimation of the moon ephemerides is more generally applicable and is thus selected as the preferred method for this analysis.

There are certain operational aspects that complicate the use of external ephemeris products in the Navigation OD. The Navigation OD is an essential part of a strict operational GNC framework. Spacecraft tracking data is made available to the Navigation OD on the shortest route possible. From there, OD solutions must be generated within less than a day to enable a timely design and processing of subsequent TCM commands (section 3.1). As a result, Navigation OD solutions have a data

cut-off lag of less than a day, (2 days w.r.t. execution of associated manoeuvre). Scientific ephemeris products on the other hand are typically developed in academic environments or research institutes and are decoupled from the operations of the associated mission. This results in a more significant lag for the availability of scientific ephemeris products, which can be in the order of weeks or months and which will hereafter be indicated by  $\ell$ .

#### 4.3. External Ephemeris Interface

As indicated in fig. 2, the analysis requires the Navigation OD framework to be capable of simulating moon ephemeris updates from external ephemeris products. In section 4.2 the ephemeris update method was chosen, which uses the external moon ephemeris as an a-priori covariance for regularising the estimation of the moon initial states on the given arc.

Recalling the nominal a-priori strategy described in section 2.4, the a-priori information of the moon initial states at arc  $i + 1$  ( $\mathbf{x}_{m,0}^{i+1}$ ) would be derived from combining the propagated estimation of moon states from previous arcs with the base moon ephemerides (eq. (12)). Instead, when an external ephemeris update is performed for the Navigation OD solution on arc  $i + 1$ , the a-priori information for the moon initial states is taken as  $\hat{\mathbf{x}}_m^{(i-\ell)\rightarrow i+1}$ , that is the propagated moon state estimate of the most recent external ephemeris solution, where  $\ell$  denotes the science data cut-off lag of unspecified magnitude.

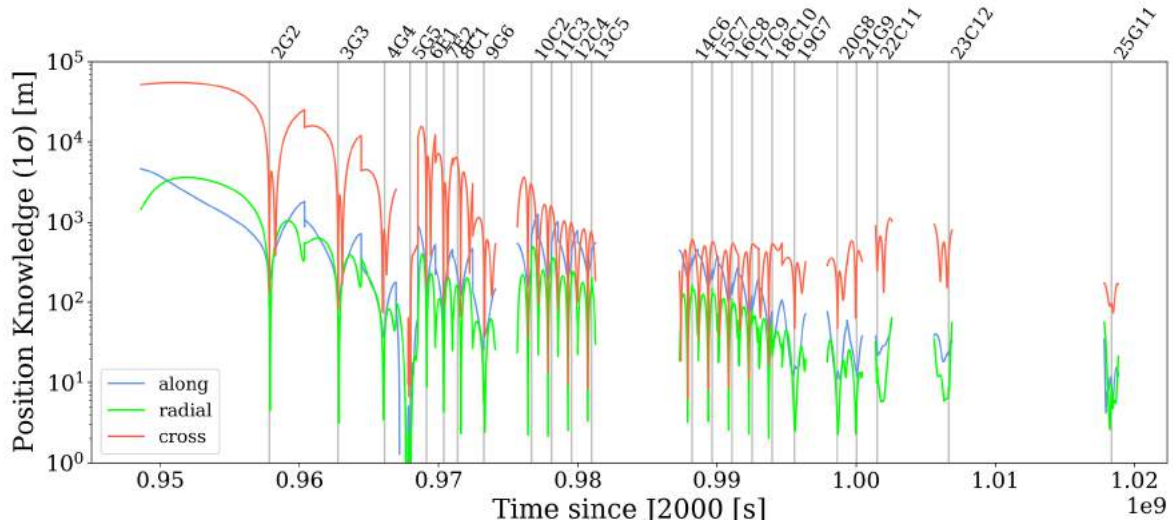
Since the Nav OD setup serves as a tool for calculating the covariances of associated OD solutions, it is sufficient to implement this functionality with regards to the covariances only. Equation (12) thus becomes

$$(\mathbf{P}_{m,0}^{i+1})^{-1} = (\mathbf{P}_m^{b,i+1})^{-1} + (\mathcal{P}_m^{(i-\ell)\rightarrow i+1})^{-1} \quad (20)$$

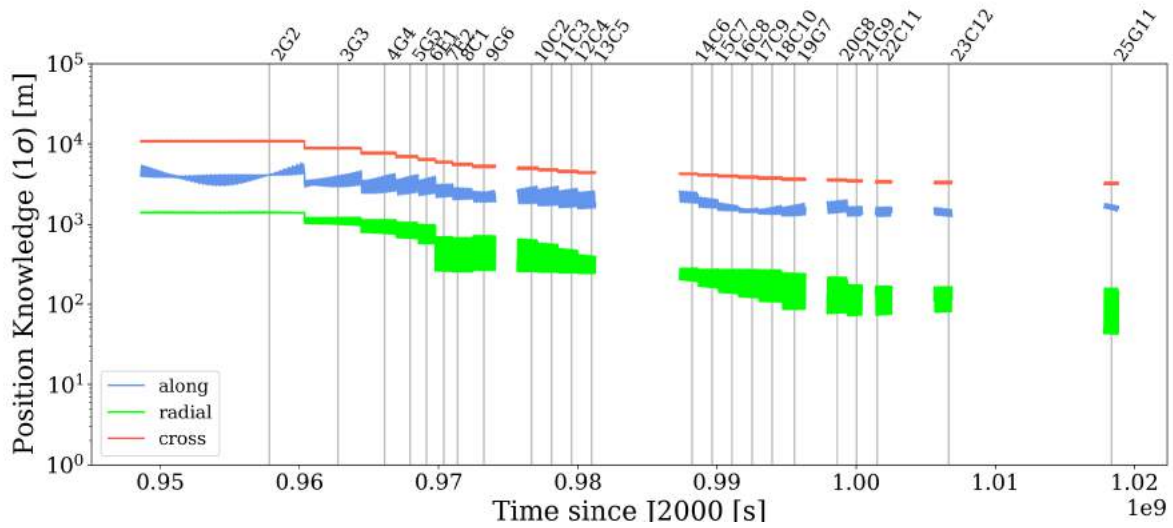
where  $\mathcal{P}_m^{(i-\ell)\rightarrow i+1}$  is the covariance matrix associated with the external moon a-priori information  $\hat{\mathbf{x}}_m^{(i-\ell)\rightarrow i+1}$ . Values for the covariances of the scientific moon ephemerides  $\mathcal{P}_m$  were produced using the setup of Fayolle et al. (2022).

## 5. Results & Discussion

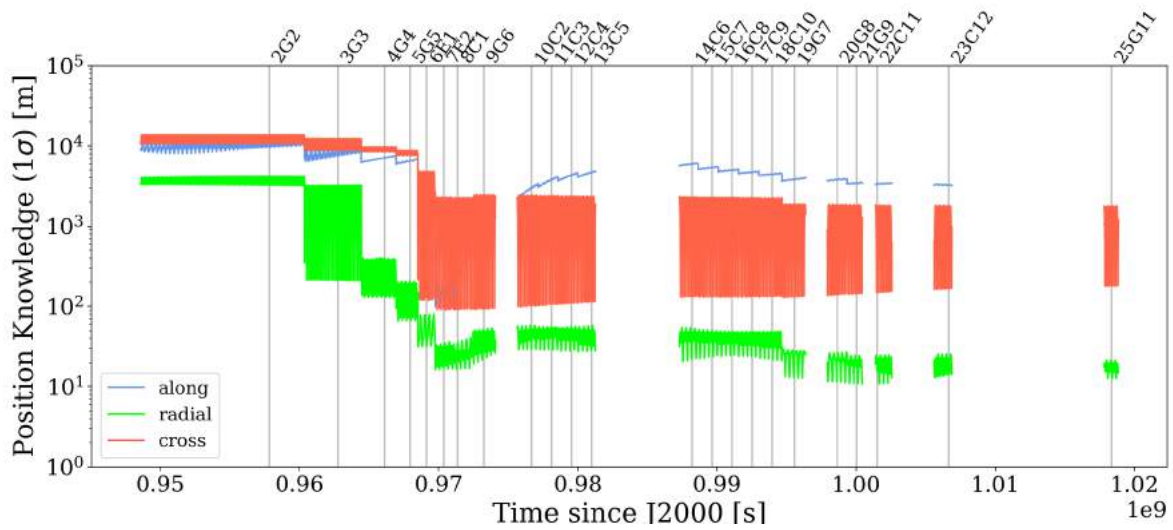
Using the setup shown in fig. 2, this work has produced multiple analyses. The uncertainty (or formal error) evolution of the Navigation OD solutions was simulated and is presented in section 5.1. By making adjustments to selected aspects of the estimation settings, their impact on the Navigation OD solutions was examined. These are presented and discussed in section 5.2. Using the external moon ephemeris interface, a comparative analysis on the statistical  $\Delta V$  cost with and without moon ephemeris updates was performed. This part constitutes the core analysis of this work, the results of which are presented in section 5.3. Lastly, the insights that were gained in the process are used to discuss potential data synergies in section 5.4.



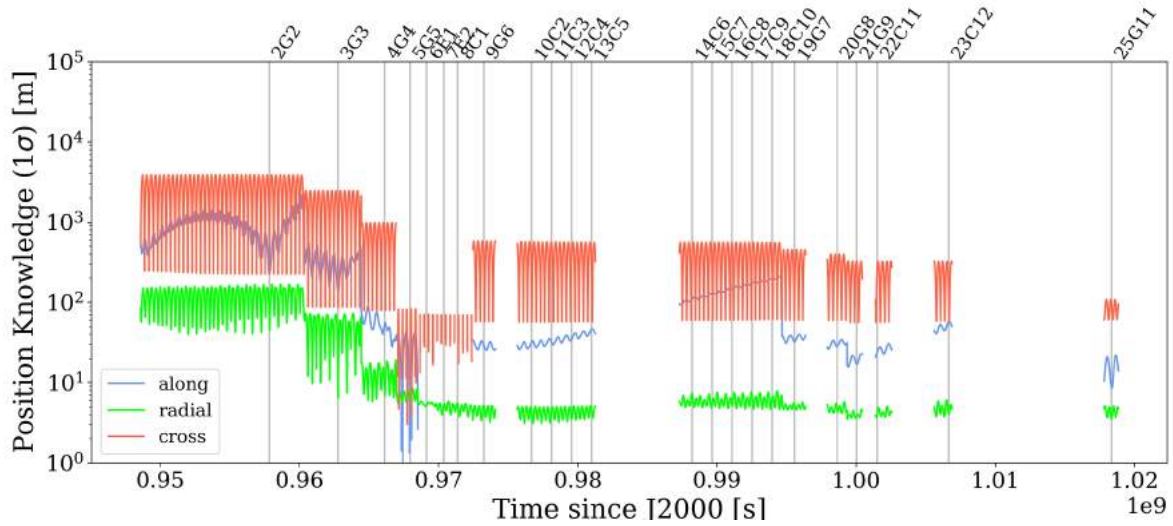
(a) Uncertainty evolution of JUICE position. The discontinuous jumps at the beginning of each flyby arc are a direct consequence of the a-priori strategy (see section 2.4), which re-sets the spacecraft a-priori to its base value for each arc-wise estimation.



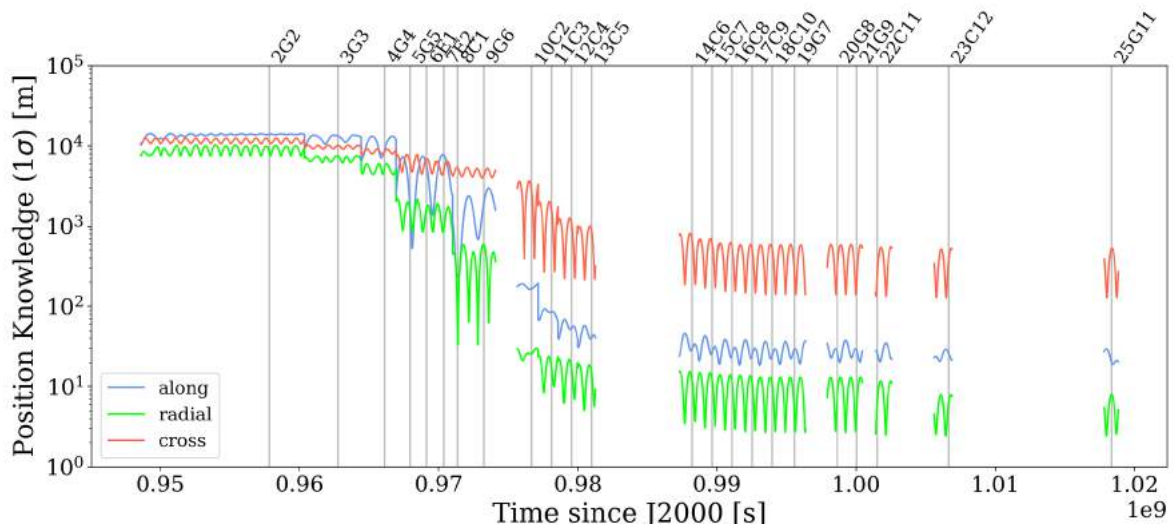
(b) Uncertainty evolution of Io position.



(c) Uncertainty evolution of Europa position.



(d) Uncertainty evolution of Ganymede position.



(e) Uncertainty evolution of Callisto position.

Figure 5: Knowledge evolution of the JUICE-Jovian system, as computed by the Nav OD setup in baseline configuration. Vertical lines mark the time of moon encounter on each considered arc. The stability issues in the JUICE and Ganymede OD solution over the 5G5 to Europa flyby sequence can be seen by erratic features in the along and cross components, as well as an entirely invalid (missing) along-track solution over the associated arcs.

### 5.1. Uncertainty Evolution: Baseline Case

The uncertainty levels from the Nav OD setup, representing state knowledge evolution during navigation operations, are the most fundamental intermediate result of the analysis. Figure 5 shows the post-fit uncertainty evolution (standard deviation  $1\sigma$  on the estimate of each position-related parameter) for JUICE and each Galilean moon, all w.r.t. Jupiter as the central body.

Before commenting on the characteristics of the uncertainty evolution, the stability issues of the presented Nav OD solution have to be discussed. Three of the four Galilean moons are in resonance and consequently the estimation of the different moons' dynamics is strongly coupled. In addition to the a-priori information, the estimation relies purely on observations from spacecraft tracking data, which for each arc will be strongly imbalanced in favour of the encountered moon. As a result, the condition numbers during inversion of the normal equations were observed to be larger than the numerical limit of the machine, meaning that the estimation of the moon ephemerides from only JUICE tracking data can become numerically unstable. Since numerical causes are mitigated by the scaling of the partials (section 2.2), the poor conditioning can be fully attributed to the physical signatures of the parameters. Similar observations have been made in previous work on ephemeris generation from JUICE (Dirkx et al. (2017)). It is suspected that the use of OpNavs as a complementary data type, especially when observing Io and Europa, mitigates this issue, and that the reference setup from ESOC (2017–2019) therefore does not experience stability issues of comparable extent.

The poor stability of the implemented Nav OD solutions first manifests itself in an invalid post-fit covariance on arc 5G5. The covariance was found to have an entry  $\sigma_k^2 < 0$ , where  $k$  refers to a Ganymede state component. Consequently, the associated estimate is deemed uninterpretable. Given the a-priori strategy from eqs. (11) and (12), the corrupted post-fit contributes to the a-priori covariance of the following arc(s). Using the scheme outlined in Appendix A, it could be shown that - for a subset of the flyby arcs - the post-fit covariance of the spacecraft and the encountered moon are not distorted by the corrupted a-priori and that the results can thus be used within the scope of this analysis. Only arcs 5G5 and 9G6 cannot be shown to be interpretable and will therefore be omitted from any quantitative discussions (indicated by grey hatching /// in figs. 8 and 9).

Keeping in mind the stability issues discussed in the previous paragraph, the discussion can be shifted towards the uncertainty evolution characteristics of the Nav OD solution (fig. 5) and how it compares to the validation data. It should be noted again, that it is the sufficiently accurate reproduction of the moon state knowledge evolution, that validates the implemented OD, and that the quantitative similarities between spacecraft trajectory knowledge is secondary in the context of this comparative statistical  $\Delta V$  analysis.

The uncertainty of the JUICE trajectory, shown in fig. 5a, varies greatly within the course of each arc. Starting at comparatively large uncertainty at apojove, the spacecraft state is much better constrained around the point of closest approach. The variations of (multiple) orders of magnitudes make it difficult to relate the solution of the implemented and reference

OD in a systematic, quantitative way. From visual comparison of the uncertainty evolution plots, it can be noted that the implemented model predicts better knowledge of the spacecraft trajectory than the reference OD. This is true especially for the state knowledge around closest approach, where the depth of the uncertainty "dips" is much more pronounced. This is believed to be due to the differences in filter setup between the two compared solutions, as well as the different treatment of manoeuvres.

Despite the a-priori covariance being reset at the beginning of each arc, one can also observe an ongoing improvement of spacecraft state knowledge over the course of the tour. This is the effect of the moon state uncertainty evolution, that shows significant improvements of the moon state knowledge over the course of the tour: the improved knowledge of the flyby moon state translates into the trajectory estimate of the spacecraft. This effect is more pronounced in the implemented OD than in the reference, which is showing slightly worse knowledge of the spacecraft trajectory during the later stages of the tour.

Studying the state uncertainty evolution of the Galilean moons (figs. 5b to 5e) over the course of the multi-flyby tour and especially during its early/mid mission stage (up to and including flyby 13C5), one can see the effect that close encounters have on the coupling of spacecraft tracking data and the encountered moon. The overall moon knowledge can be inferred much better from the spacecraft tracking data after close encounters. Knowledge of in-plane (along, radial) and especially out-of-plane (cross) position components for each given moon relies on the direct coupling between the spacecraft dynamics and the moon as encountered body.

The two in-plane components of the natural bodies show very different behaviour, which can be explained by considering the dynamical coupling in the orbital plane. When propagating the dynamics forward in time, a radial position error will spill over into downstream along-track deviations that grow with the propagation duration. The along-track uncertainty is thus much more prone to secular increase from system propagation, which can be observed in e.g. fig. 5c and fig. 5d. On the other hand this means that the along-track positions strongly depend on the upstream radial positions, such that observations of the first contribute to the determination of the latter. The radial components are therefore much more easily constrained, which is reflected in the low levels of the associated uncertainties throughout figs. 5b to 5e.

Furthermore, the in-plane resonance of the three inner Galilean moons makes the in-plane state components sensitive to spacecraft flybys of any other moon in resonance. These create "indirect" couplings of the spacecraft dynamics and the given moon, via the flyby body. This mechanism is adequately captured in the implemented Nav OD, as can be seen by comparing how the uncertainties of Io (fig. 5b) and Europa (fig. 5c) state components respond to flybys 3G3, 4G4, 5G5 of Ganymede (in resonance) and flybys 8C1, 10C2, 11C3 of Callisto (not in resonance).

As a result of this mechanism, the state knowledge of Io is improved, especially in-plane, without any direct observations or flybys. The improvement is smaller than that shown in the

reference uncertainty data, where direct observations of Io via OpNavs constrain the moon state even further. Another feature that is linked to (the absence of) indirect coupling with the spacecraft dynamics, can be seen in the along-track knowledge evolution of Europa during the sequence of 9 subsequent Callisto flybys. This constitutes a prolonged lack of direct or indirect spacecraft coupling with Europa, which results in a dramatic degrading of the along-track components. Similar but less pronounced observations can be made for Ganymede.

Overall, it is also worth highlighting the rapid improvements of the moon state knowledge from direct coupling and the implications for the navigation of subsequent flybys. In the first arc alone (2G2), post-fit uncertainty of Ganymede is reduced by up to two orders of magnitude (post-fit of  $\sim 100$  m in the radial direction). For later Ganymede flybys (20G8, 21G9), in-plane position knowledge is consistently in the order of tens of meters, while the cross components are in the order of hundreds. Similar observations can be made for Callisto, where comparable uncertainty levels are already reached after the second flyby (10C2) and stay in effect over the course of the remaining ten Callisto flybys.

From the discussion of the produced OD solutions, it can be concluded that the uncertainty evolution of the implemented OD is qualitatively consistent and quantitatively comparable with that of the reference OD from ESOC (2017–2019). This is specifically true with regards to the moon state uncertainty, which validates the implementation. In the scope of the overall analysis setup (fig. 2), the validated navigation OD framework qualifies for the computation of a baseline statistical  $\Delta V$  budget and constitutes a valid baseline for the comparison with external moon ephemerides. Recalling the stability issues discussed at the beginning of this section, arcs 5G5 and 9G6 must be excluded from this statement.

## 5.2. Effect of the Navigation OD Extensions

The reference OD setup from ESOC (2017–2019) does not include any gravity-related parameters in the estimation. This causes the neglect of gravity parameter uncertainties in the orbit determination. However, knowledge of gravity parameters in the Jovian system has already been well constrained by previous missions (*i.e.* Schubert et al. (2004)). When including the gravity-related parameters into the estimation, it was found that due to the low cadence of navigation tracking data during close encounters, the good a-priori knowledge on the parameter values cannot be constrained further within the Nav OD framework. The small gravity-related parameter uncertainty does also not generate an appreciable effect on the estimates of other system parameters - the comparison between uncertainties from the baseline and gravity estimation cases in fig. 6 does not resolve any significant differences. However, the gravity-related uncertainty does impact the propagation of the state uncertainties via the sensitivity matrix  $\mathbf{S}$  (eq. (11)). This generates a visible effect on the evolution of the Europa and Ganymede positions (predominantly the T-components), which during the 10C2 - 18C10 Callisto flyby sequence degrade more rapidly as compared to the baseline case. Furthermore, it is noted that the

estimation of the gravity-related parameters amplifies the numerical instabilities of the baseline case, which were discussed in section 5.1.

Application of the transfer factor (at a value of  $f = 3$ ) alters the OD solutions significantly, as can be seen by inspection of the uncertainty evolution plots for the "f=3" case, which are provided separately in Appendix B. When the transfer factor is applied during a sequence of repeated flybys of the same moon (see *e.g.* 2G2 - 5G5 in fig. B.15d or 10C2 - 13C5 in fig. B.15e, it effectively delays the reduction of the flyby body uncertainty. However, when another moon is encountered on the following arc, the transfer factor introduces artificial "set-backs" to moon state knowledge (*e.g.* Ganymede after 5G5, see fig. B.15d). This way the empirical penalty disrupts the natural development of the system state uncertainty, such that physical relations and the coupling mechanisms cannot be identified as clearly as in the previous discussion on the baseline case (section 5.1).

A quantitative comparison of the mean uncertainties from the baseline and "f=3" cases is given in fig. 7. Here it can be seen that the transfer factor causes a significant degrading of the moon state knowledge, especially of the late stage multi-flyby bodies Ganymede and Callisto: in-plane position uncertainties, which reduce drastically over the course of the tour and settle at a level of tens of meters, are kept in the order of hundreds of meters. Mean uncertainty levels of the cross-plane components are also raised significantly for all three flyby bodies (Europa, Ganymede and Callisto). Because of their early-stage flybys, Europa and Ganymede are affected over the full course of the mission, while the Callisto W-component is mainly affected in the late mission stages. The spacecraft position knowledge is affected too: especially during the late stages of the tour the degraded moon state knowledge translates into a less accurate determination of the spacecraft position (see B.15a).

The transfer factor extension is considered a relevant addition to the Nav OD setup and its effect will be considered in the subsequent analysis (case "f=3").

## 5.3. $\Delta V$ Savings from External Ephemeris Updates

This section addresses the findings of this paper's core investigation, that is to quantify the potential for  $\Delta V$  savings from external moon ephemeris updates. Firstly, it must be noted that the external moon ephemerides, which were adopted for this analysis, are affected by stability issues similar to those discussed in the context of the navigation OD solutions. However, only for a much smaller subset of the affected arcs could it be verified, that the corrupted a-priori covariance does not distort the relevant components of the parameter estimate estimate. External ephemeris solutions, which could not be verified for a given arc, could also not be considered for moon ephemeris updates. These arcs, indicated by grey hatching (\\) in fig. 9, had to be excluded from the analysis - on top of the arcs, which were already omitted due to stability issues in the navigation OD (///, see section 5.1). This reduces the opportunities for external moon ephemeris updates to only 12 arcs.

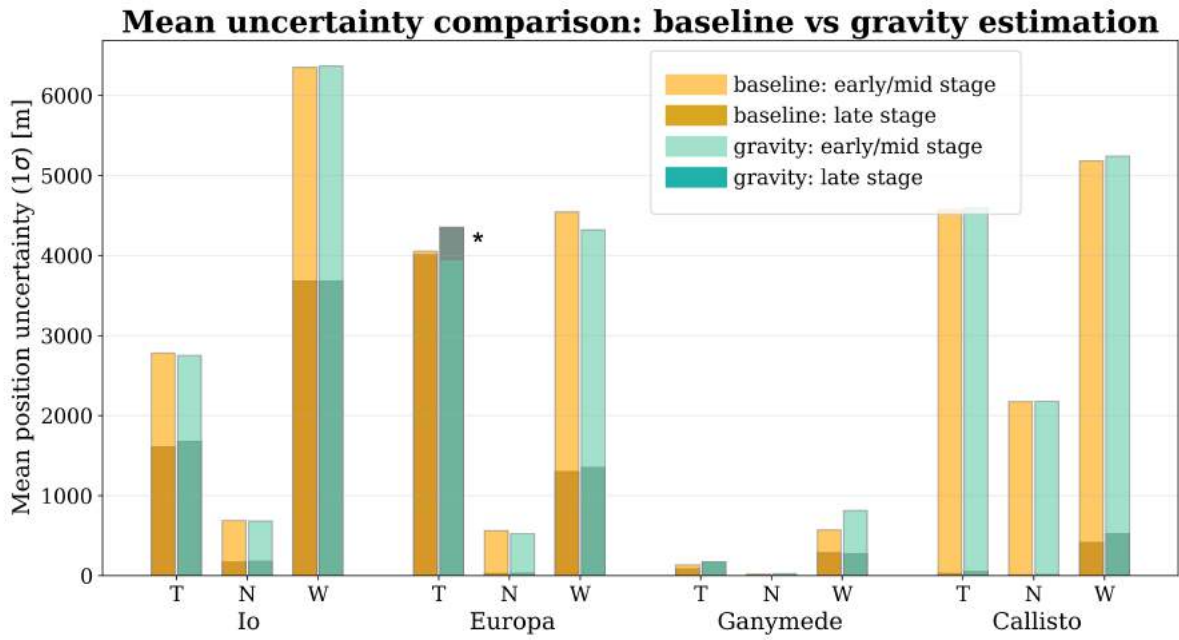


Figure 6: Average position uncertainty over early/mid and late mission stages. Early/mid mission stage is defined up to (and including) arc 13C5. The estimation of gravity-related parameters does not introduce a significant degrading of the system knowledge for either of the stages.  
 \*The grey overlap marks the exceptional case, in which mean uncertainty over the early/mid stages is smaller than the late tour stage.

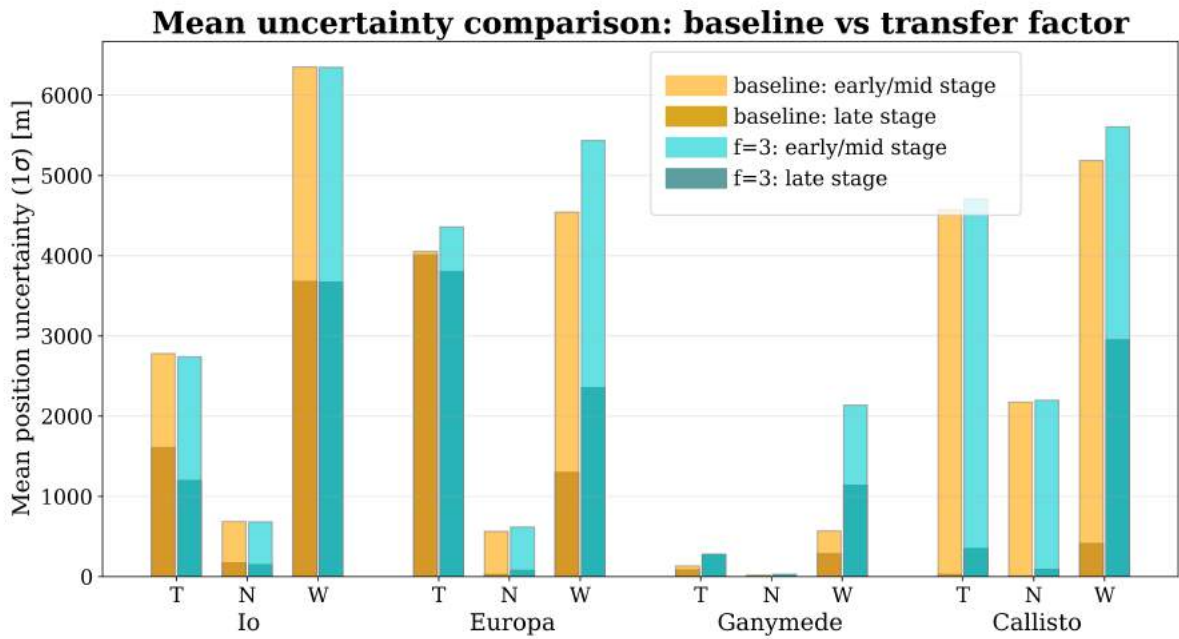


Figure 7: Average position uncertainty over early/mid and late mission stages. Early/mid mission stage is defined up to (and including) arc 13C5. Empirically degrading the moon knowledge transfer results in a significant degrading of the position knowledge associated with the multi-flyby bodies Ganymede and Callisto. Ganymede (w-component) is affected over both mission stages, while Callisto (all components) is mainly affected during the late stage.

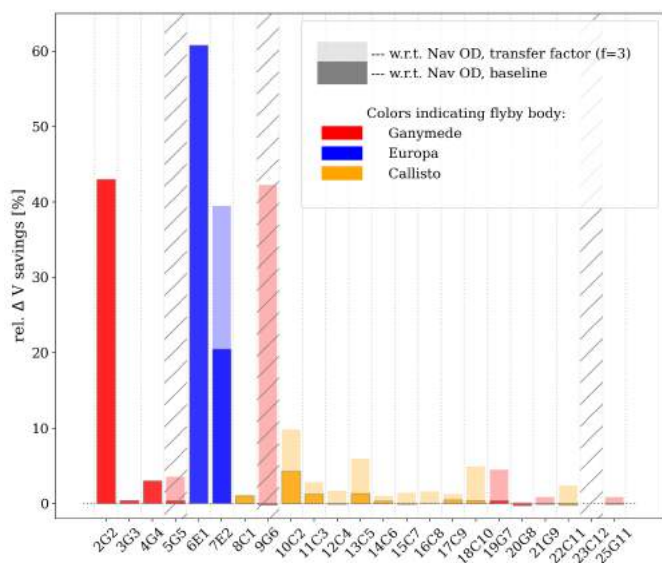


Figure 8:  $\Delta V$  savings on the  $c/u$  manoeuvre for each arc, assuming perfect moon knowledge. Computations were done over all flyby arcs, including 5G5 and 9G6, which could not be shown to be suitable for this kind of analysis. These cases are indicated by the /// hatching pattern. Arc 23C12 was also excluded, because the post-flyby section of the arc is too short to accommodate the generic guidance scheme.

Before involving the specific radio science ephemerides from [Fayolle et al. \(2022\)](#) into the analysis, it was explored to what extent generic moon ephemeris improvements can be advantageous for the statistical  $\Delta V$  expense of the clean-up manoeuvres. This was done by considering the limit case, in which the Nav OD solution assumes perfect moon state knowledge. Based on the resulting OD solution, a statistical  $\Delta V$  budget was computed for the  $c/u$  manoeuvres and compared to the budgets of the baseline and "f=3" cases. [Figure 8](#) shows the relative  $\Delta V$  savings per  $c/u$  manoeuvre of each flyby, that was introduced through the total elimination of moon ephemeris uncertainties.

By considering this limit case, it can be seen that the moon ephemeris error only acts as a  $\Delta V$ -driving factor on the arcs, on which a moon is encountered for the first or - in the case of Europa - second time. This does not apply for the first encounter of Callisto at 8C1, likely because it has already been constrained by the previous six flybys of the other moons. For the applicable cases (2G2, 6E1, 7E2), substantial ( $> 10\%$ ) savings on the  $c/u$   $\Delta V$  cost are possible. For all other flyby arcs, the savings are in the domain of low single-digit percentages. It must thus be concluded that in its baseline configuration the Nav OD constrains the moon state uncertainties so rapidly, that they effectively do no longer affect the  $c/u$  manoeuvre cost significantly for the majority of the tour. Instead the  $\Delta V$  budget appears to be almost entirely driven by the spacecraft state uncertainty. While the latter also decreases with the improved moon knowledge, there are other factors such as the noise on the tracking data, stochastic accelerations and systematic error sources (captured by the consider parameters), that impose a moon-independent limit on the quality of the spacecraft trajectory determination.

The transfer factor (case "f=3") can partially counteract the

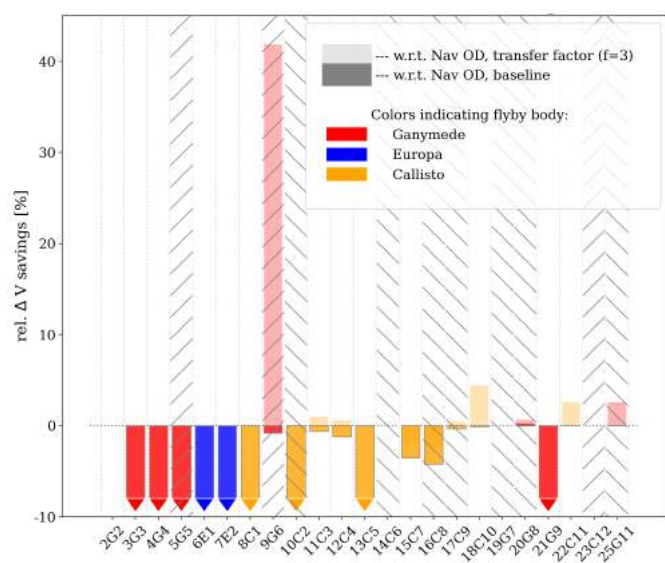


Figure 9:  $\Delta V$  savings on the  $c/u$  manoeuvre for each arc, simulating idealised updates ( $\ell = 0$  from external moon ephemerides). The truncated bars indicate statistical manoeuvre cost increases of  $\zeta 10\%$ . Note that the opportunity for reliable comparisons had to be narrowed down further, since some of the a-priori covariance provided by the external ephemerides does not match the validity criteria ([Appendix A](#)). These cases are indicated by the /// hatching pattern.

rapid improvement of moon knowledge, because it prevents the locally decreased uncertainty of the encountered moon to persist over the full course of the tour. Applying the transfer factor, the savings on 7E2 can be doubled and another substantial  $\Delta V$  reduction can be recorded on arc 10C2.

Using the individual  $c/u$  manoeuvre expenses presented by [ESOC \(2017–2019\)](#), the limit case savings from [fig. 8](#) were scaled to absolute  $\Delta V$  savings. The resulting numbers in [table 2](#) effectively indicate the theoretical limit which could be achieved by implementing external moon ephemerides. Over half of the total savings indicated by the limit case comes from the  $c/u$  manoeuvre on arc 2G2.

External JUICE ephemeris products rely equally as much - or even more so in the case of the chosen external ephemeris from [Fayolle et al. \(2022\)](#) - on the tracking data from moon encounters. They can therefore not be expected to attain significantly reduced moon state knowledge at the early stages of the tour. Recalling the observations from the theoretical limit case ([fig. 8](#)), which showed that it is only during the early stages that moon state knowledge improvement can effectuate significant  $\Delta V$  savings, it must be expected that the external ephemeris updates are not an effective way to save statistical  $\Delta V$ .

This is confirmed by [fig. 9](#), which shows the maximum savings that can be achieved by updating moon knowledge from the [Fayolle et al. \(2022\)](#) ephemerides. In the underlying computation, an update was assumed to be conducted at the beginning of each arc. For these updates, operational cut-off lags were ignored (*i.e.*  $\ell = 0$  in [eq. \(20\)](#)), such that all data of the previous flyby is assumed to be available for the generation of the external ephemeris. While the possible improvements were expected to lie in the rather small margins, that were drawn out

	$\Delta V$ savings - 99% limit case	$\Delta V$ savings - 99% external updates	Tour statistical $\Delta V$ - 99% (ESOC (2017–2019))	Cost of lower-altitude GCO-500 (ESA (2014))
baseline	12.7 m/s	n/a	158.6 m/s	~ 90 m/s
”f=3” case	14.3 m/s	0.43 m/s		

Table 2:  $\Delta V$  savings on the c/u manoeuvre - effectuated by perfect moon knowledge and idealised external ephemeris updates - next to the total statistical  $\Delta V$  expense and the cost of the lower-altitude enhancement of the GCO-500 phase. Relative savings from fig. 8 were translated to absolute savings by mapping them to the statistical c/u manoeuvre expenses presented in the JUICE navigational analysis (ESOC (2017–2019)). This method is not entirely consistent, but the resulting numbers can indicate how the maximum attainable savings from moon ephemeris updates relate to the total statistical  $\Delta V$  budget and the cost of mission extension.

by the limit case in fig. 8, the findings in fig. 9 were surprising nonetheless: Even with the idealistic assumptions about the cut-off lag, ephemeris updates were found to strongly degrade the Nav OD solution on the majority of arcs, which results in a severe increase of the associated c/u manoeuvre cost. The main reason for this observation was traced back to the coverage of the navigation tracking data, which is much more extensive than than the 3GM data on which the external ephemeris product relies (see section 5.4). The only noteworthy exceptions are arcs 18C10 and 22C11, where - given the transfer factor of  $f = 3$  is applied -  $\Delta V$  savings between 3 and 5% are possible. These improvements, which sum to a total saving of 0.43 m/s, and which degrade further when accounting for the operational cut-off lag, are too low to be considered relevant findings. Additionally, another adverse effect that is not captured in fig. 9, has to be mentioned. The external moon knowledge update, that could be introduced at either one of the arcs 18C10 and 22C11 may lead to an improved OD solution on the given arc, but can potentially degrade the OD solution on subsequent arc. This can become relevant when the external ephemeris constrains the Ganymede state less accurately than the Navigation OD, such that the OD solutions that drive manoeuvre cost on the following Ganymede flybys degrade.

Instead of in-mission ephemeris updates, a more effective way to tap into the  $\Delta V$  savings outlined by the theoretical limit (table 2) is to improve the Galilean moon ephemerides before the onset of the JUICE flyby tour. This requires the use of data sources outside the JUICE mission, such as ground-based astrometric measurements of occultations and mutual approximations, but also the Europa Clipper mission, which is scheduled to arrive in the Jovian system before JUICE (Tarzi et al. (2019)). By the time of JUICE’s first encounters with the Galilean moons, Clipper is expected to have collected approximately two years’ worth of data in the Jovian system. Since this mission is focused on acquiring data for the detailed characterisation of Europa (Verma and Margot (2018)), its consideration may be especially useful for effectuating  $\Delta V$  savings during JUICE’s Europa flybys (fig. 8, blue bars). Analyses, which quantify the expected extent of such pre-arrival improvements, are already being carried out in preparation of the JUICE mission (ESOC (2017–2019)).

#### 5.4. Further Data Synergy

In sections 5.1 and 5.3 it was discussed, that the Nav OD solution constrains moon state knowledge very rapidly. This is not trivial and does not apply for the science data based OD

solutions from e.g. Fayolle et al. (2022). In fact, the key reason why external moon ephemeris updates are unable to lead to  $\Delta V$  savings (section 5.3), is that the moon state uncertainty is reduced more gradually by the external OD setup. This can be seen by inspection of fig. 10, which shows the average moon state uncertainties in the external ephemerides over the early stages of the tour and compares them with the generally much smaller uncertainties from the Nav OD. Given that the external ephemeris solution is based on the more accurate radio science data from 3GM, this is an unexpected observation. This motivates an investigation for the decisive factor, which enables the Nav OD to rapidly improve the moon state knowledge.

This factor was identified to be the volume, and distribution of the radiometric tracking data. The continuous availability of navigation tracking data over the full length of the flyby arcs stands in stark contrast to the locally focused placement ( $c/a \pm 4$  h) of the 3GM data. This discrepancy is especially pronounced during the long arcs of the early tour stage (2G2, 3G3).

Figure 11 shows the design matrix  $\mathbf{H}$  of the inversion on arc 2G2, indicating by colour how strongly individual observations contribute to the estimation of certain parameters. With a total volume of 3286 observations - as compared to only 480 observations from 3GM - this design matrix is considerably larger. Recalling the scaling of the estimated uncertainties ( $1/\sqrt{N_{obs}}$  in the absence of systematic errors), this gives the navigation data an advantage, which can at least partially counteract the higher noise levels on the observables.

The crucial point that eventually creates the early-mission advantage for the navigation data set is the distribution of the observations in time and space. Firstly, the navigation data set contains many observations far downstream of the flyby, the furthest taken almost 30 days after the point of closest approach. These late downstream measurements are extremely sensitive to the pre-flyby state of spacecraft and encountered moon. This makes the late observations very powerful contributors in the estimation, much more powerful than the most downstream 3GM observations (at  $c/a + 4$  h). The importance of the downstream observations can also be seen in fig. 11, where their associated partials are shown to be much larger than the partials of the pre-flyby observations, especially w.r.t. spacecraft and flyby body. This effect also shows for Europa and Callisto, and to a much lesser extent for Io.

By closer inspection of the information content w.r.t. Io parameters, it can be seen that pre-flyby observations contribute more strongly to the estimation, than is the case for other bodies. This indicates, that the tracked spacecraft picks up the dy-

### Mean uncertainty comparison: Nav and External OD

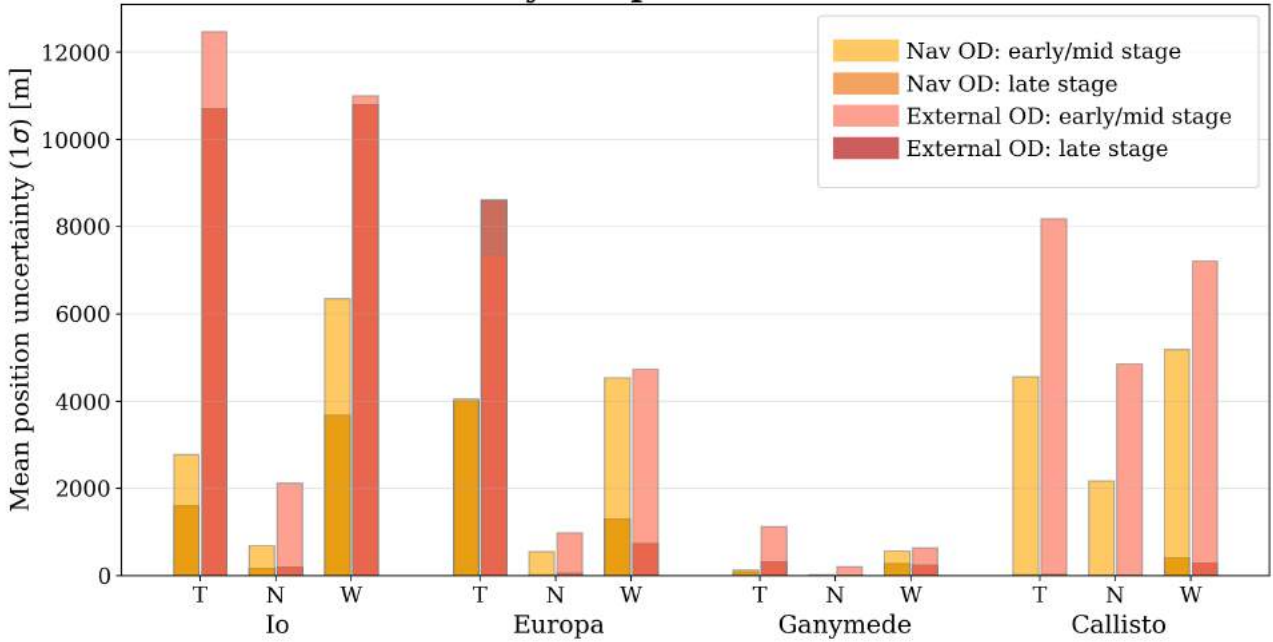


Figure 10: Average position uncertainty over early/mid and late mission stages, comparing post-arc uncertainty levels of the External and Navigation OD. It can be seen that - with few exceptions - the external ephemeris cannot match the early/mid stage levels of the Navigation OD. Late stage uncertainty levels of the multi-flyby bodies Ganymede and Callisto become comparable between Navigation OD and External OD, with small advantages for the External OD on Ganymede and Callisto w-components. Early/mid mission stage is defined up to (and including) arc 13C5.

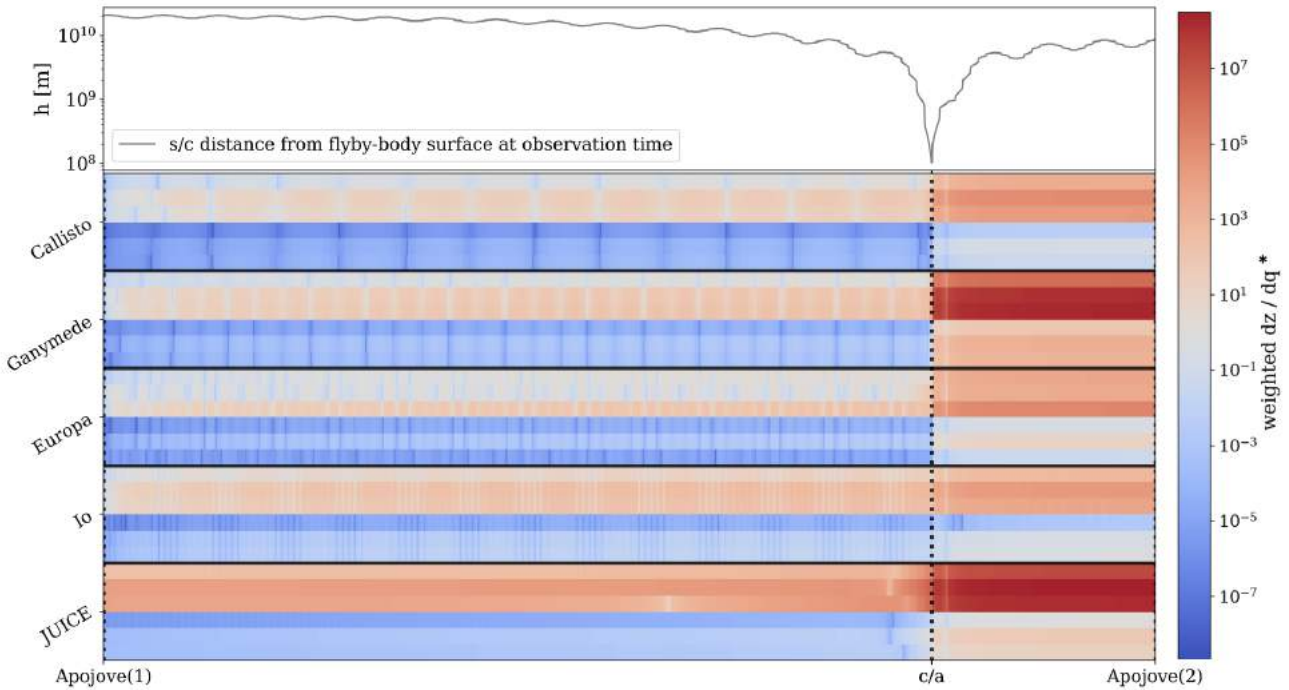


Figure 11: Weighted design matrix ( $\mathbf{H}^T$ ) of arc 2G2: the x-axis is the dimension of the observation timeline, shown from start to end of the given arc, the y-axis the dimension of the estimatable state parameters. Each entry of the design matrix relates a given observation  $z$  to an estimatable parameter  $q$ , via the partial derivative  $\partial z / \partial q$ . The magnitude of these partials indicate how influential a given observation is for constraining the knowledge of the associated parameter. The additional axis on top of the figure indicates how distant the object of measurement (spacecraft) is from the flyby body for any given observation. Note that the design matrix in this figure has been reduced to contain range-rate entries only.

\* The units of the partials are [1/m] for position (upper three) components and [s/m] for the velocity (lower three) components of each body's state.

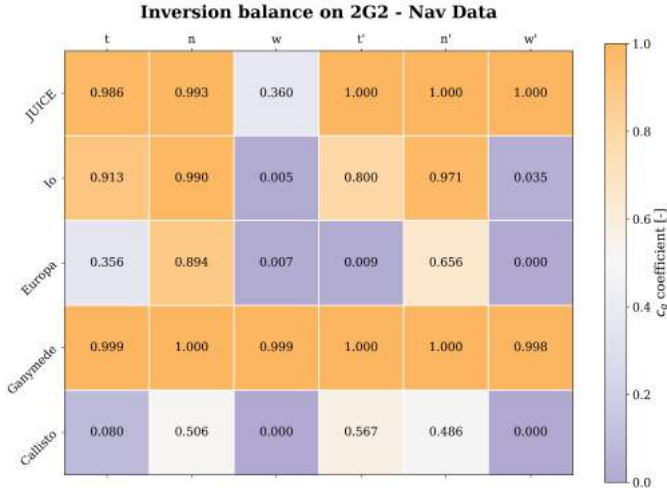


Figure 12:  $c_q$  values on arc 2G2, indicating the balance of a-priori and observation information when using the navigation tracking data. It can be seen that this observation set outweighs a-priori information for spacecraft and the encountered moon, but also for the in-plane components of non-flyby bodies, especially Io.

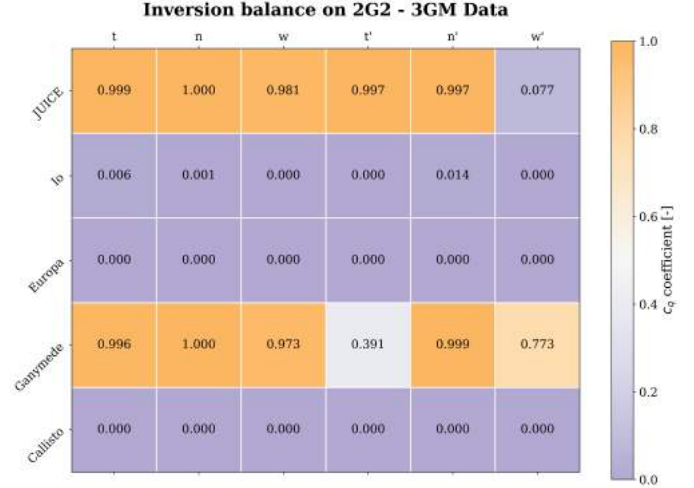


Figure 13:  $c_q$  values on arc 2G2, indicating the balance of a-priori and observation information when using radiometric data from 3GM. It can be seen that this observation set outweighs a-priori information only for spacecraft and the encountered moon. The estimation of non-flyby bodies relies almost entirely on a-priori information.

namical signature of Io prior to any close encounters, and consequently this signature is also contained in the pre-flyby observations. The impact of these pre-flyby observations can be stressed further, when looking at the extent to which the cumulative observations on the long arcs (here 2G2) improve the a-priori knowledge. This can be done by considering the contribution coefficients  $c_q$  (eq. (8)), which fig. 12 shows for each estimated state parameter. The  $c_q$  values indicate that the estimate of (in-plane) Io parameters on arc 2G2 is effectively completely dominated by observation - a large contribution to which comes from the pre-flyby measurements (by fig. 11). It also shows that the observations on arc 2G2 help improve knowledge of Io more than is the case for any other non-flyby body.

Using the locally focused tracking data from 3GM, it must be expected that the measurements pick up dynamical signals of non-flyby bodies to a much lesser extent. To confirm this, the Nav OD setup was used to produce another OD solution, but navigation data was replaced by simulated 3GM data. Indeed, it was observed that the 8 h tracking intervals on the long arcs (2G2, 3G3, 4G4) cannot improve knowledge of the non-flyby bodies. This is consistent with the interpretation of the  $c_q$  coefficients, for which the values of the associated parameters are close to zero (fig. 13 for 2G2).

While the previous paragraphs discuss the full-arc coverage as a powerful asset of the navigation data set, it must be recalled that this notion relies on the results of a covariance analysis, in which dynamical and observational models are idealised (section 2.2). The simulated tracking data is perfectly consistent with the dynamical model - an assumption which in reality applies to the navigational full-arc tracking much less than to the 8 h 3GM tracking arcs. Whether the potential benefits of the navigation data coverage can be exploited in practice depends strongly on the accurate modelling of manoeuvres and non-conservative forces over the long arcs.

To prevent the misinterpretation of the results presented thus

far, it must be emphasised that navigational tracking data can by no means act as a replacement for the 3GM data. Considering the post-mission ephemeris generation, Fayolle et al. (2022) and Dirx et al. (2017) have shown that a combination of 3GM and VLBI data from the entire flyby tour enables the creation of moon ephemerides with smaller uncertainty levels than the levels to which moon state knowledge from the navigation OD converges. This effect becomes even more pronounced when considering the contribution of 3GM data from the Ganymede orbit phase, during which the radiometric data cadence is increases significantly (Cappuccio et al. (2020)). Furthermore, 3GM data addresses other JUICE science goals, most notably the accurate determination of the moons gravity fields and tides (Cappuccio et al. (2020)), to which radiometric tracking data could not contribute to the same extent.

Instead, this work suggests a possibly beneficial data synergy between the radiometric data from the navigation subsystem and 3GM. Synergy between complementary observables from different data sources is expected to be a central aspect in the reconstruction of the JUICE trajectory and the generation of Galilean moon ephemerides (e.g. Fayolle et al. (2022); Dirx et al. (2017); Morgado et al. (2019)). Since this type of ephemeris generation is typically working with complete observation sets which consolidate data from the entire mission duration, it is not clear if the navigation data ability to enable a rapid improvement of the moon state knowledge will be of great advantage in this context. Inclusion of the navigation tracking measurements could nonetheless have beneficial effects, because it contains a stronger signature of Io's dynamics and could thus help balance the more lob-sided 3GM data set. Similar considerations would likely apply to OpNav measurements of Io and Europa, and the data produced by the JANUS instrument Della Corte et al. (2014) onboard the JUICE spacecraft, which were however not investigated in this work.

## 6. Conclusions

This work addresses potential  $\Delta V$  savings on the post-flyby cleanup manoeuvres during the JUICE multi-flyby tour, using external moon ephemerides as updates in the GNC operations. Using the capabilities of the *Tudat* software, a navigation orbit determination was simulated. Despite certain model simplifications, most notably the omission of optical navigation data and manoeuvre execution errors, the simulation results were validated with the uncertainty levels of the ESOC navigation setup (ESOC (2017–2019)).

The simulated state uncertainty evolution of the JUICE spacecraft and the Galilean moons along the multi-flyby tour was found to show the qualitative features, that are expected from the dynamical coupling in the system. One such effect of the coupling can be observed in the evolution of the Io state knowledge which is improved despite the lack of direct observations. It was furthermore noticed, that - in its baseline configuration - the navigation OD was simulated to produce rapid and significant improvements of the moon state knowledge, especially through close encounters. During the late stage of the tour, uncertainties of the Ganymede and Callisto in-plane position were found to be consistently in the order of tens of meters.

The navigation OD simulation was used to examine the effect of alternative OD settings, such as the estimation of gravity-related parameters and the empirical degrading of moon knowledge transfer along the tour. It was shown that due to well-constrained a-priori knowledge of the gravity-related parameters, the estimation of Galilean moon mass and lower order spherical harmonics coefficients does not impose a significant effect on the resulting system knowledge evolution. The empirical penalty on moon knowledge transfer was found to significantly impact the state knowledge of the multi-flyby bodies Ganymede and Callisto. It effectively biases the state uncertainty evolution of the encountered bodies, slowing the rate at which multi-flyby sequences of the same body constrain the state of the encountered body. At the same time, the transfer factor can also introduce artificial features in the uncertainty error evolution, which to some extent obscure the natural mechanisms of the multi-body OD. Overall, the transfer factor was found to be a useful empirical measure to partially prevent that idealising assumptions in the covariance analysis result in overly optimistic OD simulations. It was adopted as a free parameter for the statistical  $\Delta V$  analysis.

In the core analysis of this work it was shown that over the largest part of the tour statistical  $\Delta V$  cost of the cleanup manoeuvres is not driven by moon state uncertainty. The navigation OD solution shows rapid improvement of moon state knowledge from the first moon encounters (2G2, 6E1, 7E2 - 8C1 constitutes an exception), such that corrective manoeuvres for all subsequent flybys depend mostly on spacecraft trajectory uncertainty and cannot be influenced significantly by moon knowledge improvement. Only during the first and - in case of the Europa flybys - second encounter with a moon can the moon state uncertainty be considered a significant contributor to the manoeuvre cost. Assuming perfect moon knowledge, the limit for reducing cleanup manoeuvre cost on arcs 2G2,

6E1, 7E2 was found to be 43%, 61% and 20%, respectively, while  $\Delta V$  savings on other arcs do not exceed lower single-digit percentages. This puts a total theoretical limit of 15.6 m/s on the clean-up manoeuvre  $\Delta V$  savings from improved moon ephemeris knowledge.

Within these tight theoretical limits, updates from the radio science moon ephemerides cannot generate considerable advantages. This is mainly due to the fact that the limited 3GM tracking data coverage does not allow these moon ephemerides to converge to low-level moon state uncertainties as rapidly as the navigation solutions. Only when penalising the transfer of locally improved moon state knowledge by an empirical factor of  $f = 3$  on the state variance, and thereby limiting the pace at which the navigational solution constrains moon states, can updates from the external ephemerides generate small advantages. The greatest savings from external moon ephemeris updates were found to be at 5% and 3% for corrective manoeuvres after flybys 18C10 and 22C11, respectively, which sum up to a total saving of 0.43 m/s. Despite being computed without accounting for operational constraints, which are expected to make the use of external ephemerides even less advantageous, and especially when considering the  $\Delta V$  cost of the anticipated mission enhancements, these findings do not support the case of integrating external ephemeris updates in the JUICE GNC operations.

In order to at least partially effectuate the theoretical limits on the  $\Delta V$  savings, it may be more advantageous to consider moon ephemeris improvements prior to the mission. These could be derived from ground-based astrometric measurements as well as data products from the Europa Clipper mission, which will arrive in the Jovian system before JUICE (Tarzi et al. (2019)). The potential extent of pre-arrival ephemeris improvements is already being analysed as part of the JUICE mission preparations (ESOC (2017–2019)).

The spatial and temporal distribution of the navigation tracking data was identified to be the decisive factor, which allows the rapid conversion of navigational moon state knowledge. A large volume of post-flyby observations, some of which up to 30 days downstream of closest approach, imposes tight constraints on the pre-flyby states of the system. Furthermore, it was found that Io's dynamical signature is picked up by pre-flyby range-rate measurements of the JUICE spacecraft, which through their enormous volume allow to improve Io's a-priori position knowledge. Based on this finding, it is recommended to consider (early mission) subsets of the navigational tracking data for the ambitious data synergy projects, which in the aftermath of the JUICE and Europa Clipper missions aim to produce new high-accuracy ephemerides of the Jovian system (e.g. Dirkx et al. (2017); Fayolle et al. (2022)). This addition could help balance the observation set and add valuable information on the state of Io. In practice, the effectiveness of the proposed data synergy will depend on how well the long navigational tracking arcs can be reconstructed dynamically, and how valuable tracking data from the Ganymede orbit phase and the Europa Clipper mission, which were both not considered in this analysis, will be for the state estimation of Io.

## 7. Acknowledgements

This work constitutes the MSc thesis for the study program in Space Exploration at the Delft University of Technology. The author would like to thank Dr. Dirkx, Marie Fayolle, Dr. Lainey and Dr. Zannoni for their guidance, as well as the ESOC mission analysis group for sharing essential information on the JUICE navigation OD.

## References

- Acton Jr, C.H., 1996. Ancillary data services of nasa's navigation and ancillary information facility. *Planetary and Space Science* 44, 65–70.
- Bellerose, J., Nandi, S., Roth, D., Tarzi, Z., Boone, D., Criddle, K., Ionasescu, R., 2016. Cassini navigation: The road to consistent subkilometer accuracy satellite encounters, in: *AAS Annual Guidance and Control Conference*.
- Bellerose, J., Roth, D., Criddle, K., 2018. The Cassini mission: Reconstructing thirteen years of the most complex gravity-assist trajectory flown to date, in: *2018 SpaceOps Conference*, p. 2646.
- Boone, D., Bellerose, J., Roth, D., 2017. Resolution of orbit determination prediction instabilities at Titan during Cassini's Solstice mission, in: *International Symposium on Space Flight Dynamics*.
- Buffington, B., Strange, N., Ionasescu, R., 2005. Addition of a low altitude Tethys flyby to the nominal Cassini tour, in: *AAS/AIAA Astrodynamics Specialist Conference*.
- Cappuccio, P., Hickey, A., Durante, D., Di Benedetto, M., Iess, L., De Marchi, F., Plainaki, C., Milillo, A., Mura, A., 2020. Ganymede's gravity, tides and rotational state from JUICE's 3GM experiment simulation. *Planetary and Space Science* 187.
- Cho, D.H., Chung, Y., Bang, H., 2012. Trajectory correction maneuver design using an improved b-plane targeting method. *Acta Astronautica* 72, 47–61.
- D'Amario, L., Byrnes, D., Stanford, R., 1981. A new method for optimizing multiple-flyby trajectories. *Journal of guidance and control* 4, 591–596.
- Della Corte, V., Schmitz, N., Zusi, M., Castro, J.M., Leese, M., Debei, S., Magrin, D., Michalik, H., Palumbo, P., Jaumann, R., et al., 2014. The JANUS camera onboard JUICE mission for Jupiter system optical imaging, in: *Space Telescopes and Instrumentation 2014: Optical, Infrared, and Millimeter Wave*, International Society for Optics and Photonics. p. 914331.
- Dirkx, D., Gurvits, L.I., Lainey, V., Lari, G., Milani, A., Cimò, G., Bocanegra-Bahamon, T., Visser, P., 2017. On the contribution of PRIDE-JUICE to jovian system ephemerides. *Planetary and Space Science* 147, 14–27.
- Dirkx, D., Lainey, V., 2019. Improved Galilean Moon Ephemerides - Reanalysis of Astrometry and Contribution of JUICE mission, in: *EPSC-DPS Joint Meeting*, Geneva, Switzerland.
- Dirkx, D., Prochazka, I., Bauer, S., Visser, P., Noomen, R., Gurvits, L.I., Vermeersen, B., 2018. Laser and radio tracking for planetary science missions — a comparison. *Journal of Geodesy* , 1–16.
- Durante, D., Hemingway, D., Racioppa, P., Iess, L., Stevenson, D., 2019. Titan's gravity field and interior structure after cassini. *Icarus* 326, 123–132.
- Durante, D., Parisi, M., Serra, D., Zannoni, M., Notaro, V., Racioppa, P., Bucino, D., Lari, G., Gomez Casajus, L., Iess, L., et al., 2020. Jupiter's gravity field halfway through the juno mission. *Geophysical Research Letters* 47, e2019GL086572.
- ESA, 2014. JUICE Definition Study Report (Red Book). Technical Report.
- ESOC, 2017–2019. JUICE: Navigation Analysis of the Jupiter Tour. Technical Report v1.1–v2.2. ESA.
- Fayolle, M., Dirkx, D., Lainey, V., Gurvits, L.I., Visser, P.N.A.M., 2022. Decoupled and coupled moons' ephemerides estimation strategies application to the JUICE mission. Submitted to *Planetary and Space Science*.
- Floberghagen, R., 2001. *The Far Side: Lunar Gravimetry into the Third Millennium*. Ph.D. thesis. Delft University of Technology.
- Folkner, W.M., Williams, J.G., Boggs, D.H., Park, R.S., Kuchynka, P., 2014. The planetary and lunar ephemerides DE430 and DE431. *Interplanetary Network Progress Report* 196, 42–196.
- Fuller, J., Luan, J., Quataert, E., 2016. Resonance locking as the source of rapid tidal migration in the Jupiter and Saturn moon systems. *Monthly Notices of the Royal Astronomical Society* 458, 3867–3879.
- Grasset, O., Dougherty, M., Coustenis, A., Bunce, E., Erd, C., et al., 2013. Jupiter icy moons explorer (JUICE): An ESA mission to orbit Ganymede and to characterise the Jupiter system. *Planetary and Space Science* 78, 1–21.
- Greenberg, R., 2010. The icy jovian satellites after the galileo mission. *Reports on Progress in Physics* 73, 036801.
- Gurvits, L., Bahamon, B., Cimò, G., Duev, D., Molera Calvés, G., Pogrebenko, S., De Pater, I., Vermeersen, L., Rosenblatt, P., Oberst, J., et al., 2013. Planetary radio interferometry and Doppler experiment (PRIDE) for the JUICE mission, in: *European Planetary Science Congress*, pp. EPSC2013–357.
- Hay, H.C., Trinh, A., Matsuyama, I., 2020. Powering the galilean satellites with moon-moon tides. *Geophysical Research Letters* 47.
- Hussmann, H., Spohn, T., 2004. Thermal-orbital evolution of Io and Europa. *Icarus* 171, 391–410.
- Ionasescu, R., Martin-Mur, T., Valerino, P., Criddle, K., Buffington, B., McElrath, T., 2014. Orbit determination covariance analysis for the Europa Clipper mission, in: *AIAA Space 2014*.
- Jones, D.L., Folkner, W.M., Jacobson, R.A., Jacobs, C.S., Dhawan, V., Romney, J., Fomalont, E., 2014. Astrometry of cassini with the vlba to improve the saturn ephemeris. *The Astronomical Journal* 149, 28.
- Lainey, V., Arlot, J.E., Karatekin, Ö., Van Hoolst, T., 2009. Strong tidal dissipation in Io and Jupiter from astrometric observations. *Nature* 459, 957–959.
- Lainey, V., Casajus, L.G., Fuller, J., Zannoni, M., Tortora, P., Cooper, N., Murray, C., Modenini, D., Park, R.S., Robert, V., et al., 2020. Resonance locking in giant planets indicated by the rapid orbital expansion of Titan. *Nature Astronomy* 4, 1053–1058.
- Lainey, V., Duriez, L., Vienne, A., 2004a. New accurate ephemerides for the Galilean satellites of Jupiter - I. Numerical integration of elaborated equations of motion. *Astronomy & Astrophysics* 420, 1171–1183.
- Lainey, V., Duriez, L., Vienne, A., Arlot, J., 2004b. New accurate ephemerides for the Galilean satellites of Jupiter - II. Fitting the observations. *Astronomy & Astrophysics* 427, 371–376.
- Lainey, V., Tobie, G., 2005. New constraints on Io's and Jupiter's tidal dissipation. *Icarus* 179, 485–489.
- Lari, G., Milani, A., 2019. Chaotic orbit determination in the context of the JUICE mission. *Planetary and Space Science* 176, 104679.
- Martin-Mur, T.J., Ionasescu, R., Valerino, P., Criddle, K., Roncoli, R., 2014. Navigational challenges for a Europa flyby mission, in: *International Symposium on Space Flight Dynamics*.
- Montenbruck, O., Gill, E., 2000. *Satellite Orbits: Models, Methods and Applications*. Springer-Verlag Berlin Heidelberg.
- Morgado, B., Benedetti-Rossi, G., Gomes-Júnior, A., Assafin, M., Lainey, V., Vieira-Martins, R., Camargo, J., Braga-Ribas, F., Bouffleur, R., Fabrega, J., et al., 2019. First stellar occultation by the galilean moon europa and upcoming events between 2019 and 2021. *Astronomy & Astrophysics* 626.
- Murrow, D., Jacobson, R., 1988. Galilean satellite ephemeris improvement using Galileo tour encounter information, in: *Astrodynamics Conference*, p. 4249.
- Peale, S., 1999. Origin and evolution of the natural satellites. *Annual Review of Astronomy and Astrophysics* 37, 533–602.
- Raofi, B., Guman, M., Potts, C., 2000. Preliminary statistical analysis for a representative Europa orbiter mission, in: *AIAA/AAS Astrodynamics Specialist Conference*.
- Roth, D., Alwar, V., Bordi, J., Goodson, T., Hahn, Y., Ionasescu, R., Jones, J., Owen, W., Pojman, J., Roundhill, I., et al., 2003. Cassini tour navigation strategy, in: *Proceedings of the 16th International Technical Meeting of the Satellite Division of The Institute of Navigation*, pp. 2218–2229.
- Schubert, G., Anderson, J., Spohn, T., McKinnon, W., 2004. Interior composition, structure and dynamics of the Galilean satellites. *Jupiter: The planet, satellites and magnetosphere* 1, 281–306.
- Tarzi, Z., Boone, D., Mastrodemos, N., Nandi, S., Young, B., 2019. Orbit determination sensitivity analysis for the Europa Clipper Mission tour, in: *AIAA/AAS Space Flight Mechanics Meeting*.
- Verma, A.K., Margot, J.L., 2018. Expected precision of Europa Clipper gravity measurements. *Icarus* 314, 35–49.
- Wagner, S., 2014. Maneuver performance assessment of the cassini spacecraft through execution-error modeling and analysis, in: *AAS/AIAA Space Flight Mechanics Meeting*.
- Weeks, C., 2008. A statistical analysis of spacecraft maneuvers for a deep space mission, in: *AIAA/AAS Astrodynamics Specialist Conference and Exhibit*, p. 7194.
- Wolf, A., Smith, J., 1995. Design of the cassini tour trajectory in the saturnian system. *Control Engineering Practice* 3, 1611–1619.

## Appendix A. Testing invalid OD solutions.

Numerical instabilities during the inversion in eq. (7) have surfaced corrupted covariance results. These can be identified by negative variances ( $\sigma^2 < 0$ ) and non-sensical correlation coefficients ( $|\rho| > 1$ ) in the post-fit and propagated covariance ( $\mathbf{P}_{qq}$  and  $\mathbf{P}_{yy}$ , respectively). Given the a-priori strategy of the OD setup (section 2.4), corrupted covariance is mapped into the a-priori covariance of the subsequent arcs, which may render the following estimates invalid. Even if the results of these estimates do not show any of the mentioned issues, they can still be incorrect in ways that go unnoticed.

This issue is addressed by the following scheme, which examines if the post-fit covariance, which is based on corrupted a-priori covariance, can be used in the analysis. In order for the OD solutions to be applicable within the scope of the statistical  $\Delta V$  analysis, it must be shown that the estimate of the spacecraft and the encountered moon are not distorted by the corrupted a-priori covariance.

This was done by replacing the corrupted covariance  $\mathbf{P}_0$  with a covariance matrix, in which the corrupted entries were artificially removed through a correction  $\mathcal{C}$ :

$$\mathbf{P}_0^* = \mathcal{C}(\mathbf{P}_0) \quad (\text{A.1})$$

A key requirement on this step is that the correction  $\mathcal{C}()$  alters the regularisation of spacecraft (subscript  $sc$ ) and flyby moon (subscript  $k$ ) states as little as possible. This allows for a direct comparison between their re-estimated (based on the artificial a-priori) and original post-fit uncertainties.

Any significant differences on the flyby-relevant fields would therefore indicate a distortion by the corrupted a-priories - an undistorted estimation requires

$$\sigma_{sc}^* \approx \sigma_{sc} \quad (\text{A.2})$$

$$\sigma_k^* \approx \sigma_k \quad (\text{A.3})$$

where  $\sigma^*$  and  $\sigma$  are the uncertainties obtained from estimating with the artificially corrected ( $\mathbf{P}_0^*$ ) and original a-priories ( $\mathbf{P}_0$ ), respectively. It was found that the conditions described by eq. (A.2) were met for all tested arcs (this does not include arcs 5G5 and 9G6) and thus it could be concluded that the corrupted a-priori covariances did not distort the flyby-relevant components of the estimate. Figure A.14 shows how this test is successfully applied to the exemplary arc 8C1.

The requirement of not altering the regularisation of flyby-relevant components by  $\mathcal{C}()$  limits this test scheme to those cases, in which the corrupted entries in the a-priori matrix are only associated with the moons that are not encountered on the arc. For arcs 5G5 and 9G6, on which this is not the case, the interpretability of the post-fit covariances cannot be verified.

## Appendix B. Full uncertainty evolution for the "f=3" case.

Section 2.5 describes the "transfer factor", which was implemented into the navigation OD setup to mitigate some possible shortcomings of the OD covariance analysis. The impact of this extension is discussed in section 5.2, after which the transfer factor is adopted as a free parameter in the statistical  $\Delta V$  analysis (case "f=3").

As such, it takes a significant role in this work. Thus some additional material, specifically the uncertainty evolution of the case "f=3" OD solution, is provided in fig. B.15.

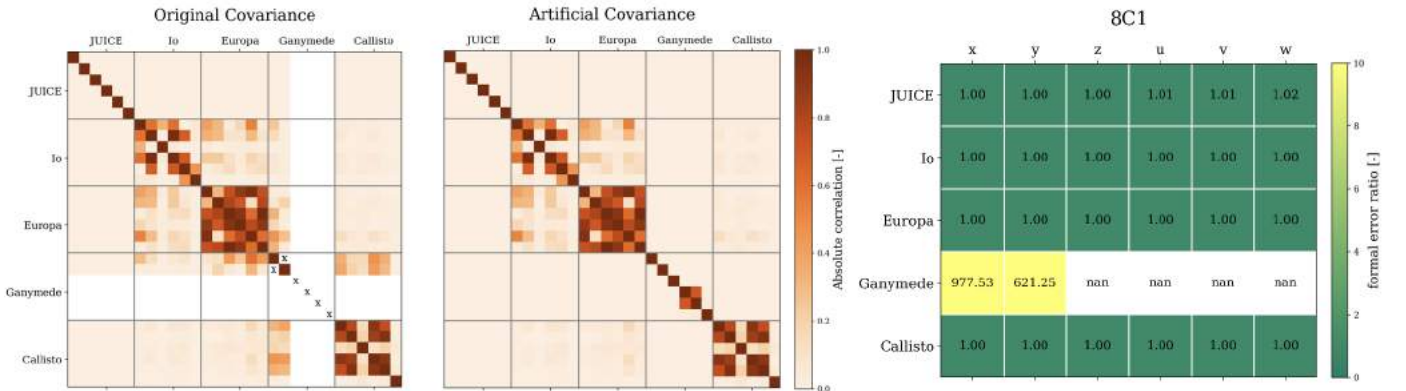
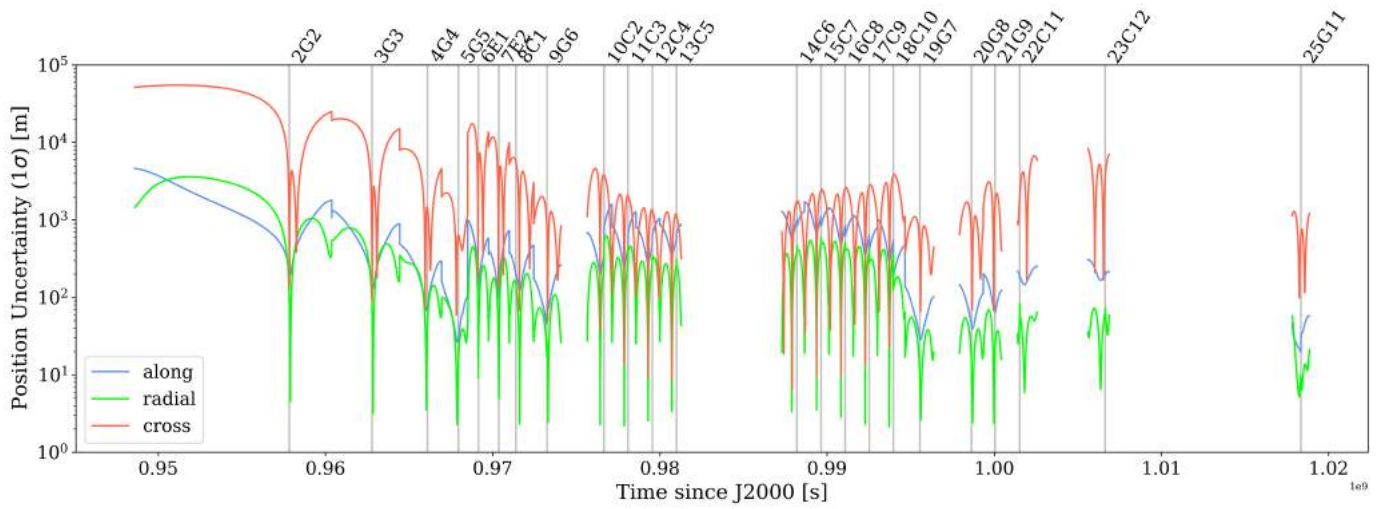
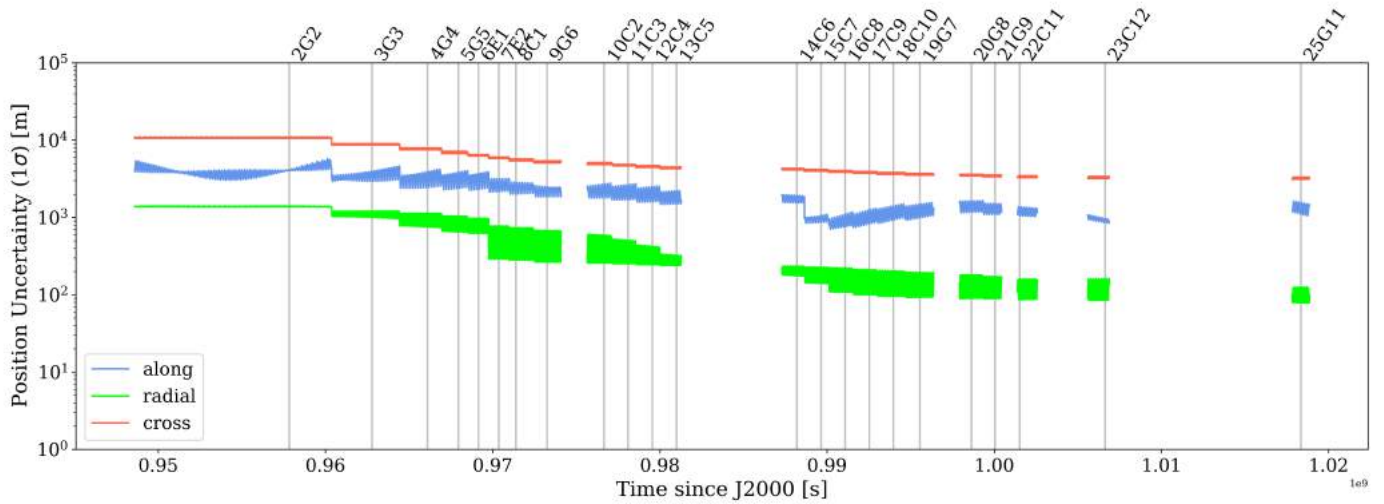


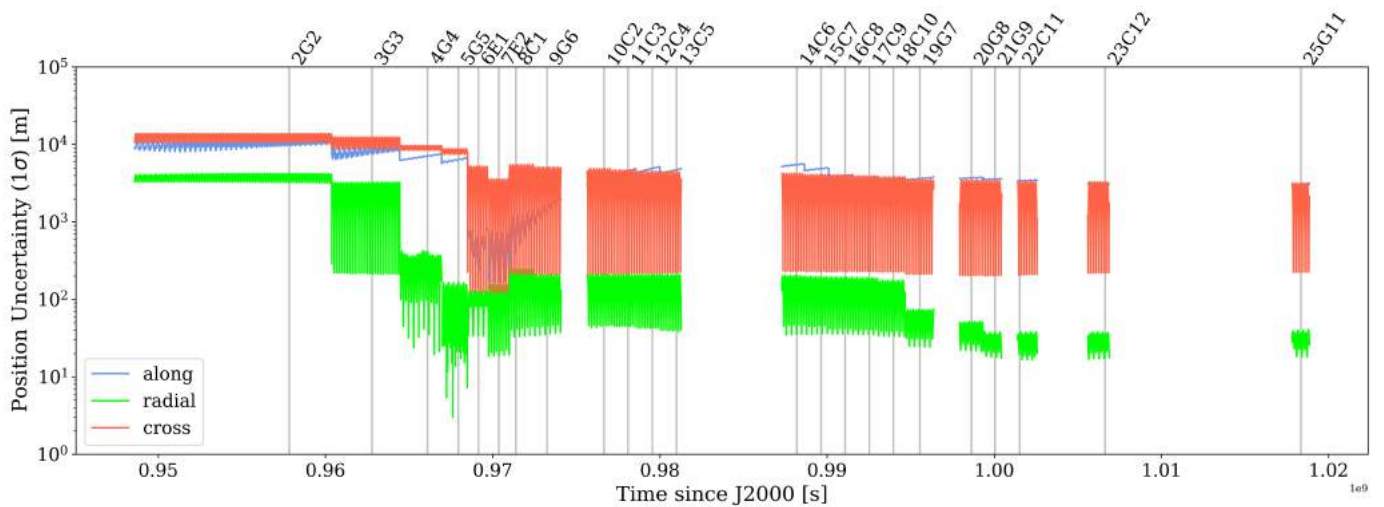
Figure A.14: Successfully conducted testing scheme on exemplary arc 8C1: The two plots on the left show the normalised covariance matrix before and after correction. The "x" indicate the originally corrupted fields, white (nan) fields are the result of the corrupted elements during normalisation of the matrix. For correction, the block including the corrupted entries is replaced by the IMCCE base covariance ( $\mathbf{P}_0$ , see section 2.4). The rightmost grid shows the ratios of original and re-estimated uncertainties: all relevant entries show negligible deviations.



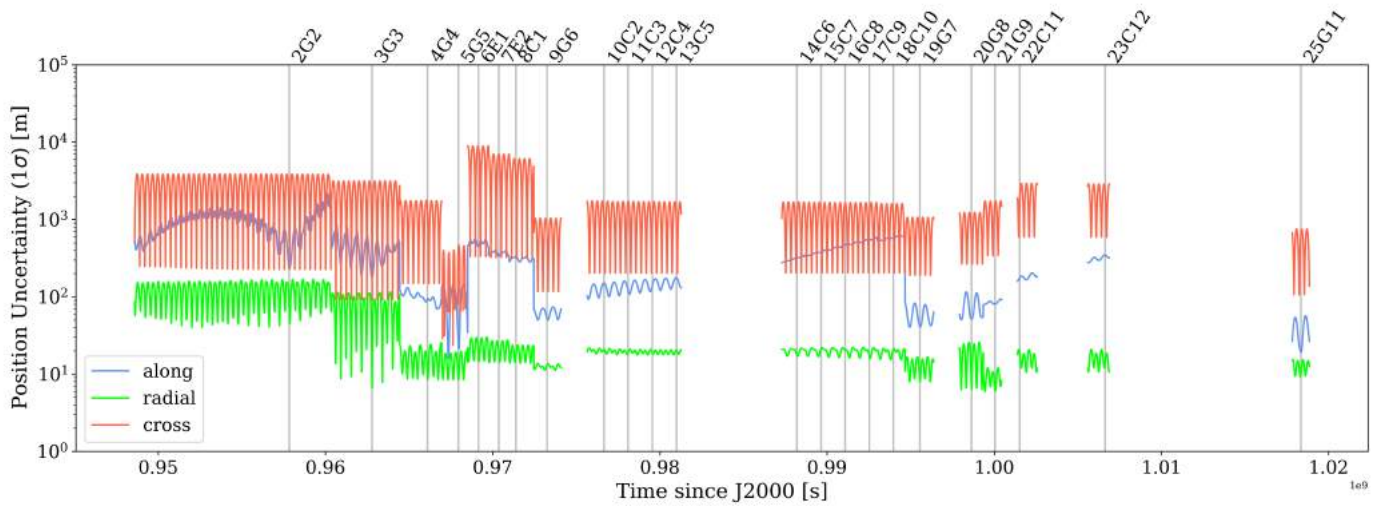
(a) Uncertainty evolution of JUICE position, under the impact of the transfer factor at  $f = 3$ . The discontinuous jumps at the beginning of each flyby arc are a direct consequence of the a-priori strategy (see section 2.4), which re-sets the spacecraft a-priori to its base value for each arc-wise estimation.



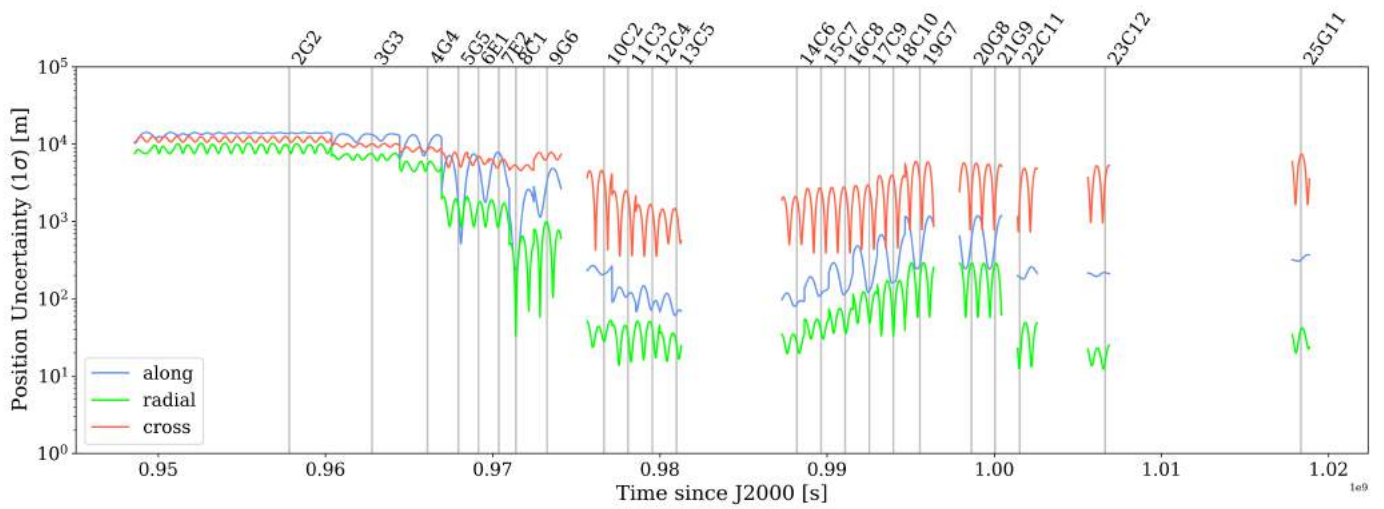
(b) Uncertainty evolution of Io position, under the impact of the transfer factor at  $f = 3$ .



(c) Uncertainty evolution of Europa position, under the impact of the transfer factor at  $f = 3$ .



(d) Uncertainty evolution of Ganymede position, under the impact of the transfer factor at  $f = 3$ .



(e) Uncertainty evolution of Callisto position, under the impact of the transfer factor at  $f = 3$ .

Figure B.15: Knowledge evolution of the JUICE-Jovian system, as computed by the Nav OD setup with a transfer factor of  $f = 3$ . Similar to the baseline case, numerical instabilities produce erratic features in the early mission stage. Vertical lines mark the time of moon encounter on each considered arc.

# 3

## Conclusions & Recommendations

This chapter draws conclusions (section 3.1) with respect to the research questions and gives recommendations for future work (section 3.2).

### 3.1. Conclusions

The conclusions of the work address the research questions from section 1.1. Sub-questions are addressed first, the answers to which will then be used to motivate the conclusions on the leading and extended research questions. Note that the statements made in this section are supported by results and discussions in the journal paper (Chapter 2).

#### **Q1. How can external ephemerides be integrated into the GNC operations of the JUICE mission?**

Studying publications of the GNC operations during the Cassini multi-flyby tour, two options were identified to be applicable to the JUICE operations: The first option introduced external ephemerides into the navigational orbit determination (OD) setup as fixed parameters, entirely eliminating the need for moon state estimation; uncertainties associated with the external ephemeris product are accounted for as consider parameters. The second option uses the external ephemerides to derive an a-priori guess of the moon state parameters, which apply to the regularisation of the moon state estimation in the navigation OD. The latter is chosen as the preferred option for this analysis, because it is less prone to inconsistencies and instabilities in the navigation OD solution.

#### **Q2. How strongly is the statistical $\Delta V$ expense of corrective manoeuvres driven by moon state uncertainty?**

The statistical  $\Delta V$  expense of the post-flyby corrective manoeuvre is generally most sensitive to moon state uncertainties. However, it was found that moon ephemeris quality only has an appreciable effect on the magnitude of these manoeuvres, when the given flyby moon is encountered for the first or (in the case of Europa) the second time. Assuming perfect moon state knowledge, the cost of correcting trajectory dispersion after the first considered Ganymede encounter (2G2) were cut by 43%; 61% and 20% savings could be possible on the first (6E1) and second (7E2) encounter of Europa, respectively. The  $\Delta V$  cost reductions from perfect moon knowledge on subsequent arcs were found to be in the low single-digit percentages, resulting in total theoretical limit of 15.6 m/s on the clean-up manoeuvre  $\Delta V$  savings. This can be linked to the characteristics of the navigation OD solution, which the manoeuvre cost computation is based on. The navigation OD displays a strong capability to rapidly constrain the moon state knowledge: from first encounter with a moon, the moon state uncertainties are reduced to levels in which they do no longer exert an significant effect on the downstream flyby dispersion and the associated corrective manoeuvre.

This may in fact be an overestimation of the state knowledge improvement by the OD covariance analysis, which is based on the assumptions of perfect dynamical and observational models. To partially counteract the undesired effects of these idealisations, an empirical penalty was applied to the navigation-internal moon knowledge transfer ("transfer factor"), which effectively prevented the strong uncertainty reductions of moon knowledge from individual encounters from persisting over the full remainder of the tour. This practice mitigates the rapid constraining of moon state knowledge, which gives rise to more opportunity for moon knowledge driven  $\Delta V$  savings.

**Q3. How does the in-mission uncertainty evolution of the radio science ephemeris solution compare to the moon knowledge improvement from the navigation operations?**

Comparison of the moon knowledge evolution was done ignoring operational constraints, most notably data cut-off lags for the data transfer and in-mission generation of the external radio science ephemeris products. Despite this assumption, it was found that the uncertainty levels of these ephemerides are all around higher than those associated with the moon knowledge evolution from navigation operations. During the early mission stages, the average position uncertainty ( $1\sigma$ ) levels of the encountered Galilean moons are larger by factors as high as two (with  $1\sigma$  values in the order of 0.1 to 10 km), while the disadvantage with regards to Io (no direct encounters) is at a factor of four in the along-track sense of the moon's orbit. During the mid-section and late stage of the tour, the radio science ephemeris uncertainties converge towards the levels of the navigation solution, where  $1\sigma$  values are in the order of tens of metres to a few hundred meters for the multi-flyby bodies Ganymede and Callisto. Only for few components, exclusively in the out-of-plane moon position, do the uncertainty levels of the radio science ephemerides drop slightly below the navigational ones. These findings were not in agreement with our expectations, as the radio science moon ephemerides, which are based on more accurate data from 3GM, were expected to outperform the navigational moon knowledge evolution. The reason for this observation was identified and will be addressed in the context of the extended research question.

**Q4. To what extent can external ephemeris updates effectuate  $\Delta V$  savings by improving moon knowledge? At what point in time are ephemeris updates most effective?**

As was mentioned in the context of Q2, the largest - and only truly significant - potential for saving on the statistical  $\Delta V$  cost was identified to be during the first few moon encounters. At the same time, it was found that the in-mission radio science ephemeris products cannot compete with the early-mission uncertainty levels of the navigation solution (see Q3). It is therefore not able to effectuate any of the restricted opportunities for  $\Delta V$  savings. Applying the "transfer factor" at a value of  $f=3$  to the navigation OD solution, new opportunities arise. In this case, external moon ephemeris updates were found to yield  $\Delta V$  savings between 3 and 5% on corrective manoeuvres after flybys 18C10 and 22C11, which sum up to a total saving of 0.43 m/s. Considering that these small benefits will be further degraded by the operational constraints of external update implementation, and the adverse downstream effects of the particular updates, these findings are insufficient to support the case for an implementation of external moon ephemeris updates.

Based on these conclusions, the leading research question can be addressed:

**Leading Research Question**

To what extent can in-mission ephemeris updates be used in the JUICE GNC operations to relax the constraints on the mission's statistical  $\Delta V$  budget?

The extent to which in-mission ephemeris updates can be used in the JUICE GNC operations to relax the constraints on the mission's statistical  $\Delta V$  is essentially negligible and does not give grounds for the implementation of such external ephemeris updates. This follows from the findings that

- a) moon ephemeris knowledge only impacts post-fly corrective manoeuvres on the first Ganymede encounter and the first and second Europa encounter
- b) the in-mission radio science ephemerides, that were chosen to evaluate external ephemeris updates, constrain moon state knowledge more slowly than the navigation-internal moon knowledge improvement

A more effective way to effectuate statistical  $\Delta V$  savings could be to further improve the moon state knowledge prior to the mission. This could be achieved from the use of ground-based astronomy and Europa Clipper data, which will become available before JUICE's arrival in the Jovian system.

The findings of this work, especially navigation OD's pronounced ability to rapidly constrain moon state knowledge motivate the extension of the research scope, resulting in the extended research question:

**Extended Research Question**

How do JUICE navigation tracking data and 3GM radio science experiment products complement each other and how could such data synergies be exploited?

It was shown that the navigational tracking data, despite having much higher noise levels than the science data from 3GM, captures system information that the science data is less sensitive to. Specifically, the range-rate measurements of the spacecraft at epochs far downstream of the flybys were found to be very effective at constraining the initial, upstream spacecraft state. Through the close encounter with the flyby body and its dynamical coupling with the other moons, this enables an accurate determination of the natural bodies in the system. Moreover, the large volume of range-rate measurements upstream of the first two Ganymede flybys appears to capture the dynamical signature of all Galilean moons, including Io which - apart from OpNav measurements - is not directly observed. The navigation tracking data and especially its early-mission subset could therefore be an interesting component in the post-mission generation of high-fidelity moon ephemerides.

**3.2. Recommendations for future work**

- During the course of this work, selected characteristics of the navigation data set were analysed. For the reasons mentioned throughout the applicable sections, it is believed that a subset of this data can be a valuable addition to the post-mission ephemeris solution. The potential benefits, that the data could bring to the moon ephemerides could be evaluated in a covariance analysis similar to Dirkx et al., 2017 and Fayolle et al., 2022. A positive outcome of this study could motivate the effort that is required to pre-process this data for the concurrent inversion with the other observation sets.
- The conclusions of this work were derived using an approximate re-construction of the operational statistical  $\Delta V$  analysis of the ESOC Mission Analysis group. The implementation effort and the impact of model simplifications (omitting Optical Navigation measurements, ignoring manoeuvre execution errors, simplifying the TCM targeting scheme and focus on clean-up TCMs) were carefully traded off, and the results of the analysis are believed to be valid. Nonetheless, it is encouraged to bring together the newest high-fidelity ephemeris solutions from Fayolle et al., 2022 and the original ESOC mission analysis software, and to repeat this analysis.
- The mission profile that was chosen for this analysis (CReMA 3.2) is outdated by the time this work is being concluded. Repetition of the analysis using the most recent (and likely final) JUICE mission profile (CReMA 5.0) is not expected to fundamentally change the outcome of this analysis, but is recommended nonetheless.
- This work has found that the most effective way to reduce statistical  $\Delta V$  expenditure during the JUICE multi-flyby tour is to improve the moon ephemerides prior to the mission. In order to do so, astrometric measurements of occultations and mutual approximations (Morgado et al., 2019, Fayolle et al., 2021), as well as Europa Clipper radio science data (Tarzi et al., 2019; Verma and Margot, 2018), could be integrated into the existing ephemerides from the IMCCE (Lainey et al., 2004b). This possibility is already considered by the IMCCE and ESOC and an investigation on the effect of the future observation is in progress (ESOC, 2017–2019). Upon completion of this analysis, the statistical  $\Delta V$  budget of the JUICE mission can (and will) be re-evaluated.



# A

## Numerical implementation of the JUICE mission trajectory

In the following the details of the numerical modelling of the JUICE mission trajectory are presented. Appendix A.1 discusses how the mission was reduced to a series of simplified arcs, that could easily be used for the analysis. Appendix A.2 gives the conditions for which the numerical setup, *i.e.* propagator and integrator, were tuned.

### A.1. Mission trajectory simplifications

Starting from the CReMA 3.2 spice kernels, the JUICE mission trajectory was reconstructed in a slightly modified form. This reconstruction aims to create the simplest version of the mission trajectory, that adequately supports the moon orbit determination (OD) from spacecraft tracking. Since it is assumed that the mission sections without any close moon encounters do not contribute significantly to the moon OD solutions, these sections will not be included in the reconstruction. First, all close encounters ( $h < 20000$  km) are identified on the spice trajectory; epoch and system state at point of closest approach are retrieved. Pre- and post-flyby apojove epochs and system states are likewise retrieved from spice. The pre-flyby apojove state, from which a "freely" propagated spacecraft will satisfy the spice flyby conditions. From this state, the spacecraft is then freely propagated through the point of closest approach to the post-flyby apojove; the resulting trajectory constitutes a "flyby arc". This way the JUICE flyby-tour trajectory was reduced to a sequence of simplified, manoeuvre-less flyby-arcs, where subsequent flyby arcs do not necessarily connect to each other continuously. The reconstructed mission trajectory is visualised in fig. A.1.

It is important to note that the trajectory reconstruction into a discontinuous sequence of "flyby arcs" applies only to the spacecraft trajectory. Moon dynamics are not affected by this division and can easily be propagated across and between these arcs.

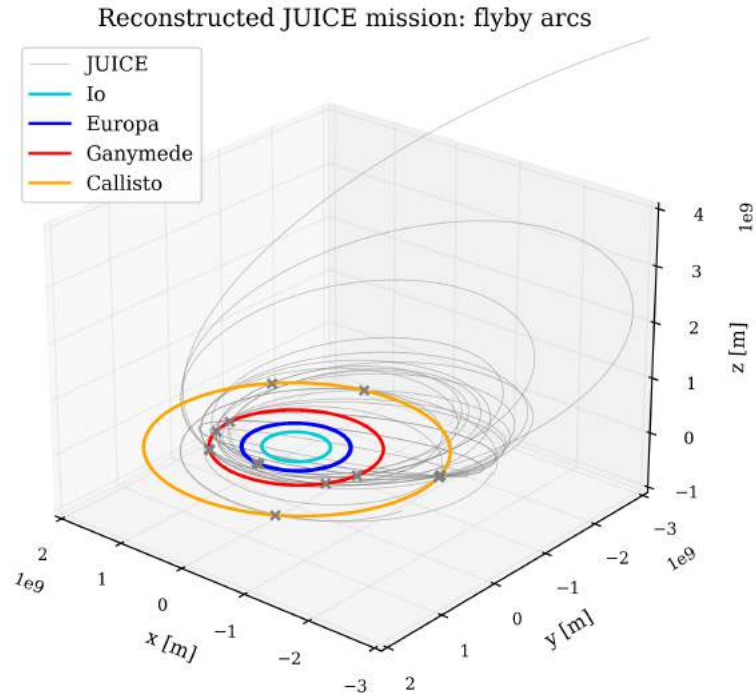


Figure A.1: Visualisation of the JUICE mission reconstruction using a non-continuous sequence of flyby arcs. For each arc the close encounter is marked by an X.

Modelling the flyby arcs by freely propagating the spacecraft means that any manoeuvres are omitted from the spacecraft dynamics, which naturally leads to a deviation between spice reference trajectory and the modelled flyby arcs. This also leads to a simplified orbit determination setup which will not be able to consider manoeuvre execution errors in the estimation. This simplification and the associated consequences for the OD solution have to be accepted, because a proper identification and implementation of all deterministic manoeuvres, as well as the coupling (journal paper, section 3.3) required for the modelling of stochastic correction manoeuvres, exceed the scope of this work.

Figure A.2 shows the extend of the deviations between the spice trajectory and modelled flyby arcs up- and downstream of the flyby epoch. The maximum position deviations occur at the far ends of the arc, with most values well below  $10^7$  m (outlier arc 2G2 has deviations up to  $10^8$  m). In order to judge the significance of these numbers appropriately, the deviations can be expressed as a percentage of the total distance between spacecraft and flyby moon. This way maximum deviations are found to be smaller than 1% for most arcs, with a few (5) arcs in single-digit percentages. Since the simplified flyby arcs were constrained at the point of closest approach and the deviations from the spice trajectory at the far ends of the arcs are relatively small, the modelled flyby arcs are expected to undergo the same dynamical influence of the natural bodies in the system and can be considered representative of the original mission trajectory for the sake of the orbit determination.

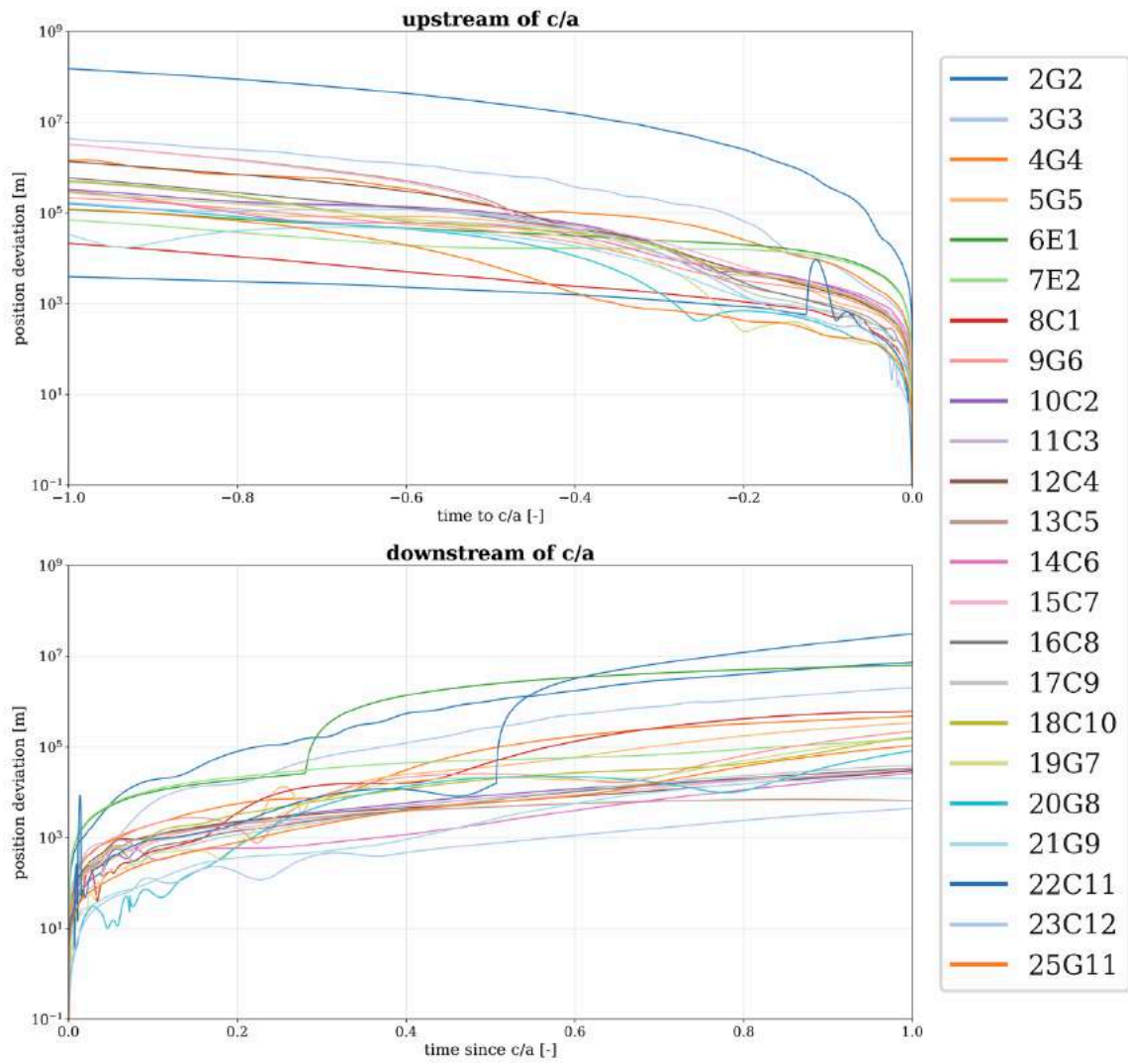


Figure A.2: Deviations between spice trajectory and the simplified flyby arcs, measured on the relative position of spacecraft to the given flyby body. In order to accommodate all flyby arcs of greatly varying length into one plot, the timescale on the x-axis were normalised by the duration of each arc. Reaction wheel saturation manoeuvres affect the trajectory only locally; their omission does therefore not result in a secular growth of position deviations. Omitted trajectory shaping manoeuvres can be identified at the onset of growing position deviations. The propagated flyby arcs for this comparison were computed using the benchmark integrator settings, that are introduced in appendix A.2.

## A.2. Integrator & Propagator selection

This section addresses the tuning of the numerical solver, that is employed for the propagation of spacecraft and moon dynamics on the flyby arcs. The requirements on the solver are defined to enforce the flyby conditions adequately. The solver is tuned to meet these requirements. A benchmark is established to quantify the numerical error and to show that it lies well below the modelling errors that were introduced by the omission of manoeuvres from the spacecraft dynamics.

### A.2.1. Requirements on numerical solver

During propagation of long flyby arcs accelerations are almost constant for the longest part of the arc and then change rapidly on a small section around closest approach. The computational effort, which - using a sufficiently small fixed step size - can become a limiting factor in the analysis, can be alleviated very well by use of variable step size integrators.

The primary requirement on the integrator and step size control choice is to guarantee that the system state at closest approach is constrained to the spice reference value. This requires the scheme to produce a sufficiently consistent solution between propagating from closest approach to pre-flyby apojoove (backwards in time) and propagating from pre-flyby apojoove to closest approach. The requirement allows for:

- a maximum deviation of 10% or 100 km from the nominal flyby altitude - this requirement effectively ensures that the acceleration, experienced by the spacecraft due to the flyby body gravitational parameter does not deviate by more than 5%.
- a maximum deviation of 5 minutes from the nominal flyby epoch - this requirement acts as an additional constraint to ensure the also the point of closest approach (w.r.t. to the flyby body coordinates) does not deviate too much from the reference trajectory.

Appendix A.2.2 shows how integrator and step size control scheme were tuned to fulfil this requirement.

The geometry of the flyby arcs does not call for special requirements on the propagator. The standard Cowell propagator, which formulates the equations of motion in the cartesian coordinates of a quasi-inertial Jovicentric reference frame, is used.

### A.2.2. Integrator settings selection

The Runge-Kutta-Fehlberg 7(8) method is adopted as an competitive and robust variable step size integrator scheme. The integrator scheme was initiated with lenient constraints on relative, absolute tolerances, and minimum step size, which are the free settings that are to be found in the tuning process. The maximum step size was fixed at 1000s, to avoid interpolation issues during the creation of the synthetic observables (at a cadence of 3600s). Then the following algorithm was used to tune the free integrator settings:

1. Starting from the spice state of the JUICE-Jovian system at closest approach, it was used to propagate the system state backwards in time to the pre-flyby apojoove, which marks the beginning of the given flyby arc. The propagated system state at pre-flyby apojoove is recorded.
2. The numerical solver is re-initialised with identical settings to propagate the recorded pre-flyby system state along the entire length of the flyby arc. During the full propagation, the spacecraft distance from the flyby body surface (flyby altitude) is monitored and its minimum value is recorded.
3. The occurrence of the minimum value marks the propagated point of closest approach. The minimum altitude, and the epoch at which it was detected, is compared to the nominal flyby conditions from spice. Based on this comparison, it is evaluated if the propagated flyby is constrained to the nominal flyby conditions according to the requirements (appendix A.2.1).
4. If the requirements are met, the integrator settings are stored and the propagated flyby arc is saved as the numerical reference trajectory. If any of the requirements are not fulfilled, the integrator settings are incrementally made more stringent and the process is repeated.

After integrator settings were tuned for each arc, the most stringent settings were identified and adopted for all arc. The final integrator configuration is given in table A.1. It should be noted that during generation of synthetic 3GM data, that is generated at a much higher cadence (60s), the maximum time step was adjusted to a value of 30s.

integrator scheme	order	max. step size	min step size	abs. tolerance	rel. tolerance
Runge-Kutta-Fehlberg	7(8)	1000 s	n/a	1e-10	1e-10

Table A.1: Summary of the final integrator settings.

### A.2.3. Numerical accuracy quantification

To quantify the numerical accuracy of the solver settings in table A.1, a benchmark, that acts like a numerical ground truth, has to be established. This was done by employing the same integrator scheme, but limiting it to the smallest, fixed step size that is truncation error dominated. The transition between rounding and truncation error domain was found by comparing the maximum deviation from various fixed step settings against a very conservative step of  $\Delta t = 10$ s. Due to the computational burden of fixed step size integration at small  $\Delta t$ , this analysis had to be performed over a shortened 8h section of the flyby arcs ( $\pm 4$ h around closest approach). It was conducted for three representative arcs, one per each flyby body. The outcome, which is presented by fig. A.3, suggests that a  $\Delta t = 120$  s is a suitable choice for all considered arcs.

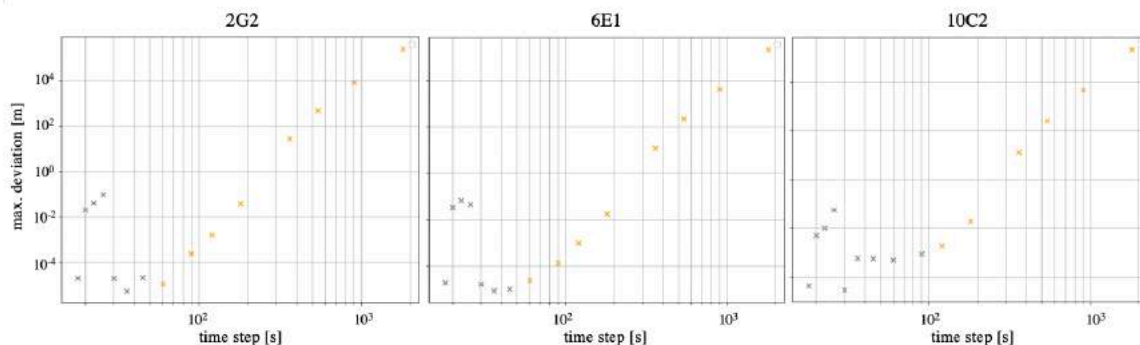


Figure A.3: Maximum position deviation (spacecraft w.r.t. flyby body) between candidate time step and conservative reference time step. Truncation error dominated samples form a linear trend of slope  $p-1$  (with  $p = 8$ ) on the Log-Log scale. These samples are highlighted by orange markers. Samples that lie within the rounding error domain are characterised by random walk and are marked in grey.

Using this fixed step size of  $\Delta t = 120$  s, a numerical ground truth was established for each flyby arc. The accuracy of the selected numerical solver (table A.1) evaluated against the numerical ground truth trajectories and the results are shown in fig. A.4. Comparison with the model accuracy in fig. A.2, it can be seen that the numerical errors are orders of magnitude smaller. It is therefore concluded that the integrator settings are suitable.

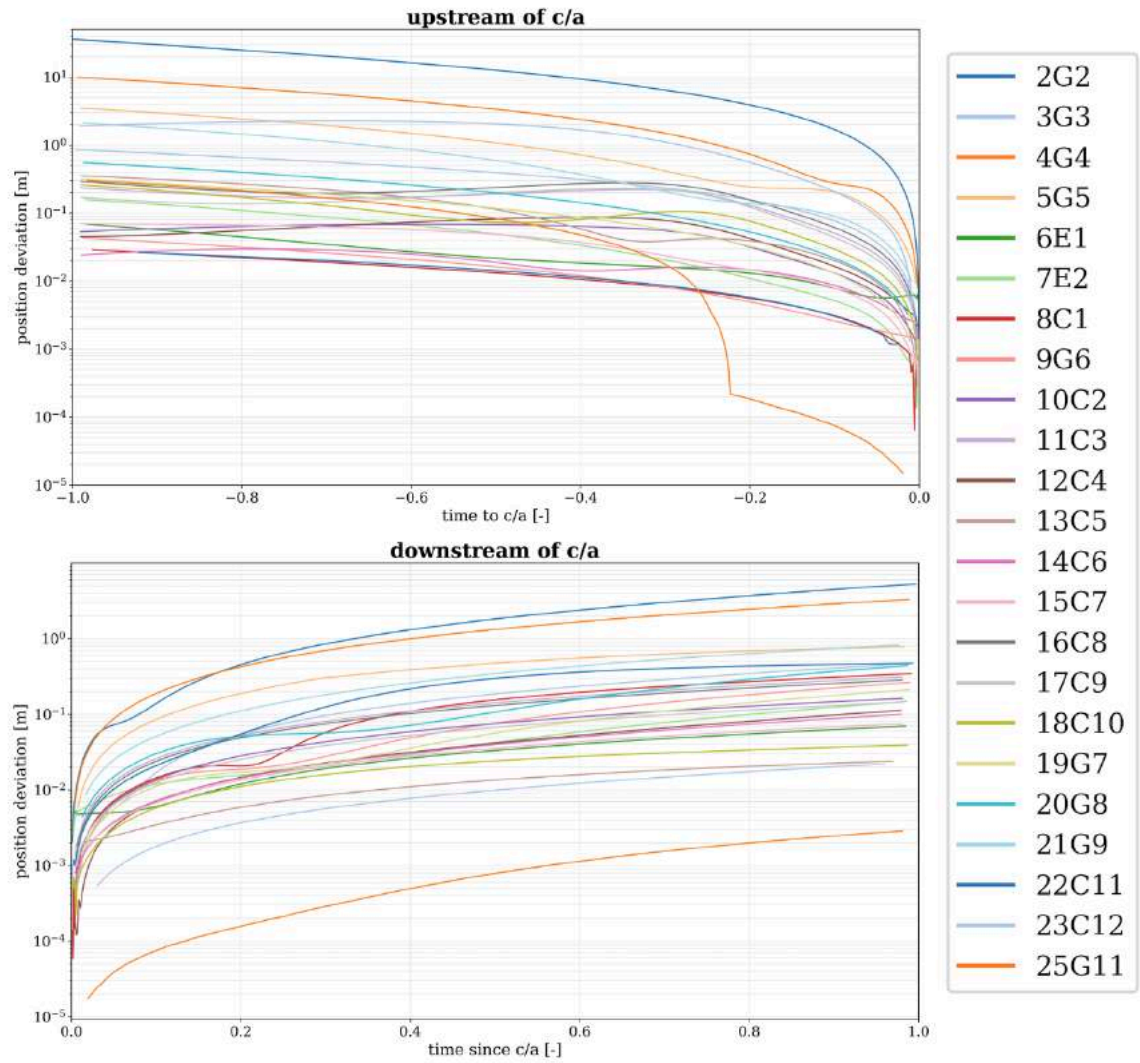


Figure A.4: Deviations between numerical ground truth and arcs from the selected integrator settings (table A.1), measured on the relative position of spacecraft to the given flyby body. In order to accommodate all flyby arcs of greatly varying length, the timescale on the x-axis were normalised by the duration of each arc.

# B

## Verification & Validation

This chapter outlines the steps taken to validate the methodology and its numerical implementation in this work. All simulations have relied on the *tudat* software developed at the Astrodynamics & Space Missions department of Delft University of Technology<sup>1</sup>. *tudat* was used to facilitate the numerical simulation of the JUICE-Jovian system dynamics, which is underlying all orbit determination and manoeuvre design calculations. Observation simulation and parameter estimation tools were taken from *tudat* alike. The software undergoes verification tests upon installation, and has been used for earlier publications in the field of orbit determination (Bauer et al., 2016; Dirkx et al., 2014; Dirkx et al., 2017). Validating the software itself is therefore deemed unnecessary. Nonetheless, the implementation of the navigation OD is validated in appendix B.1 and the manoeuvre design algorithm is verified in appendix B.2.

### B.1. Verification & Validation: Navigation OD

As was mentioned multiple times in the journal paper (Chapter 2), a critical aspect of the conducted analysis is the validity of the implemented navigation OD. The validity is in this case defined via the qualitative and quantitative similarity of its OD solutions w.r.t. the reference OD from ESOC, 2017–2019, specifically on the uncertainty evolution of the Galilean moons' states. The extend of similarity is examined in appendix B.1.2. Furthermore, indicators for the instability of the OD solution were observed in the process. This issue is addressed in appendix B.1.1, where these indicators are investigated and their impact on the validity of the analysis is examined.

#### B.1.1. Consistency of Navigation OD Results (Verification)

Before validation by comparison with the reference uncertainty levels, the internal consistency of our navigation OD solutions is investigated. It was found that the OD solution is not stable throughout the entire tour - the inversion of the normal equations on many arcs is characterised by condition numbers exceeding the numerical limit of the machine. This is not surprising, given that the state of multiple bodies, some of which are strongly dynamically coupled, is to be estimated from a lobe-sided set of observations. It is suspected that the use of OpNavs, which - especially when targeting Io - balances the distribution of observations, can mitigate the instabilities and that the reference OD setup therefore does not experience this issue to the same extent.

The instabilities manifest themselves in the occurrence of post-fit covariance with invalid properties, such as negative entries on the diagonals ( $\sigma_i^2 < 0$ ) and correlation coefficients larger than one ( $|\rho_{ij}| > 1$ ). The first instance of an invalid post-fit covariance was identified to occur over arc 5G5 ( $\sigma_i^2 < 0$ , where  $i$  refers to a Ganymede state component), followed by arcs 6E1 and 7E2 (also  $\sigma_i^2 < 0$ , on Ganymede state components). As a consequence, the Ganymede ephemeris uncertainty cannot be reliably described over this period, the uncertainty evolution is characterised by erratic features (see fig. B.5). Within the time-constraints of the analysis, it was not possible to implement OpNavs for the mitigation of this issue. Other mitigation strategies were considered, but were found to be incompatible with the required similarity between the implemented OD setup and the reference. Instead, state estimates that are associated with such invalid post-fit covariances, that means specifically Ganymede state estimates on arcs 5G5, 6E1 and 7E2, must be deemed uninterpretable.

---

<sup>1</sup>Documentation and user guide can be found at: <https://tudat-space.readthedocs.io/en/latest/>

On arc 5G5, the Ganymede flyby couples spacecraft dynamics to the corrupted Ganymede state estimate. The spacecraft trajectory estimate thus shows similar erratic features fig. B.7. Since state estimate of spacecraft and flyby body form the basis of the computation of statistical manoeuvre cost on the arcs, this arc cannot be considered in the statistical  $\Delta V$  analysis.

Given the applicable a-priori strategy, in which post-fit moon covariance is passed on to act as a-priori covariance for the subsequent arc, the invalid estimates from arcs 5G5, 6E1 and 7E2 can result in a-priori covariances of invalid nature. To ensure the interpretability of the estimates on subsequent arcs, it must therefore be examined to what extent OD solutions can be considered correct, when based on an a-priori covariance of invalid nature. Specifically, the scope of the comparative statistical  $\Delta V$  analysis requires the "arc-relevant" estimate, *i.e.* the estimate of the flyby body as well as the spacecraft, to be quantitatively correct. It is thus most important to examine the impact of invalid a-priori covariance features on the arc-relevant components of the estimate. Hereafter, the covariance entries of the flyby body are indicated by subscript  $k$ , and the corresponding indices by the set  $\mathcal{K}$ , while entries associated with the spacecraft are indicated by the subscript  $sc$ . For the examination, an inventory of the invalid features in the a-priori covariance matrix of each arc was made (table B.1). The following distinction proved useful:

**degree 1** invalid by  $|\rho_{ij}| > 1$ , where  $i, j \notin \mathcal{K}$

**degree 2** invalid by  $\sigma_i^2 < 0$ , where  $i \notin \mathcal{K}$

**degree 3** invalid by  $\sigma_i^2 < 0$  and / or  $|\rho_{ij}| > 1$ , where  $i \in \mathcal{K}$  or  $j \in \mathcal{K}$

For invalid a-priori covariances of **degree 1** and **degree 2**, a test was constructed, that follows the following argument: By eliminating the invalid features, while affecting the regularising of the arc-relevant uncertainty as little as possible, one can establish a way to artificially correct corrupted a-priori covariances.

$$\mathbf{P}_0^* = \mathcal{C}(\mathbf{P}_0) \quad (\text{B.1})$$

If the invalid entries of the original a-priori matrix have affected the arc-relevant estimates in a significant way, one would be able to observe a notable difference in the associated components of the post-fit covariance, which is based on the artificially corrected a-priori. If the notable difference is not observable, it can be concluded that the invalid entries do not have a significant impact on the arc-relevant estimate. For this comparison, the focus is put on the diagonal entries of the post-fit covariance, which contain the uncertainties  $\sigma$  of each state component. The condition, which has to be satisfied for showing a negligible effect of the corrupted a-priori entries is formulated in eq. (B.2).

$$\sigma_{sc}^* \approx \sigma_{sc} \quad (\text{B.2})$$

$$\sigma_k^* \approx \sigma_k \quad (\text{B.3})$$

where  $\sigma^*$  and  $\sigma$  are the uncertainties obtained from estimating with the artificially corrected ( $\mathbf{P}_0^*$ ) and original a-priori covariance ( $\mathbf{P}_0$ ), respectively.

The test requires a scheme  $\mathcal{C}$  for artificially correcting a-priori covariances that are corrupted by degree 1 and/or degree 2. This is done by first identifying which bodies are associated with the invalid covariance entries. Then, all entries associated with this body (these bodies) are replaced by a conservative, uncorrelated covariance, which is taken to be the IMCCE base covariance (Lainey et al., 2004b, see also Chapter 2). An example of this artificial correction is shown in fig. B.1: all entries that are associated with the corrupted body (here Ganymede) are replaced by the uncorrelated base covariance. Since all covariance entries in fig. B.1 are normalised, it does not become apparent that the correction results in much larger a-priori formal errors for the corrupted body. Using this method, an artificially corrected a-priori covariance  $\mathbf{P}_0^*$  regularises the estimate of the corrupted bodies differently, such that they cannot be compared to the original. The test therefore only applies, when the corrupted bodies do not include the flyby body, *i.e.* only corruption by degree 1 and 2.

This test was performed over all arcs following flyby 7E2. Figure B.2 shows an exemplary excerpt of three arcs from the analysis - one example of a degree 2 case (8C1), and two examples of degree 1 cases (15C7, 20G8) with two different flyby bodies (Callisto and Ganymede). As can be seen by inspection of fig. B.2, it was found that in all cases the estimates based on the artificially corrected a-priori match the original estimates very well. The uncertainties of arc-relevant entries differ by factors  $< 1.4$  for the flyby bodies, while

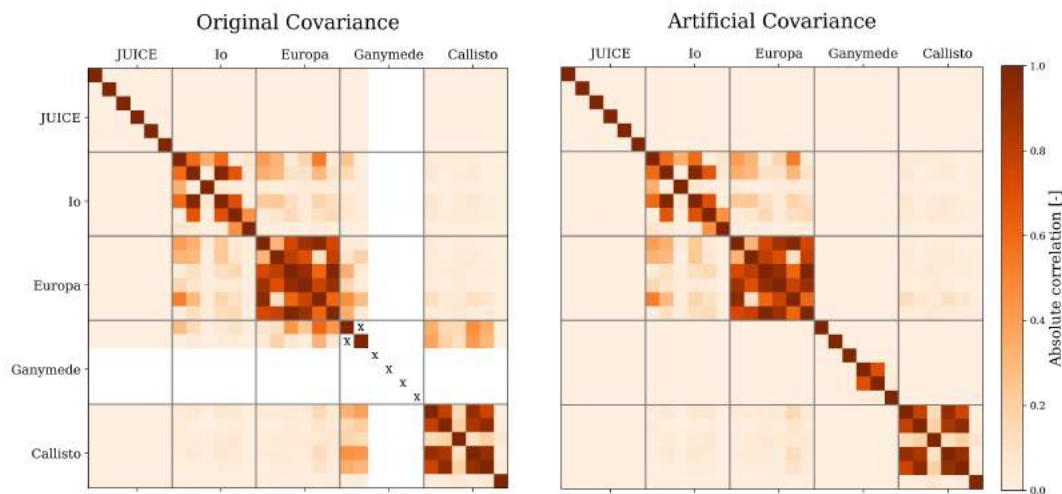


Figure B.1: Illustration of the correction scheme  $\mathcal{C}$  on arc 8C1, showing the normalised a-priori covariance (correlation) matrix before and after correction. Note that before correction, the a-priori matrix is corrupted by degree 1 (in-plane Ganymede correlations), as well as degree 2 (negative variances on the remaining Ganymede state components). The artificially corrected covariance does not contain any invalid entries and the regularisation of the flyby body (Callisto) is altered as little as possible.

the spacecraft state uncertainty (which is the driving component of the  $c/u$  manoeuvre cost) only differs by single-digit percentages. Uncertainties of the corrupted bodies, which as a consequence of the correction method are regularised differently, form the expected exception. It can thus be concluded that in-valid a-priori covariances, that are corrupted by degree 1 and 2 do not affect the covariance of the resulting estimate for the sake of the statistical  $\Delta V$  analysis.

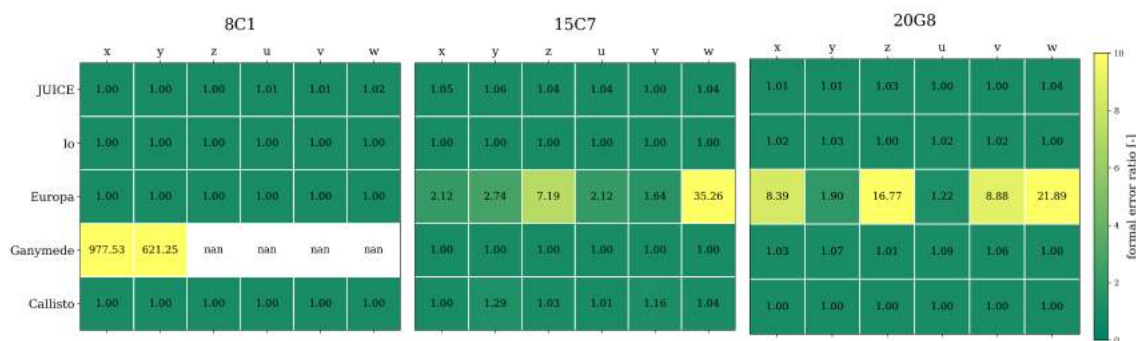


Figure B.2: Uncertainty ratio  $\sigma^* / \sigma$  for three exemplary arcs. The examples were chosen to show a degree 2 case (8C1), and two examples of degree 1 cases (15C7, 20G8) with two different flyby bodies (Callisto and Ganymede). Ratios close to unity indicate that the estimate of the associated system state component is not affected by the corrupted a-priori. Ratios associated with the corrupted body are - as expected - significantly greater than unity. Nan values in the comparison of Ganymede state components on 8C1 are caused by the  $\sigma^2 < 0$  in the estimate covariance, which follow from the degree 2 corruption of the 8C1 a-priori covariance.

For selected arcs, however, it is the a-priori entries of the flyby body that are corrupted (**degree 3**, table B.1). As previously mentioned, the test is not designed for such cases and it cannot be shown that the resulting estimates are quantitatively correct. Note that this does not necessarily mean that the resulting estimates are incorrect. Taking for example the ephemeris uncertainty of Ganymede on arc 9G6, it was found that it is based on a degree 3 corrupted a-priori covariance (see table B.1). By inspection of fig. B.5, however,

the evolution of the Ganymede ephemeris can be seen to qualitatively match that of the reference OD solution and is quantitatively comparable (different by a factor of 2). Since the effect of the corrupted a-priori on this estimate cannot be systematically examined, this arc is nonetheless excluded from the computation of statistical  $\Delta V$ .

arc id	Navigation OD		External OD		DV comparison
	valid	invalid	valid	invalid	
2G2	x		n/a	n/a	n/a
3G3		degree 1	x		x
4G4		degree 1	x		x
5G5	-	-		degree3	
6E1		degree 2		degree 1+2	x
7E2		degree 2		degree 1+2	x
8C1		degree 2		degree 1	x
9G6		degree3		degree 1	
10C2	x			degree3	
11C3		degree 1		degree 1+2	x
12C4		degree 1		degree 1	x
13C5		degree 1		degree 1+2	x
14C6		degree 1		degree3	
15C7		degree 1		degree 1+2	x
16C8		degree 1		degree3	
17C9	x			degree3	
18C10	x			degree 1+2	x
19G7	x			degree3	
20G8		degree 1		degree3	
21G9		degree 1		degree 1	x
22C11	x			degree 1	x
23C12		degree 1		degree 1+2	x
25G11				degree3	

Table B.1: Inventory of invalid elements in a-priori covariance - for navigation OD solution and external ephemeris, per arc. The last column indicates the arcs where both solutions are deemed interpretable and where a comparison of the manoeuvre cost is possible.

It is emphasised that the conditions in eq. (B.2) do not test for the characteristics of a particular a-priori covariance, but of the arc's sensitivity to invalid features in the a-priori covariance. It was concluded that the inversion on any arc works sufficiently well with a-priori corruptions of degree 1 and 2, regardless of the origin of the a-priori covariance. This means that a moon ephemeris update via the external ephemeris interface can be considered, so as long as the a-priori covariance derived from the external ephemeris is either uncorrupted or classifies as degree 1 or degree 2 corrupted. This requirement results in a drastic reduction of moon ephemeris update opportunities that can be evaluated in this work. The opportunities are indicated in the right-most column of table B.1.

### B.1.2. Comparison to reference data (Validation)

The analysis in appendix B.1.1 has confirmed the internal consistency of the Nav OD solutions over wide stretches of the flyby tour, with the exception of the flyby sequence 5G5-6E1-7E2, during which Ganymede and spacecraft state estimates must not be interpreted. It already referred to fig. B.5, where it can be seen that over the given stretch the behaviour of the uncertainty evolution is erratic and does not match that of the reference solution. For the remainder of the tour, Nav OD solutions were compared closely to the solutions of the reference setup. The comparison is based on figs. B.3 to B.6, each of which shows the two OD solutions for one body side by side. Results of our OD implementation were plotted such that a visual comparison with the reference graphs is as easy as possible.

Before diving into the comparison, it is worth pointing out the following difference: the reference graphs show the instantaneous knowledge moons' states, while the results of the implementation show the arc-wise post-fit knowledge. When comparing the two, one can expect the instantaneous uncertainty levels at the beginning of each arc to be larger than the post-fit ones, while approaching them towards the end of the arc. One can also observe some visible difference between Io's position uncertainty evolution. These are likely

due to the absence of OpNavs in the implemented Nav OD.

The mid- and late-tour phases, that are dominated by the long sequence of Callisto flybys are at focus of the comparative statistical  $\Delta V$  analysis. It should be noted that especially for these phases, the Callisto reference uncertainties are matched very nicely. This holds also true for the Ganymede position uncertainties in the late mission phase, although in-plane components are estimated at a slightly more optimistic uncertainty than the reference.

From the quantitative comparison of predicted uncertainty levels in the analysis-critical domains, it can be concluded that the implemented OD qualifies for the computation of a baseline statistical  $\Delta V$  budget and constitutes a valid baseline for the comparison with external moon ephemerides.

Considering the qualitative similarities, e.g. in terms of the general uncertainty trends and features over the course of the whole flyby tour, the implementation can furthermore be assumed to exert the same mechanisms and to exhibit the same behaviour when subjected to modifications, such as added estimation parameters or empirical factors. This property was exploited for extending the scope of the analysis, examining the OD solution sensitivity to model fidelity (by introducing the transfer factor, gravitational parameter estimation).

A visual comparison of the spacecraft OD solutions from the two OD setups (see fig. B.7) is more difficult. In both cases, the state uncertainty fluctuates greatly on each arcs. Again, it can be concluded that the main features, that is the trends of the along, radial and cross components, are matched. It must also be noticed, that the implemented model features more pronounced uncertainty dips on and around closest approach points, and that it appears to have an amplified improvement of the overall sc knowledge over the course of the tour. This could be at least partially related to the different filter types, where in the sequential filter the spacecraft knowledge is forced to be close to the *base* a-priori uncertainty (Chapter 2) at the beginning of each arc. Additionally, the omission of corrective (TCMs) and deep space manoeuvres (DSMs) as well as reaction wheel de-saturation burns, which are all included in the JUICE reference OD solution could contribute to this. As has been mentioned on previous occasion, the comparative statistical  $\Delta V$  analysis does not require strict quantitative equivalence of the spacecraft trajectory uncertainties between the implemented and reference model.

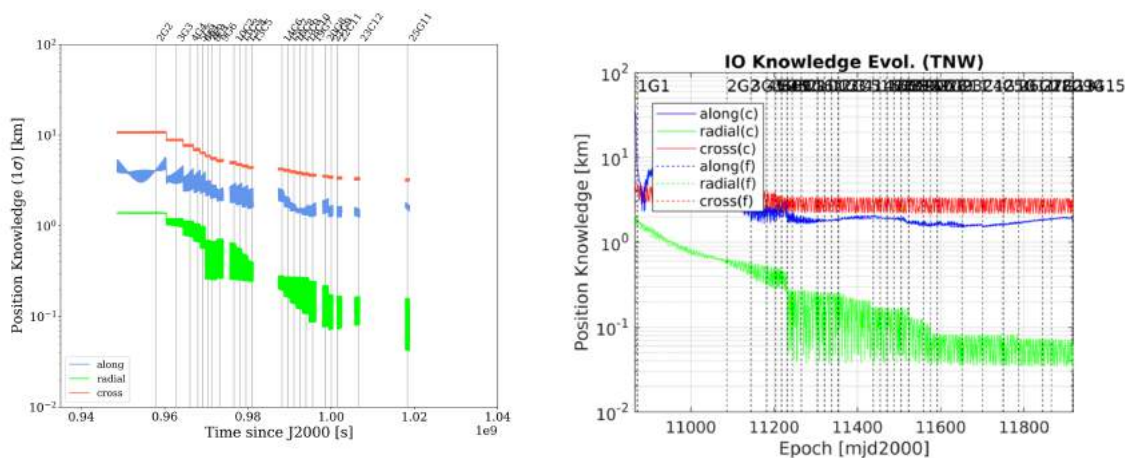


Figure B.3: Uncertainty evolution of Io ephemeris from implemented model (left) and reference (right).

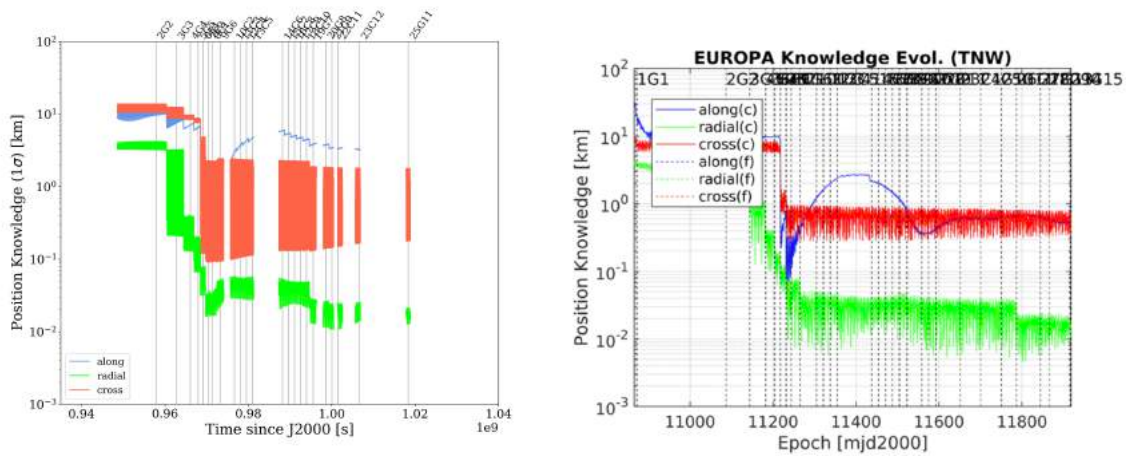


Figure B.4: Uncertainty evolution of Europa ephemeris from implemented model (left) and reference (right).

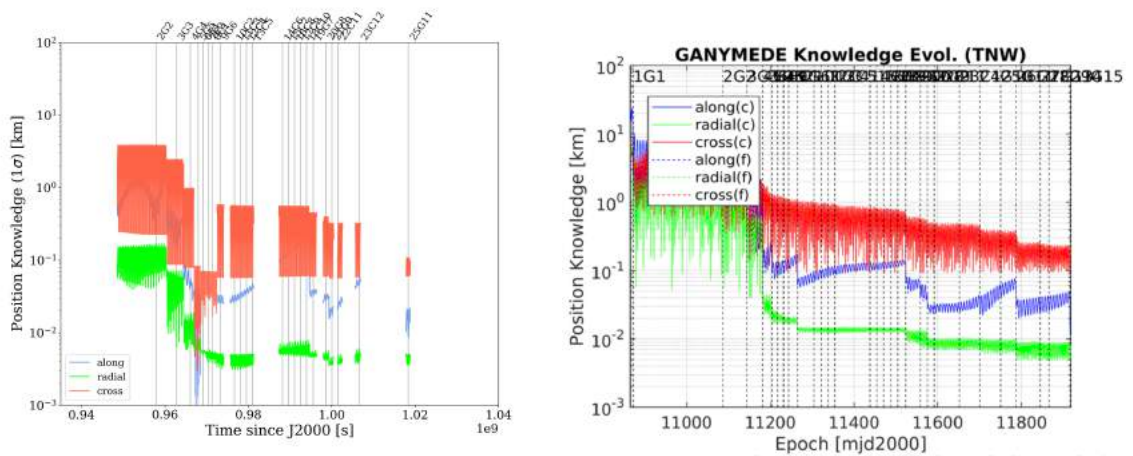


Figure B.5: Uncertainty evolution of Ganymede ephemeris from implemented model (left) and reference (right).

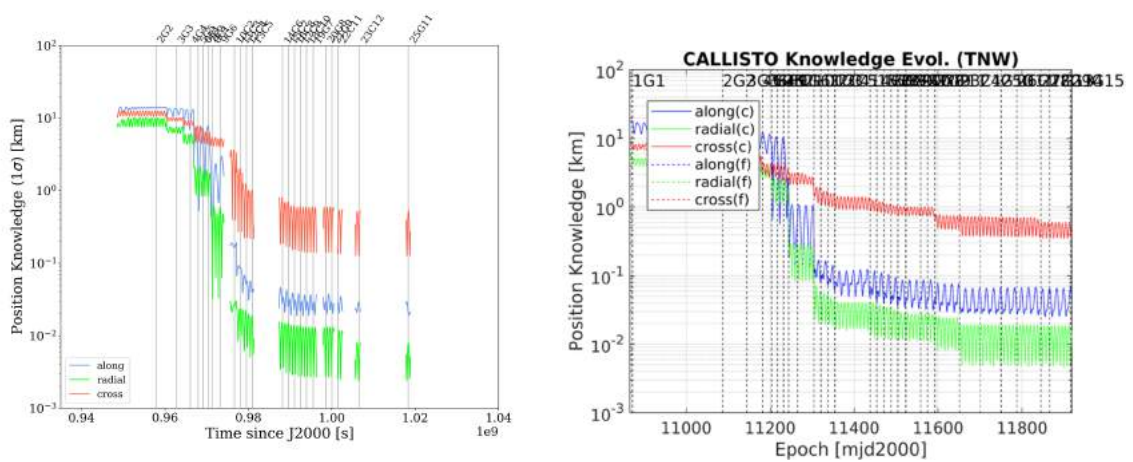


Figure B.6: Uncertainty evolution of Callisto ephemeris from implemented model (left) and reference (right).

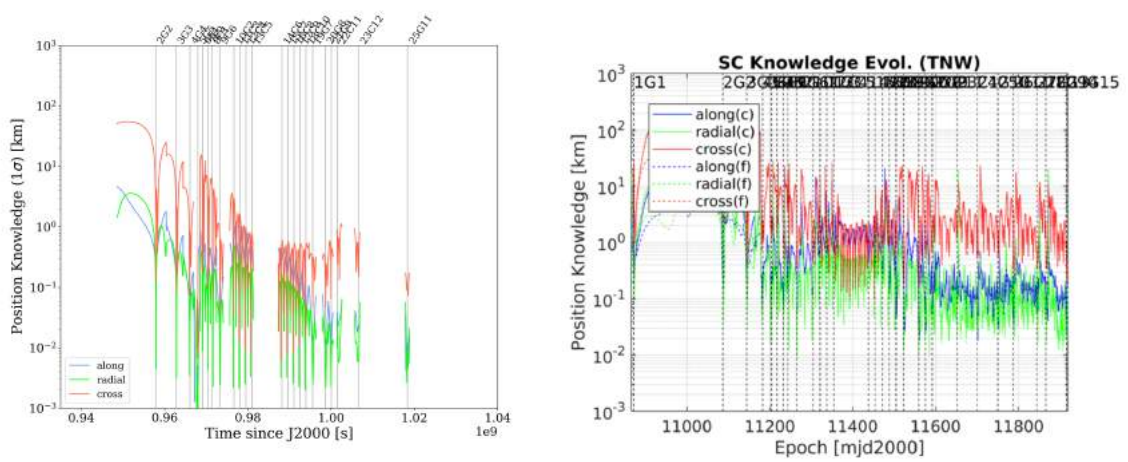


Figure B.7: Uncertainty evolution of JUICE ephemeris from implemented model (left) and reference (right).

## B.2. Validation: Manoeuvre Design Algorithm

The clean-up manoeuvre computation is another crucial building block of the comparative statistical  $\Delta V$  analysis. These manoeuvres are designed following a simple targeting strategy, namely the targeting of the nominal spacecraft position at the first downstream apojoive. It should be emphasised that targeting of the nominal spacecraft position does not allow for simultaneously targeting the spacecraft velocity.

This strategy differs from the targeting strategy in the reference documents ESOC, 2017–2019, and can therefore not be validated using the reference data. Instead, the clean-up manoeuvre design algorithm is verified by examining its effectiveness with which it can hit the chosen targets. The effectiveness is primarily defined via the ability to reduce spacecraft position error at the target epoch. However, the manoeuvre effect on the velocity error is also monitored. The latter step is considered necessary in order to confidently argue for the validity of the resulting manoeuvre designs.

An explicit formulation of the manoeuvre design algorithm is given in Chapter 2. Figure B.8 shows the effectiveness in reducing position residuals at target epoch. It also shows the single-iteration residual on the target position hit, which is well within the negligible regime.

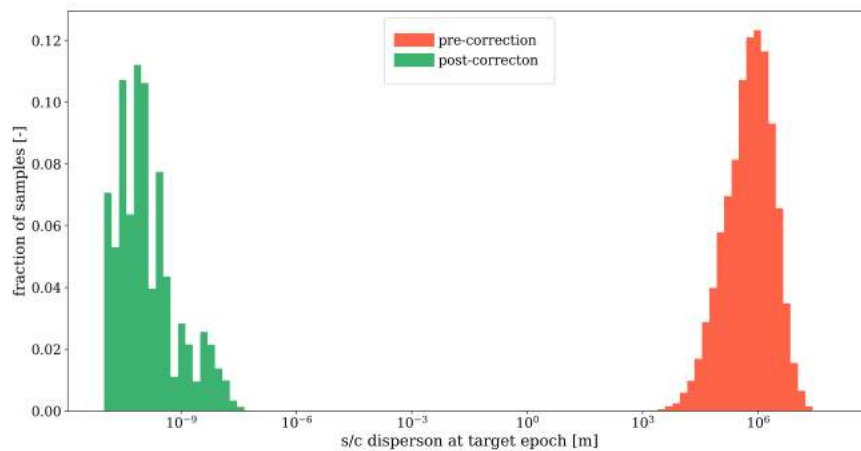


Figure B.8: Histogram showing the distribution of pre- and post-correction spacecraft position error at target epoch. The 1000 corrective manoeuvres were designed for spacecraft errors downstream of each tour flyby. Error samples were drawn from the same distribution  $S$  (journal paper, Eq. 5), on which the statistical  $\Delta V$  budget for the Nav OD baseline case was computed.

Figure B.9 documents the post-correction velocity residuals at target time. Since the targeting scheme does not constrain the velocity components, it is expected to see large residuals. The comparison with the pre-correction velocity error shows, that the residuals tend to be smaller than the original velocity deviation - large errors are reduced and not amplified. From this it can be concluded that the position-targeting scheme has the natural tendency to mitigate deviations in the velocity components, which suggests that the manoeuvre designs do not only eliminate target position errors, but also guide the spacecraft towards its nominal trajectory.

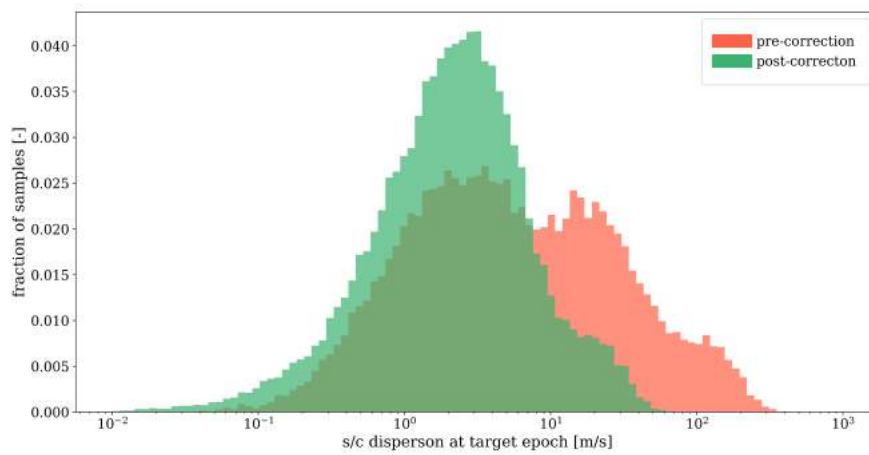


Figure B.9: Histogram showing the distribution of pre- and post-correction spacecraft velocity dispersion at target epoch. The 1000 corrective manoeuvres were designed for spacecraft dispersions downstream of each tour flyby. Dispersion samples were drawn from the same distribution  $S$  (journal paper, Eq. 5), on which the statistical  $\Delta V$  budget for the Nav OD baseline case was computed.



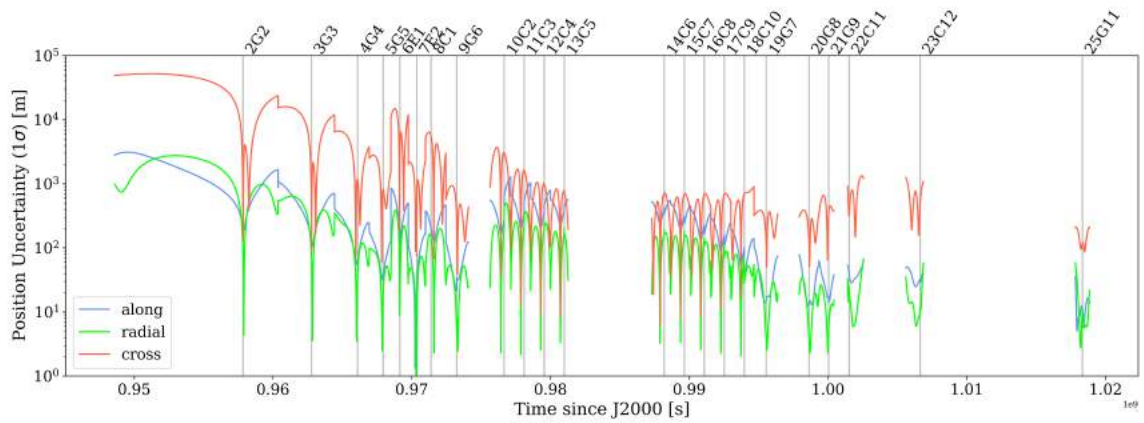
# C

## Supplementary material on selected OD solutions

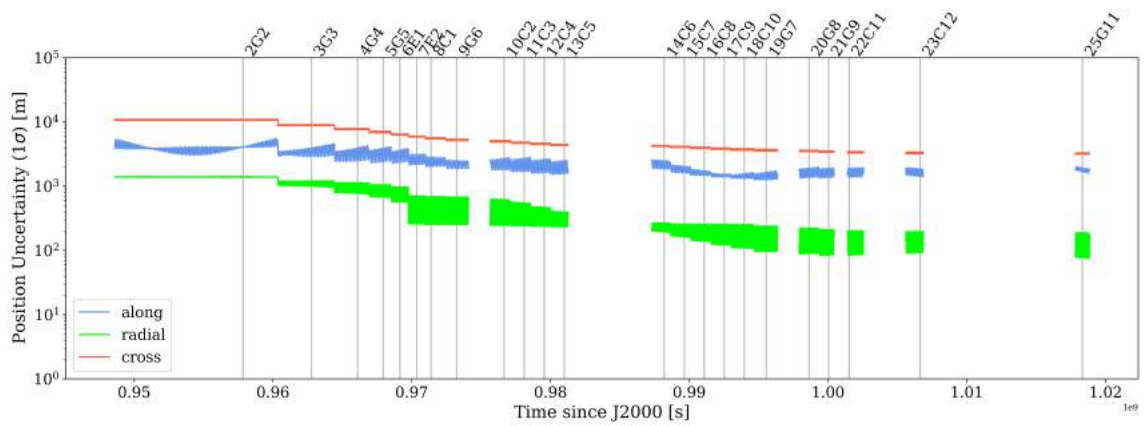
This appendix provides some additional material, specifically the uncertainty evolution and a summary on the numerical stability of modified navigation OD solutions. Appendix C.1 addresses the gravity estimation modification, appendices C.2 and C.3 the transfer factor and science data substitution cases, respectively.

### **C.1. System knowledge evolution with gravity estimation**

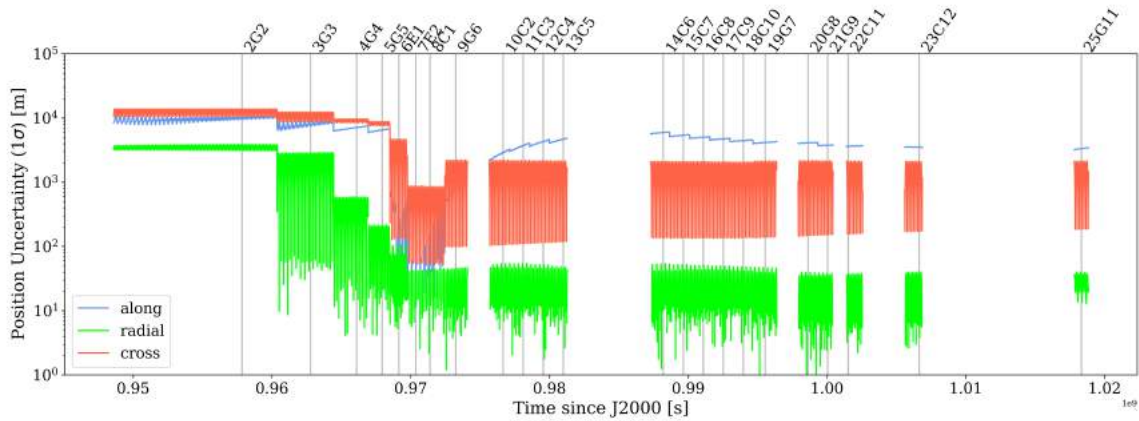
This section presents the uncertainty evolution plots and the inventory of invalid covariances for the navigation OD solution, when gravity-related parameters are included into the estimation. This modification was implemented to test the sensitivity of the OD setup to the uncertainties of these parameters.



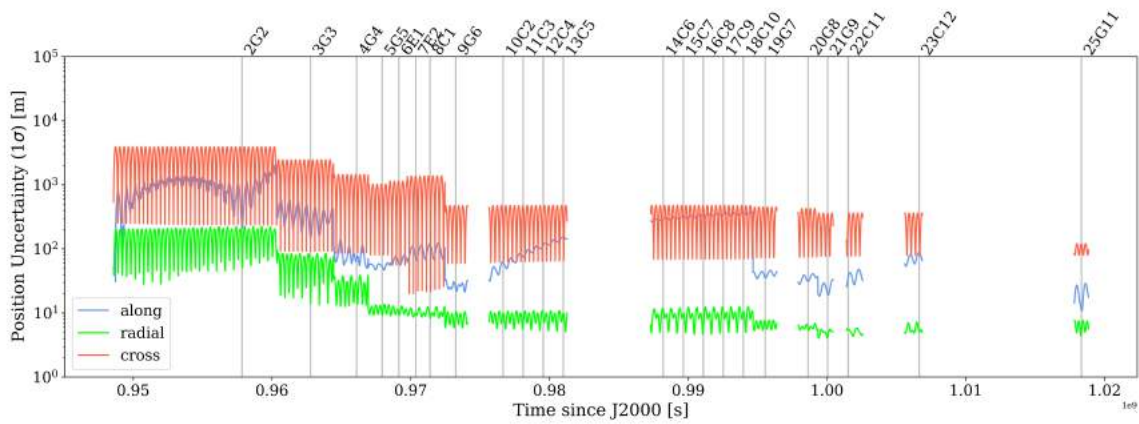
(a) Uncertainty evolution of JUICE position.



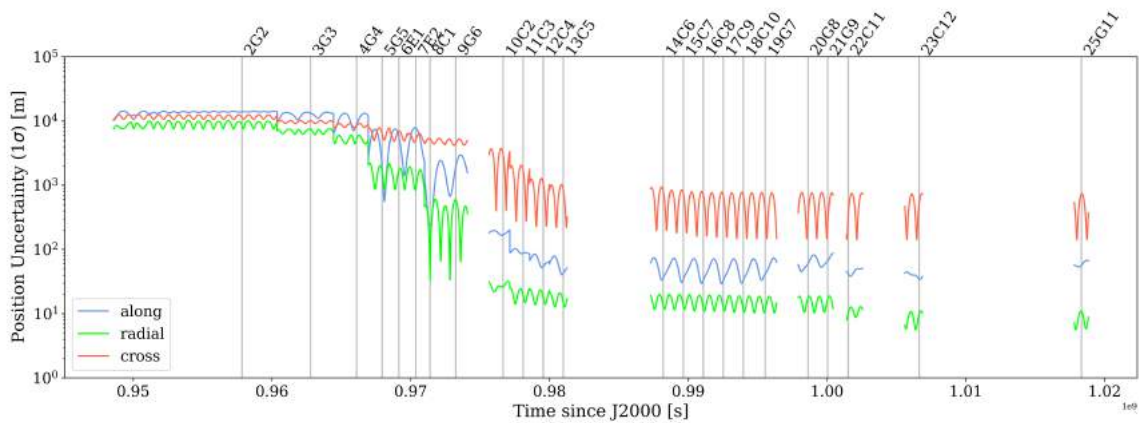
(b) Uncertainty evolution of Io position.



(c) Uncertainty evolution of Europa position.



(d) Uncertainty evolution of Ganymede position.



(e) Uncertainty evolution of Callisto position.

Figure C.1: Knowledge evolution of the JUICE-Jovian system, as computed by the Nav OD setup with gravity estimation. Vertical lines mark the time of moon encounter on each considered arc.

arc id	Navigation OD	
	valid	invalid
2G2	x	
3G3	x	
4G4	x	
5G5	x	
6E1		degree 3
7E2		degree 3
8C1		degree 3
9G6		degree 3
10C2		degree 1
11C3		degree 1
12C4		degree 1
13C5		degree 1
14C6		degree 1
15C7		degree 1
16C8		degree 1
17C9		degree 1
18C10		degree 1
19G7		degree 1
20G8		degree 3
21G9		degree 3
22C11		degree 1
23C12		degree 1
25G11		degree 3

Table C.1: Inventory of invalid elements in a-priori covariance - for Nav OD solution with gravity estimation, per arc. For definition of the degrees of invalid covariances, and the implications on the interpretability, please refer to appendix B.1.1.

## C.2. System knowledge evolution with transfer factor (f=3)

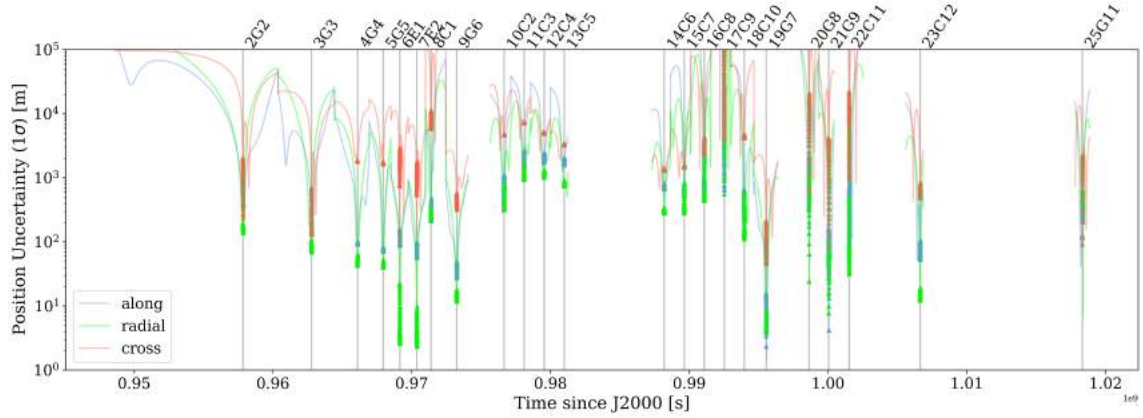
This section presents the inventory of invalid covariances for the navigation OD solution, when the empirical transfer factor of  $f=3$  is applied to the setup. The transfer factor was implemented to mitigate the idealising assumptions of the OD covariance analysis and was adopted as a free parameter in the statistical  $\Delta V$  analysis. As such, it played an important role in this work and thus uncertainty evolution plots of this case were already provided in the appendix of Chapter 2.

arc id	Navigation OD	
	valid	invalid
2G2	x	
3G3		degree 1
4G4	x	degree 3
5G5	x	
6E1		degree 2
7E2		degree 2
8C1	x	
9G6	x	
10C2	x	
11C3	x	
12C4	x	
13C5	x	
14C6	x	
15C7	x	
16C8	x	
17C9	x	
18C10	x	
19G7	x	
20G8	x	
21G9	x	
22C11	x	
23C12	x	
25G11	x	

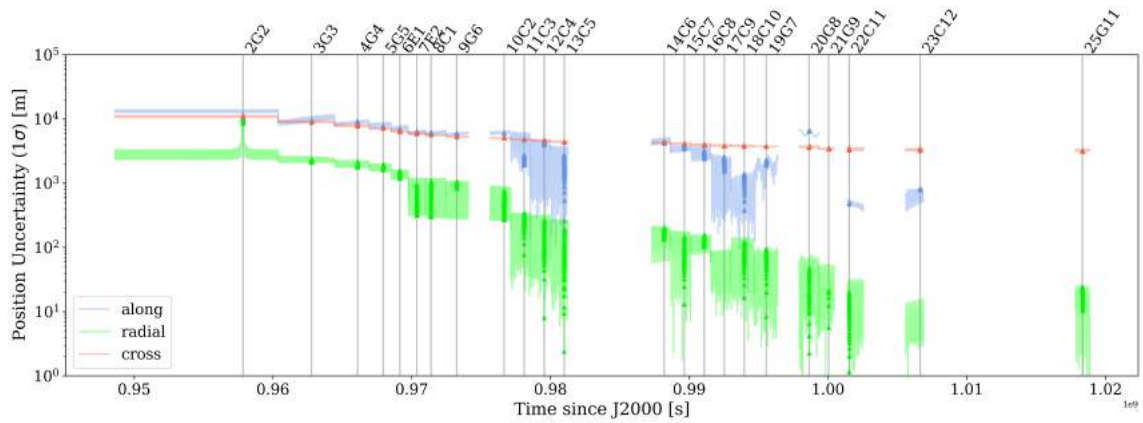
Table C.2: Inventory of invalid elements in a-priori covariance - for Nav OD solution with transfer factor at  $f=3$ , per arc. For definition of the degrees of invalid covariances, and the implications on the interpretability, please refer to appendix B.1.1.

### C.3. System knowledge evolution from simulated 3GM data

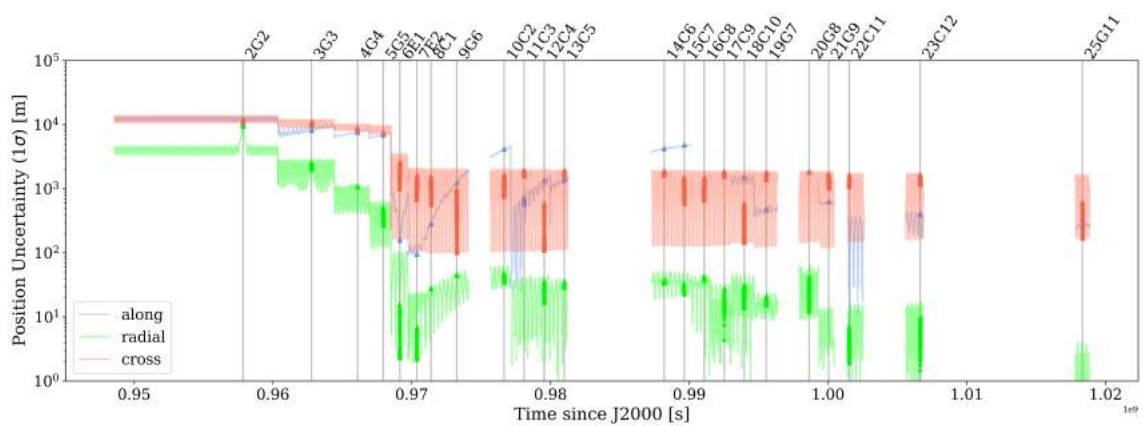
This section presents the uncertainty evolution plots and the inventory of invalid covariances for the navigation OD solution, when simulated with the 3GM radio science data. This modification was implemented for the direct comparison of radio science and navigation tracking data characteristics.



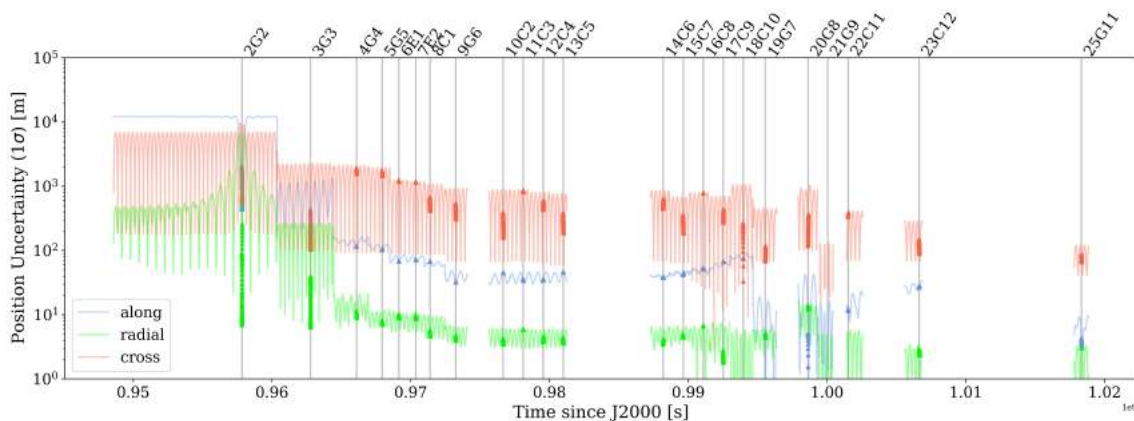
(a) Uncertainty evolution of JUICE position.



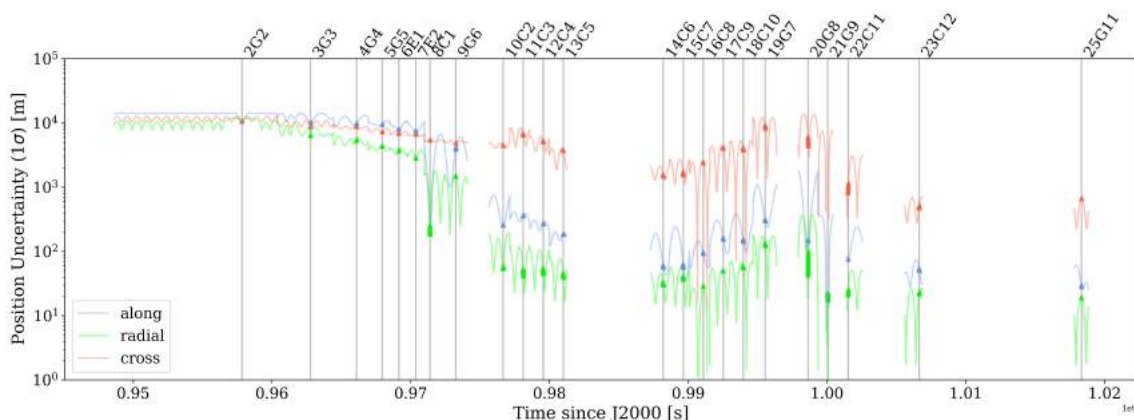
(b) Uncertainty evolution of Io position.



(c) Uncertainty evolution of Europa position.



(d) Uncertainty evolution of Ganymede position.



(e) Uncertainty evolution of Callisto position.

Figure C.2: Knowledge evolution of the JUICE-Jovian system, as computed by the Nav OD setup using simulated 3GM data. Vertical lines mark the time of moon encounter on each considered arc.

arc id	Navigation OD	
	valid	invalid
2G2	x	
3G3	x	
4G4	x	
5G5	x	
6E1	x	
7E2	x	
8C1	x	
9G6	x	
10C2	x	
11C3		degree 3
12C4		degree 3
13C5	x	
14C6		degree 3
15C7		degree 3
16C8		degree 3
17C9		degree 3
18C10	x	
19G7		degree 1
20G8		degree 1
21G9	x	
22C11	x	
23C12		degree 3
25G11		degree 1

Table C.3: Inventory of invalid elements in a-priori covariance - for Nav OD solution from simulated 3GM data, per arc. For definition of the degrees of invalid covariances, and the implications on the interpretability, please refer to appendix B.1.1.

# Bibliography

- Archinal, B. A., AHearn, M. F., Bowell, E., Conrad, A., Consolmagno, G. J., Courtin, R., Fukushima, T., Hestrofer, D., Hilton, J. L., Krasinsky, G. A., et al. (2011). Report of the IAU working group on cartographic coordinates and rotational elements: 2009. *Celestial Mechanics and Dynamical Astronomy*, 109(2), 101–135.
- Bauer, S., Hussmann, H., Oberst, J., Dirx, D., Mao, D., Neumann, G. A., Mazarico, E., Torrence, M., McGarry, J., Smith, D., et al. (2016). Demonstration of orbit determination for the lunar reconnaissance orbiter using one-way laser ranging data. *Planetary and Space Science*, 129, 32–46.
- Bellerose, J., Nandi, S., Roth, D., Tarzi, Z., Boone, D., Criddle, K., & Ionasescu, R. (2016). Cassini navigation: The road to consistent subkilometer accuracy satellite encounters. *39th AAS Annual Guidance and Control Conference, Breckenridge, Colorado*.
- Buffington, B., Strange, N., & Smith, J. (2008). Overview of the cassini extended mission trajectory. *AIAA/AAS Astrodynamics Specialist Conference and Exhibit*, 6752.
- Cappuccio, P., Hickey, A., Durante, D., Di Benedetto, M., Iess, L., De Marchi, F., Plainaki, C., Milillo, A., & Mura, A. (2020). Ganymede's gravity, tides and rotational state from JUICE's 3GM experiment simulation. *Planetary and Space Science*, 187.
- Dirx, D., Vermeersen, L., Noomen, R., & Visser, P. (2014). Phobos laser ranging: Numerical geodesy experiments for Martian system science. *Planetary and Space Science*, 99, 84–102.
- Dirx, D., Gurvits, L. I., Lainey, V., Lari, G., Milani, A., Cimò, G., Bocanegra-Bahamon, T., & Visser, P. (2017). On the contribution of PRIDE-JUICE to jovian system ephemerides. *Planetary and Space Science*, 147, 14–27.
- ESA. (2014). *Juice definition study report (red book)* (tech. rep.). ESA.
- ESOC. (2017–2019). *Juice: Navigation analysis of the jupiter tour* (tech. rep. No. 1.1–2.2). ESA.
- Fayolle, M., Dirx, D., Visser, P., & Lainey, V. (2021). Analytical framework for mutual approximations-derivation and application to jovian satellites. *Astronomy & Astrophysics*, 652, A93.
- Fayolle, M., Dirx, D., Lainey, V., Gurvits, L. I., & Visser, P. N. A. M. (2022). *Decoupled and coupled moons ephemerides estimation strategies application to the JUICE mission* [submitted to Planetary and Space Science].
- Grasset, O., Dougherty, M., Coustenis, A., Bunce, E., Erd, C., Titov, D., Blanc, M., Coates, A., Drossart, P., Fletcher, L., et al. (2013). JUpiter ICy moons Explorer (JUICE): An ESA mission to orbit Ganymede and to characterise the jupiter system. *Planetary and Space Science*, 78, 1–21.
- Greenberg, R. (2010). The icy jovian satellites after the galileo mission. *Reports on Progress in Physics*, 73(3), 036801.
- Hussmann, H., Sohl, F., & Spohn, T. (2006). Subsurface oceans and deep interiors of medium-sized outer planet satellites and large trans-neptunian objects. *Icarus*, 185(1), 258–273.
- Lainey, V., Arlot, J., & Vienne, A. (2004b). New accurate ephemerides for the Galilean satellites of Jupiter-II. fitting the observations. *Astronomy & Astrophysics*, 427(1), 371–376.
- Lainey, V., Arlot, J.-E., Karatekin, Ö., & Van Hoolst, T. (2009). Strong tidal dissipation in io and jupiter from astrometric observations. *Nature*, 459(7249), 957–959.
- Lainey, V., & Tobie, G. (2005). New constraints on Io's and Jupiter's tidal dissipation. *Icarus*, 179(2), 485–489.
- Lynam, A. E., & Longuski, J. M. (2012). Preliminary analysis for the navigation of multiple-satellite-aided capture sequences at jupiter. *Acta Astronautica*, 79, 33–43.
- Morgado, B., Benedetti-Rossi, G., Gomes-Júnior, A., Assafin, M., Lainey, V., Vieira-Martins, R., Camargo, J., Braga-Ribas, F., Bouffleur, R., Fabrega, J., et al. (2019). First stellar occultation by the galilean moon europa and upcoming events between 2019 and 2021. *Astronomy & Astrophysics*, 626, L4.
- Murrow, D., & Jacobson, R. (1988). Galilean satellite ephemeris improvement using Galileo tour encounter information. *Astrodynamics Conference*, 4249.
- Raofi, B., Guman, M., & Potts, C. (2000). Preliminary statistical analysis for a representative Europa orbiter mission. *Astrodynamics Specialist Conference Denver, CO, USA*.
- Schubert, G., Anderson, J., Spohn, T., & McKinnon, W. (2004). Interior composition, structure and dynamics of the Galilean satellites. *Jupiter: The planet, satellites and magnetosphere*, 1, 281–306.

- Tarzi, Z., Boone, D., Mastrodemos, N., Nandi, S., & Young, B. (2019). Orbit determination sensitivity analysis for the Europa Clipper Mission tour. *AIAA/AAS Space Flight Mechanics Meeting*.
- Titov, D., Bibring, J.-P., Cardesin, A., Duxbury, T., Forget, F., Giuranna, M., Holmstroem, M., Jaumann, R., Martin, P., Montmessin, F., et al. (2016). Mars express: Status and recent findings. *EGU General Assembly Conference Abstracts*, EPSC2016–14576.
- Vance, S., Bouffard, M., Choukroun, M., & Sotin, C. (2014). Ganymede's internal structure including thermodynamics of magnesium sulfate oceans in contact with ice. *Planetary and Space Science*, 96, 62–70.
- Verma, A. K., & Margot, J.-L. (2018). Expected precision of Europa Clipper gravity measurements. *Icarus*, 314, 35–49.
- Wertz, J. R., Larson, W. J., Kirkpatrick, D., & Klungle, D. (1999). *Space mission analysis and design* (Vol. 8). Springer.